



THE HONG KONG  
POLYTECHNIC UNIVERSITY

香港理工大學

Pao Yue-kong Library

包玉剛圖書館

---

## Copyright Undertaking

This thesis is protected by copyright, with all rights reserved.

**By reading and using the thesis, the reader understands and agrees to the following terms:**

1. The reader will abide by the rules and legal ordinances governing copyright regarding the use of the thesis.
2. The reader will use the thesis for the purpose of research or private study only and not for distribution or further reproduction or any other purpose.
3. The reader agrees to indemnify and hold the University harmless from and against any loss, damage, cost, liability or expenses arising from copyright infringement or unauthorized usage.

### IMPORTANT

If you have reasons to believe that any materials in this thesis are deemed not suitable to be distributed in this form, or a copyright owner having difficulty with the material being included in our database, please contact [lbsys@polyu.edu.hk](mailto:lbsys@polyu.edu.hk) providing details. The Library will look into your claim and consider taking remedial action upon receipt of the written requests.

The Hong Kong Polytechnic University  
Department of Building Services Engineering

**An Experimental and Numerical Study on  
Improving Defrosting Performances for an Air  
Source Heat Pump Unit Having a Multi-circuit  
Outdoor Coil**

**SONG Mengjie**

**A thesis submitted in partial fulfillment of the requirements  
for the Degree of Doctor of Philosophy**

August 2014

## **CERTIFICATE OF ORIGINALITY**

I hereby declare that this thesis is my own work and that, to the best of my knowledge and belief, it reproduces no material previously published or written, nor material that has been accepted for the award of any other degree or diploma, except where due acknowledgement has been made in the text.

SONG Mengjie

Department of Building Services Engineering

The Hong Kong Polytechnic University

Hong Kong SAR, China

August, 2014

## **Abstract**

Air source heat pump (ASHP) units have found wide applications worldwide in recent decades as an energy efficient and environmental friendly means for indoor environmental control. However, when an ASHP unit operates in heating mode, frost might be formed and accumulated on the surface of its outdoor coil. Frosting deteriorates its operational performance and energy efficiency, and therefore periodic defrosting is necessary.

Currently, reverse cycle defrosting is the most widely used standard defrosting method for ASHP units. For an outdoor coil in an ASHP unit, multiple parallel refrigerant circuits are commonly seen for minimized refrigerant pressure loss and enhanced heat transfer efficiency. However, uneven defrosting over the entire airside surface of a vertically installed multi-circuit outdoor coil was observed during reverse cycle defrosting for ASHP units. Uneven defrosting could lead to a prolonged defrosting duration and a lower defrosting efficiency. One of the reasons for uneven defrosting was downwards flowing of melted frost over the surface of a vertically installed multi-circuit outdoor coil due to gravity. Therefore, it is necessary to experimentally study the negative impacts of downwards flowing of melted frost on defrosting performance for ASHP units, by comparing the measured defrosting performances with and without the melted frost downwards flowing from up circuit(s) to down circuit(s) in an experimental multi-circuit outdoor coil. On the other hand, to enable further quantitatively analyzing the effects of locally draining away the melted frost on reverse cycle defrosting performance of an

ASHP unit, and to develop methods to alleviate the negative effects of uneven defrosting on defrosting performance of an existing ASHP unit, modeling studies should also be carried out.

This thesis begins with reporting an experimental study on the negative effects of downwards flowing of melted frost over a vertically installed experimental three-circuit outdoor coil in an experimental ASHP unit on defrosting performance during reverse cycle defrosting. Three experimental study cases, with different arrangements of water collecting trays placed between or under circuit(s), were designed and carried out. The temperatures of tube surface at the exits of each refrigerant circuit, coil fin surface at the center of each circuit, and the melted frost collected were measured. The experimental results and corresponding quantitative analysis revealed the negative effects of allowing melted frost to freely flow downwards due to gravity over the airside surface of the vertically installed experimental three-circuit outdoor coil in the experimental ASHP unit on defrosting performance during reverse cycle defrosting: a longer defrosting duration and more energy consumption. In addition, the study results also suggested that the use of water collecting trays between circuits for locally draining away the melted frost before flowing into down circuit(s) was effective in mitigating these negative effects.

Secondly, the thesis presents a mathematical modeling study on the defrosting performance for the experimental ASHP unit with local drainage of the melted frost from its vertically installed three-circuit outdoor coil. Two semi-empirical mathematical models, corresponding to two settings of with and without the use of water collecting

trays between circuits, were developed. In this modeling study, a defrosting process on the airside of an outdoor coil was divided into four stages: (1) preheating, (2) frost melting without water flowing away from a circuit, (3) frost melting with water flowing away from a circuit, and (4) water layer vaporizing. The two semi-empirical models were validated by comparing the experimental data obtained in the experimental study and the predicted data using the models for the key operating parameters of the experimental ASHP unit, with good agreements. The validated models could adequately describe the defrosting operation for the experimental ASHP unit with local drainage of the melted frost from its outdoor coil.

Finally, to explore the potential methods of alleviating the negative effects of downwards flowing of melted frost and thus improving the defrosting performance of an existing ASHP unit, a modeling study on alleviating uneven defrosting for the experimental vertical three-circuit outdoor coil in the experimental ASHP unit during reverse cycle defrosting was carried out and the study results are reported. To alleviate uneven defrosting for an existing ASHP unit, it can be effective to vary the heat supply (via refrigerant flow) to each refrigerant circuit by varying the openings of modulating valves installed at an inlet pipe to each circuit. Three study cases, with different mechanisms of both varying the openings of modulating valves and introducing other operational changes, were designed and corresponding modeling studies carried out using the validated semi-empirical model developed at the setting of without the use of water collecting trays between circuits. Modeling results suggested that the best defrosting performances in terms of shortening defrosting durations and reducing defrosting energy

use were achieved in the study case of fully closing the modulating valve on the top circuit when its tube surface temperature at the exit of the circuit reached defrosting termination point. While further experimental studies to validate the modeling results are to be carried out, it is however expected that with more refrigerant circuits in an outdoor coil in an ASHP unit, the method of fully closing the modulating valves on top circuit(s) would yield better defrosting performance for the ASHP unit.

## Publications Arising from the Thesis

### I. Journal Papers

- **Song Mengjie**, Deng Shiming, Pan Dongmei and Mao Ning. An experimental study on the effects of downwards flowing of melted frost over a vertical multi-circuit outdoor coil in an air source heat pump on defrosting performance during reverse cycle defrosting. *Applied Thermal Engineering*. Vol. 67, pp. 258-265. 2014 (Based on Chapter 5).
- **Song Mengjie**, Deng Shiming and Xia Liang. A semi-empirical modeling study on the defrosting performance for an air source heat pump unit with local drainage of melted frost from its three-circuit outdoor coil. *Applied Energy (Accepted)*. 2014 (Based on Chapter 6).
- **Song Mengjie**, Xia Liang and Deng Shiming. A modeling study on alleviating uneven defrosting for a vertical three-circuit outdoor coil in an air source heat pump unit during reverse cycle defrosting. *Submitted to Building Services Engineering Research and Technology*. 2014 (Based on Chapter 7).

## II. Conference Papers

- **Song Mengjie**, Pan Dongmei, Li Ning and Deng Shiming. An experimental study on the negative effects of downwards flow of the melted frost over a multi-circuit outdoor coil in an air source heat pump during reverse cycle defrosting. *The 5<sup>th</sup> International Conference on Applied Energy*, Pretoria, South Africa, 1-4 July, 2013.
- **Song Mengjie**, Xu Xiangguo, Deng Shiming and Mao Ning. An experimental study on performance during reverse cycle defrosting of an air source heat pump with a horizontal three-circuit outdoor coil. *The 6<sup>th</sup> International Conference on Applied Energy*, Taipei, Taiwan, 30 May-2 June, 2014.

## **Acknowledgements**

I must express my grateful thanks to my Chief Supervisor, Prof. Deng Shiming, Professor and Associate Head, and my Co-Supervisor, Dr. Chan Mingyin, Assistant Professor, both from Department of Building Services Engineering (BSE), The Hong Kong Polytechnic University, and my Co-Supervisor, Dr. Xia Liang, Assistant Professor, Department of Building Services Engineering and Building Physics, Faculty of Science and Engineering, The University of Nottingham Ningbo China, for their readily available supervision, valuable suggestions, patient guidance, continuous helps and encouragement throughout the course of the work.

My special thanks go to The Hong Kong Polytechnic University for financially supporting my study. I would also like to thank all members in my research group, for their assistances during my experimental and simulation work. In addition, I wish to express my gratitude to the technicians in the Heating Ventilation and Air Conditioning Laboratory of BSE Department for their supports during my experimental work.

Finally, I would like to express my deepest appreciation to my parents, my wife Ms. Luo Xiaoyan and all other family members. I could not have finished my work without their encouragement, supports and understandings.

## Table of Contents

	<b>Page</b>
<b>Certificate of Originality</b>	<b>i</b>
<b>Abstract</b>	<b>ii</b>
<b>Publications Arising from the Thesis</b>	<b>vi</b>
<b>Acknowledgements</b>	<b>viii</b>
<b>Table of Contents</b>	<b>ix</b>
<b>List of Figures</b>	<b>xiii</b>
<b>List of Tables</b>	<b>xvi</b>
<b>List of Abbreviations</b>	<b>xvii</b>
<b>Nomenclature</b>	<b>xviii</b>
<b>Subscripts</b>	<b>xxii</b>
<b>Chapter 1      Introduction</b>	<b>1</b>
<b>Chapter 2      Literature Review</b>	<b>6</b>
2.1 Introduction	6
2.2 Operating performances of ASHP units under frosting conditions	8
2.2.1 Mechanisms of frost formation	8
2.2.2 Frost formation on the surface of a heat exchanger	10
2.2.3 Frost formation on the outdoor coil surface of an ASHP unit	13
2.2.4 Numerical studies on the operating performances of ASHP units under frosting conditions	16
2.3 Frost retarding measures and defrosting methods for ASHP units	18
2.3.1 Changing ambient air parameters	18
2.3.2 Optimizing the structure of an outdoor coil	21
2.3.3 Other frost retarding measures	25

2.3.4	Defrosting methods	28
2.4	Operating performances of ASHP units during reverse cycle defrosting	33
2.4.1	Experimental studies on ASHP units during reverse cycle defrosting	34
2.4.2	Performance improvements for ASHP units during reverse cycle defrosting	37
2.4.3	Studies on multi-circuit outdoor coil of ASHP units during reverse cycle defrosting	40
2.4.4	Numerical studies on the operating performances of ASHP units during reverse cycle defrosting	43
2.5	Control methods to start and end a defrosting operation	46
2.5.1	Defrosting initiation	46
2.5.2	Defrosting termination	50
2.6	Conclusions	52
<b>Chapter 3</b>	<b>Proposition</b>	<b>55</b>
3.1	Background	55
3.2	Project title	56
3.3	Aims and objectives	57
3.4	Research methodologies	58
<b>Chapter 4</b>	<b>An Experimental Setup for an Experimental ASHP Unit Having a Multi-circuit Outdoor Coil</b>	<b>60</b>
4.1	Introduction	60
4.2	Detailed descriptions of the experimental setup	61
4.2.1	The experimental ASHP unit	63
4.2.2	The specially-made vertically-installed outdoor coil and its airside details	65
4.2.3	Environmental chamber	68

4.3	Computerized instrumentation and data acquisition system (DAS)	69
4.3.1	Sensors/measuring devices for temperatures, pressures and flow rates	70
4.3.2	The DAS	73
4.4	Evaluating the mass of accumulated frost on outdoor coil surface	73
4.5	Conclusions	75
<b>Chapter 5</b>	<b>An Experimental Study on Improving Defrosting Performances for an ASHP Unit Having a Multi-circuit Outdoor Coil</b>	<b>76</b>
5.1	Introduction	76
5.2	Experimentation	78
5.2.1	Experimental ASHP unit	78
5.2.2	Experimental procedures and conditions	78
5.3	Experimental results	80
5.4	Conclusions	94
<b>Chapter 6</b>	<b>A Semi-empirical Mathematical Modeling Study on Improving Defrosting Performances for an ASHP Unit Having a Multi-circuit Outdoor Coil</b>	<b>95</b>
6.1	Introduction	95
6.2	Development of the semi-empirical mathematical models	96
6.2.1	Assumptions and calculation conditions	99
6.2.2	Model development	102
6.2.2.1	Model 1 development (all four stages)	102
6.2.2.2	Model 2 development (only Stage 3)	115
6.2.2.3	Modeling a water collecting tray and a water collecting cylinder	116
6.2.2.4	The method of solving the two models	119

6.3	Experimental validation of the two models	121
6.3.1	Validation of Model 1	121
6.3.2	Validation of Model 2	124
6.4	Discussions	129
6.4.1	Potential uses of the two models developed	129
6.4.2	Limitations of the modeling work	130
6.5	Conclusions	131
<b>Chapter 7</b>	<b>A Modeling Study on Alleviating Uneven Defrosting for the Experimental Three-circuit Outdoor Coil during Reverse Cycle Defrosting</b>	<b>132</b>
7.1	Introduction	132
7.2	Methodology and study cases	134
7.2.1	The three study cases	134
7.2.2	The assumptions used in the modeling study	143
7.3	Modeling results	144
7.4	Energy use for defrosting in the three study cases	153
7.5	Conclusions	154
<b>Chapter 8</b>	<b>Conclusions and Future Work</b>	<b>155</b>
8.1	Conclusions	155
8.2	Proposed future work	159
	<b>References</b>	<b>161</b>
	<b>Appendix A Photos of the Experimental Setup</b>	<b>188</b>
	<b>Appendix B Program Listing of Model 1</b>	<b>191</b>

## List of Figures

	<b>Page</b>
<b>Chapter 2</b>	
Figure 2.1	Schematic diagram illustrating reverse cycle defrosting of an outdoor coil cell [Krakow et al. 1992a, 1992b] 44
<b>Chapter 4</b>	
Figure 4.1	Schematics of the experimental setup for an experimental ASHP unit installed in an environmental chamber 62
Figure 4.2	Details of the three-parallel refrigerant circuit outdoor coil and locations of solenoid valves and manual stop valves 65
Figure 4.3	The schematic diagram of the environmental chamber 68
Figure 4.4	The airside details of the experimental outdoor coil in the experimental ASHP unit installed in the frosting outdoor space 70
<b>Chapter 5</b>	
Figure 5.1	Airside surface conditions of the outdoor coil during defrosting in three cases (twelve photographs) 81
Figure 5.1 (Cond.)	Airside surface conditions of the outdoor coil during defrosting in three cases (twelve photographs) 82
Figure 5.2	Measured tube surface temperatures at the exits of the three refrigerant circuits during defrosting (Case 1) 85
Figure 5.3	Measured tube surface temperatures at the exits of the three refrigerant circuits during defrosting (Case 2) 86
Figure 5.4	Measured tube surface temperatures at the exits of the three refrigerant circuits during defrosting (Case 3) 87
Figure 5.5	Measured fin temperatures at the center of the three refrigerant circuits during defrosting (Case 1) 88

Figure 5.6	Measured fin temperatures at the center of the three refrigerant circuits during defrosting (Case 2)	89
Figure 5.7	Measured fin temperatures at the center of the three refrigerant circuits during defrosting (Case 3)	90
Figure 5.8	Temperatures of melted frost collected in the water collecting cylinders in the three cases	91
 <b>Chapter 6</b>		
Figure 6.1	Conceptual models for the airside of the three-circuit outdoor coil in the experimental ASHP unit	97
Figure 6.2	Schematics of mass and energy flows in the four defrosting stages for Model 1	103
Figure 6.3	Schematics of mass and energy flows in Stage 3 of defrosting for Model 2	116
Figure 6.4	Schematics of mass and energy flows in a water collecting tray and a water collecting cylinder during defrosting	117
Figure 6.5	The computational algorithm for the four defrosting stages in two models	120
Figure 6.6	Comparison between the measured and predicted tube surface temperatures at the exit of each circuit (Model 1)	122
Figure 6.7	Comparison between the measured and predicted temperatures of melted frost collected in Cylinder C (Model 1)	123
Figure 6.8	Comparison between the measured and predicted tube surface temperatures at exits of the three circuits (Model 2)	125
Figure 6.9	Comparison between the measured and predicted temperatures of melted frost collected in Cylinder A (Model 2)	126
Figure 6.10	Comparison between the measured and predicted temperatures of melted frost collected in Cylinder B (Model 2)	127

Figure 6.11	Comparison between the measured and predicted temperatures of melted frost collected in Cylinder C (Model 2)	128
-------------	--	-----

## **Chapter 7**

Figure 7.1	Measured refrigerant mass flow rate	137
Figure 7.2	Assumed refrigerant mass flow rates to three circuits in Study Case 1	138
Figure 7.3	Assumed refrigerant mass flow rates to three circuits in Study Case 2	140
Figure 7.4	Assumed refrigerant mass flow rates to three circuits in Study Case 3	142
Figure 7.5	Predicted tube surface temperatures at circuit exits (Case 1)	146
Figure 7.6	Predicted tube surface temperatures at circuit exits (Case 2)	148
Figure 7.7	Predicted tube surface temperatures at circuit exits (Case 3)	150
Figure 7.8	Measured tube surface temperatures at circuit exits	151
Figure 7.9	Predicted tube surface temperatures at circuit exits	152

## **Appendix A**

Photo 1	Overview of the indoor part of the experimental setup	188
Photo 2	Overview of the outdoor part of the experimental setup	189
Photo 3	Air velocity grid in the outdoor part of the experimental setup	189
Photo 4	Outdoor coil the experimental setup	190

## List of Tables

		<b>Page</b>
<b>Chapter 2</b>		
Table 2.1	Temperature settings to end a reverse cycle defrosting operation for ASHP units	51
<b>Chapter 4</b>		
Table 4.1	Specifications of the experimental ASHP unit excluding the outdoor coil	64
Table 4.2	Specifications of the vertically installed outdoor coil	67
Table 4.3	Measurement/calculation errors of system parameters	72
<b>Chapter 5</b>		
Table 5.1	Experimental conditions	79
Table 5.2	Three experimental cases	80
<b>Chapter 6</b>		
Table 6.1	Two semi-empirical models	98
<b>Chapter 7</b>		
Table 7.1	Valves opening of modulating and other operational changes in the three study cases	135
Table 7.2	Defrosting durations in the three study cases and in the previous experimental and modeling studies	153

## List of Abbreviations

A/C	air-conditioning
ASHP	air source heat pump
ASHRAE	American Society of Heating, Refrigerating and Air-conditioning Engineers
ANSI	American National Standard Institute
COP	coefficient of performance
DAS	data acquisition system
DX	direct-expansion
EEV	electronic expansion valve
FTVI	flash tank vapor injection
HVAC	heating, ventilation and air conditioning
LGU	load generating unit
PCM	phase change material
SCVI	sub-cooler vapor injection
TEV	thermal expansion valve

## Nomenclatures

Variable	Description	Unit
$A_0$	equivalent airside surface area of a refrigerant circuit	$m^2$
$A_{d-a}$	effective dry airside surface area of a refrigerant circuit (used in the fourth stage)	$m^2$
$A_{f-a}$	the effective airside surface area covered by only the melted frost of a refrigerant circuit (used in the second and third stages)	$m^2$
$A_t$	total refrigerant tube surface area of each circuit (used in the first stage)	$m^2$
$A_{tube}$	total refrigerant tube surface area of the entire three-circuit outdoor coil (used in the first stage)	$m^2$
$A_{tw}$	surface area of the melted frost in contact with ambient air in a water collecting tray (used in the modeling a water collecting tray and a water collecting cylinder part)	$m^2$
$A_{w-a}$	effective wetted airside surface area of a refrigerant circuit (used in the fourth stage)	$m^2$
$c_{Al}$	specific heat of aluminum	$kJ/(kg \text{ } ^\circ C)$
$c_{Cu}$	specific heat of copper	$kJ/(kg \text{ } ^\circ C)$
$c_p$	specific heat of water	$kJ/(kg \text{ } ^\circ C)$
$c_{PMe}$	average specific heat of metal (copper and aluminum)	$kJ/(kg \text{ } ^\circ C)$
$d_i$	inner diameter of refrigerant tube	$m$
$g$	gravity acceleration	$m/s^2$
$Gr$	Grashof Number	ND
$h_c$	coefficient of natural convective heat transfer	$W/(m^2 \text{ } ^\circ C)$

$h_D$	coefficient of convective mass transfer	m/s
$h_L$	liquid refrigerant heat transfer coefficient	W/(m <sup>2</sup> °C)
$h_{r,e}$	refrigerant enthalpy at the outlet of each circuit	kJ/kg
$h_{r,in}$	refrigerant enthalpy at the inlet of each circuit	kJ/kg
$h_{r,tp}$	convective heat transfer coefficient of refrigerant in the two-phase region	W/(m <sup>2</sup> °C)
$h_{r,sh}$	convective heat transfer coefficient of refrigerant in the superheated region	W/(m <sup>2</sup> °C)
$h_{TPM}$	refrigerant side mean heat transfer coefficient	W/(m <sup>2</sup> °C)
$h_w$	average coefficient of convective heat transfer caused by water flow inside a control volume	W/(m <sup>2</sup> °C)
$h_{w,x}$	coefficient of local convective heat transfer caused by water flow	W/(m <sup>2</sup> °C)
$H$	height of a refrigerant circuit	m
$L$	tube length of a refrigerant circuit	m
$Le$	Lewis Number	ND
$L_{sf}$	latent heat of frost melting (334)	kJ/kg
$L_v$	latent heat of water vaporization (2443)	kJ/kg
$\Delta m_f$	total mass of frost accumulated on the surface of a refrigerant circuit in a multi-circuit outdoor coil during the period of $\Delta t$	kg
$m_{r,j}$	mass flow rate of refrigerant in Control Volume $j$	kg/s
$m_{v,j}$	mass rate of the retained water vaporized from Circuit $j$	kg/s
$m_{v,tw}$	rate of vaporization for the melted frost vaporized from a cylinder	kg/s
$m_{w,j}$	mass flow rate of the melted frost falling from Circuit $j$	kg/s
$M_{f,j}$	total mass of frost accumulated on the surface of Circuit $j$	kg
$M_{tf}$	total mass of the melted frost collected in the cylinder(s)	kg

$M_{tw}$	accumulated mass of the retained melted frost in a water collecting tray	kg
$M_{tw,max}$	maximum mass of the retained water that can be held on the collecting tray	kg
$M_{w,j}$	accumulated mass of the retained melted frost in the Control Volume $j$	kg
$M_{w,max}$	maximum of the melted frost held on the surface of a refrigerant circuit	kg
$Nu$	Nusselt Number	ND
$P$	actual compressor discharge pressure	MPa
$P_c$	critical pressure	MPa
$P_{re}$	reduced pressure	MPa
$Pr$	Prandtl Number	ND
$q$	power consumption	kW
$q_{Me}$	power consumption to heat the metal of outdoor coil	kW
$R$	thermal resistance	(m <sup>2</sup> °C)/W
$R_r$	thermal resistance of refrigerant	(m <sup>2</sup> °C)/W
$Re$	Reynold Number	ND
$\Delta t$	measuring time interval	s
$\Delta T_{Me}$	average temperature difference of outdoor coil metal	°C
$t$	time	s
$t_d$	defrosting duration	s
$T$	temperature	°C
$T_0$	average temperature of outdoor coil metal at the start of a defrosting process	°C
$T_a$	temperature of ambient air around a refrigerant circuit	°C
$T_e$	outlet tube surface temperature of outdoor coil	°C
$T_{ICW}$	temperature at the interface between coil surface and water layer	°C

$T_{in}$	inlet tube surface temperature of outdoor coil	°C
$T_{r,j}$	average temperature of refrigerant in Circuit $j$	°C
$T_t$	average temperature of outdoor coil metal at the end of a defrosting process	°C
$T_{tp}$	triple point of water	°C
$T_{tw}$	temperature of the melted frost collected	°C
$T_{w,j}$	temperature of the retained water on the surface of tubes and fins of each circuit	°C
$v$	average velocity of water layer downwards flowing	m/s
$x$	thermodynamic vapor quality	%

*Greek symbols*

$\beta$	volumetric thermal expansion coefficient	1/°C
$\lambda$	thermal conductivity	W/(m °C)
$\nu$	kinematic viscosity	m <sup>2</sup> /s
$\rho_a$	density of ambient air	kg/m <sup>3</sup>
$\rho_{va}$	density of water vapor within ambient air	kg/m <sup>3</sup>
$\rho_{vs}$	density of water vapor at the interface (saturated density)	kg/m <sup>3</sup>

Note: ND = No Dimensions

## Subscripts

<i>a</i>	air
<i>d</i>	defrosting
<i>e</i>	outlet
<i>f</i>	frost
<i>i</i>	inner
<i>in</i>	inlet
<i>ICW</i>	interface between the coil surface and the water layer
<i>j</i>	circuit number or control volume ( $j = 1 - 3$ )
<i>L</i>	liquid
<i>m</i>	melting
<i>Me</i>	metal
<i>max</i>	maximum
<i>r</i>	refrigerant
<i>re</i>	reduced
<i>r,sh</i>	refrigerant in superheated region
<i>r,tp</i>	refrigerant in the two-phase region
<i>sh</i>	superheated
<i>tp</i>	triple point
<i>w</i>	water or melted frost layer
<i>v</i>	vaporization

# **Chapter 1**

## **Introduction**

The development of air conditioning and refrigeration technology is a natural consequence to both pursuing high quality living and working environments for thermal comfort and/or improved productivity, and at the same time addressing the issue of sustainability. Air source heat pump (ASHP) units have been widely used for space cooling in summer and space heating in winter for many years, due to their distinguished advantages of energy saving and environmental protection. However, when an ASHP unit is used for space heating in winter time, frost may be formed on its outdoor coil's surface. Frosting deteriorates its operational performance and energy efficiency, and reduces its output heating capacity, therefore periodic defrosting is necessary.

While defrosting may be realized by a number of methods including compressor shut-down, electric heating, hot gas by-pass, the most widely used standard defrosting method has been reverse cycle defrosting for many years. When a space heating ASHP unit is operated at a reverse cycle defrosting mode, its outdoor coil acts as a condenser and its indoor coil as an evaporator. Hence during defrosting, a space heating ASHP unit can actually cool a space, degrading indoor thermal comfort while consuming electrical energy for melting frost. Therefore, a defrosting period should be controlled to as short as possible. During defrosting, while most melted frost drains off from the surface of a finned outdoor coil in an ASHP unit, the surface may however retain residual water which

must be removed to prevent it from becoming ice when the ASHP unit returns to heating mode. Therefore a complete defrosting process covers both melting frost and drying coil surface. On the other hand, for an outdoor coil used in an ASHP unit, on its refrigerant side, multiple parallel circuits are commonly used for minimized refrigerant pressure loss and enhanced heat transfer efficiency. Furthermore, for saving floor space for installation, usually outdoor coils are vertically installed. However, uneven defrosting over the entire airside surface of a vertical multi-circuit outdoor coil during reverse cycle defrosting operation of ASHP units, which would prolong a defrosting duration and therefore deteriorate defrosting efficiency, has been reported. One of the reasons for uneven defrosting was downwards flowing of melted frost over the surface of a vertically installed multi-circuit outdoor coil due to gravity. Therefore, it is necessary to experimentally and numerically study the negative impacts of downwards flowing of melted frost on defrosting performance for ASHP units, and to develop methods to alleviate the negative effects of uneven defrosting on defrosting performance of an existing ASHP unit.

An extensive literature review on the operating performance of ASHP units under both frosting and defrosting conditions is presented in Chapter 2. A review of the previous related studies on the operating performances of ASHP units under frosting condition is firstly reported, covering mechanisms of frost formation, frost formation on the surfaces of a heat exchanger (or an outdoor coil) in an ASHP unit, as well as numerical studies on the operating performances of ASHP units under frosting conditions. This is followed by reviewing the previous related studies on frost retarding measures and various defrosting

methods for ASHP units. Reviews on both the operating performances of ASHP units during defrosting and various control methods on starting and ending a defrosting operation are also included. A number of important issues where further extensive research work in achieving a better defrosting performance for ASHP units having a multi-circuit outdoor coil have been identified and are summarized. These issues are the expected targets of the project to be carried out and reported in this thesis.

The research proposal covering the aims and objectives, the project title and the methodologies adopted in this project is presented in Chapter 3.

Chapter 4 describes an experimental ASHP setup specially established to facilitate carrying out the research project presented in this thesis. The experimental setup consisted of an experimental ASHP unit, an environmental chamber including one simulated heated indoor space and one simulated frosting outdoor space. A computerized data measuring, logging and control system was built into the experimental setup. A vertically installed three-circuit outdoor coil, which was a key component to the successful study on the negative effects of melted frost flowing downwards along the surface of a multi-circuit outdoor coil in an ASHP unit during reverse cycle defrosting, was specially made as part of the experimental ASHP unit.

Chapter 5 presents an experimental study on the effects of downwards flowing of melted frost due to gravity over the experimental vertical three-circuit outdoor coil surface on the defrosting performance of the experimental ASHP unit during reverse cycle defrosting.

The experimental results and corresponding quantitative analysis revealed the negative effects of allowing melted frost to freely flow downwards due to gravity over the airside surface of the specially-made experimental three-circuit outdoor coil in the experimental ASHP setup on defrosting performance during reverse cycle defrosting: a longer defrosting duration and more energy consumption. In addition, the study results also suggested that the use of water collecting trays between circuits for locally draining away the melted frost before flowing into down circuit(s) was effective in mitigating these negative effects.

To enable further quantitative analysis on the effects of locally draining away the melted frost on reverse cycle defrosting performance in the experimental ASHP unit, a further mathematical modeling study on defrosting performance with local drainage using water collecting trays was considered necessary. Therefore, a modeling study of the defrosting process taking place in the specially-made vertical three-circuit experimental outdoor coil, at two experimental settings of with and without the use of water collecting trays between circuits was carried out and the modeling results are reported in Chapter 6. Two semi-empirical mathematical models, corresponding to the two settings, were developed, and validated by comparing the experimental data reported in Chapter 5 and the predicted data using the models. The validated models could adequately describe the defrosting operation for the experimental ASHP unit with local drainage of the melted frost from its three-circuit outdoor coil.

While the outcomes from the studies reported in Chapters 5 and 6 suggested the effectiveness of locally draining away the melted frost from a vertically installed multi-circuit outdoor coil, for existing ASHP units, however, it is hardly possible to install water collecting trays between circuits. Nonetheless, for existing ASHP units, it is still possible to vary the heat input to each refrigerant circuit through varying refrigerant supply to each circuit. Therefore, in Chapter 7, using one of the developed empirical models reported in Chapter 6, a modeling study on varying heat (via refrigerant flow) supply to each refrigerant circuit in the specially-made experimental three-circuit outdoor coil to alleviate uneven defrosting is reported. Three study cases, with different mechanisms of both varying the openings of modulating valves and introducing other operational changes, were designed and corresponding modeling studies carried out. Modeling results suggested that the best defrosting performances in terms of shortening defrosting durations and reducing defrosting energy use were achieved in the study case of fully closing the modulating valve on the top circuit when its tube surface temperature at the exit of the circuit reached defrosting termination point.

The conclusions of the thesis and the proposed future work are presented in the final Chapter.

## **Chapter 2**

### **Literature Review**

#### **2.1 Introduction**

A heat pump unit is an environmentally friendly and reliable means to maintain thermal comfort level in an indoor space, and can be used for both space heating and cooling. During a cooling season, it transfers heat from the indoor space to a heat sink, in the same way as an air conditioner does. During a heating season, it extracts heat from a heat source such as ambient air, waste water, etc., and delivers the extracted heat energy to a heated indoor space. With the rising cost of energy being at the forefront of world attention, there has been a growing interest in using heat pump technology as a means to save energy, as it offers one of the most practicable solutions to the mitigation of greenhouse emissions. Studies have shown the potentials of using heat pump units to drastically reduce greenhouse gases, in particular CO<sub>2</sub>, emissions, for space heating and for heat generation. From a global point of view, over 90% of the world population resides in the regions where heat pump units can be suitably used for indoor environmental control. Almost for the whole Pacific region including the highly urbanized areas in both China and Japan except during extremely cold winter [Nishimura 2002, Wang et al. 2012a, Mohanraj et al. 2012], the use of heat pump units for space heating in winter is appropriate.

A number of heat sources are available for space heating heat pump units, such as air, and geothermal sources, including underground water and soil, etc. Among these, air and water are the mostly common heat sources for space heating heat pumps. Therefore, air to air heat pump units, air to water heat pump units, water to air heat pump units, water to water heat pump units are commonly used in buildings.

ASHP units are relatively easy and inexpensive to install, and have therefore been the most widely used types of heat pump units for many years. In 1970's the National Bureau of Standards on The Building Science Series in The United State of America conducted extensive tests on residential heat pump units. Their tests revealed two effects that significantly degraded heat pump performance: (1) the 'cycling effect' resulting from the need to establish a dynamic equilibrium during an off-cycle, and (2) the 'frosting effect' on outdoor coils, which increased both heat transfer resistance and air flow passage resistance during heating operation [Kelly and Bean 1977]. Since then, extensive experimental and theoretical investigations have been carried out on ASHP units to study their operating performances under frosting and/or defrosting conditions.

In this Chapter, a review of the previous related studies on the operating performances of ASHP units under frosting conditions is firstly reported, covering mechanisms of frost formation, frost formation on the surfaces of a heat exchanger and/or an outdoor coil in an ASHP unit, as well as numerical studies on the operating performances of ASHP units under frosting conditions. This is followed by reviewing the previous related studies on frost retarding measures and various defrosting methods for ASHP units. Reviews on both

the operating performances of ASHP units during defrosting and various control methods of starting and ending a defrosting operation are also included. A number of important issues where further extensive research work in achieving a better defrosting performance for ASHP units having a multi-circuit outdoor coil have been identified and are summarized.

## **2.2 Operating performances of ASHP units under frosting conditions**

Frost formation on the outdoor coil of a space heating ASHP unit deteriorates its operating performance and energy efficiency. This has attracted a lot of research interests over the past many years. A large number of experimental and theoretical investigations on this subject area have been reported.

### **2.2.1 Mechanisms of frost formation**

The mechanism for frost growth is the diffusion of water onto a cold surface due to the temperature difference between the water vapor of an air stream and that of the surface of a frost layer [Sanders 1974]. The water mass that is transferred to the frost surface creates two distinct effects in the frost layer. A portion of the water vapor is deposited onto the frost layer, thereby contributing to the further frost growth while the remainder of the water vapor diffuses into the frost layer where it changes phase and increases the density of the frost.

Experimental studies on frosting concentrated on frost properties, mechanisms of frost growth and heat transfer in different types of heat exchangers, covering flat plate [Yonko and Sepsy 1967, Jones and Parker 1975, Mao et al. 1999, Cheng and Shiu 2002, Kwon et al. 2006, Wang et al. 2012b], vertical plate [Fossa and Tanda 2002, Lee and Ro 2002], vertical channel [Tanda and Fossa 2006], parallel plates [Lüer and Beer 2000], and horizontal cylinder [Lee and Ro 2001, Mago and Sherif 2003]. A typical frost growth process was described by Hayashi et al. [1977]. An initial one-dimensional crystal growth period was followed by a frost layer growth period. Finally, a so-called frost layer full-growth period concluded a frost growth process. Each growth period was characterized by specific values of frost density which in turn affected the other frost properties, such as thickness, thermal conductivity, etc.

Many researchers have also studied the influences of ambient conditions and the surface temperature of a heat exchanger on frost growth. Nowadays, it is commonly acknowledged that frost formation on the surface of a heat exchanger is associated with the following factors:

- Heat exchanger structure: fin and tube pitches, surface roughness, tube arrangement;
- Fin surface temperature on a heat exchanger;
- Inlet airflow: temperature, humidity and flow rate;
- Frosting duration.

### **2.2.2 Frost formation on the surface of a heat exchanger**

Frost formation on the surface of a heat exchanger is a complex process because of the continuous changes in frost properties and the air-frost interface temperature, with respects to both time and position, during the growth of a frost layer.

The drops in both overall heat transfer coefficient and airside pressure are the two major concerns, because not only they are the two important factors used in evaluating the performance of a heat exchanger, but also frost growth may be quantitatively evaluated by airside pressure drop across the heat exchanger. As reported by Emery and Siegel [1977], 50% - 75% decrease in heat transfer and a substantial increase in pressure drop were caused by frost formation on a compact heat exchanger. Moreover, the effects of ambient air and the geometrical parameters of a heat exchanger on frost growth have been studied comprehensively. Kondepudi and O'Neal [1989] experimentally studied the effects of frost growth on the performances of louvered finned-tube heat exchangers. It was reported that frost growth, pressure drop and heat transfer coefficient increased with air humidity, air velocity and fin density. Thereafter, Kondepudi and O'Neal [1990] compared the performances of finned-tube heat exchangers with that of other heat exchangers having different fin configurations. It was found that the heat exchangers with louvered fins had the best thermal performance under frosting conditions, followed by those with wavy fins and flat fins. Rite and Crawford [1991a, 1991b] investigated the effects of different ambient and operational parameters on frost formation of a finned-tube evaporator used in a domestic refrigerator-freezer. They concluded that frosting rate

was increased at a higher air humidity, or a higher air temperature, or a higher airflow rate and a lower refrigerant evaporating temperature. The overall heat transfer coefficient and the airside pressure drop were also increased with the growth of frost on the evaporator coil surface at a constant airflow rate. Yan et al. [2003a] experimentally investigated the performances of a flat plate finned-tube heat exchanger operated under frosting conditions. Airflow rate remained unchanged during each test. It was shown that frost formation was faster at a lower airflow rate (which contradicted to what Kondepudi and O'Neal [1989], and Rite and Crawford [1991a, 1991b] reported). The results also showed that an increase in air temperature at different ranges of ambient temperature would have different effects on frost growth as evaluated by the pressure drop across the heat exchanger. When the ambient air temperature was increased from 2.5 °C to 5 °C, the amount of frost was increased. However, on the contrary, when it was increased from 5 °C to 7.5 °C, the amount of frost was actually decreased. On the other hand, the performance of a heat exchanger was not significantly affected when its fin pitch was increased. Yan et al. [2005] studied the operating performances of frosted finned-tube heat exchangers with three different types of fins, namely, flat plate fins, one-sided louver fins and re-direction louver fins. As Rite and Crawford [1991a, 1991b] reported, the effects of airflow rate, inlet air relative humidity, refrigerant evaporating temperature and different types of fins on the thermal fluid characteristics of the heat exchangers were discussed. It was also pointed out that the amount of frost formation was the highest when re-directional louver fins was used. Xia et al. [2006] studied the airside thermal-hydraulic performances of a louvered-finned flat-tube heat exchanger under frosting, defrosting and re-frosting conditions. The overall heat transfer coefficient, pressure drop,  $j$  and  $f$  factors

were compared with those of a fold-louvered-fin, micro-channel heat exchanger. Comparison results showed a decrease in the overall heat transfer coefficient and an increase in pressure drop during a frosting process. Both the reduction in airside flow rate and the bridging of louver gaps by frost significantly reduced the airside heat transfer coefficient as frost was accumulated. For heat exchangers with a large fin length, their averaged heat transfer value per unit volume of heat exchanger was much lower. The study results also suggested that the pressure drop across a heat exchanger during re-frosting was largely affected by the water retained on the surface of the heat exchanger.

The previous experimental studies reviewed above described the impacts of ambient parameters, such as inlet air temperature, relative humidity, air velocity and geometrical parameters of a finned-tube heat exchanger, such as fin spacing, fin and tube arrangements on frost growth and the operating performances of the finned-tube heat exchanger.

It appeared that there were different results from previous studies related to frosting. This may well be due to the strong dependence of frost thermal properties on individual experimental conditions. Albeit the differences, almost all of the previous experimental studies gave the similar results regarding the effect of inlet air relative humidity and fin spacing on the performances of a finned-tube heat exchanger under frosting conditions.

These results may be summarized as follows:

- A higher inlet air relative humidity led to a faster frost formation on, and thus a

greater pressure drop across, a heat exchanger;

- The effect of frost growth on the operating performances of a finned-tube heat exchanger was decreased significantly as its fin pitch was increased.

### **2.2.3 Frost formation on the outdoor coil surface of an ASHP unit**

As discussed above, frost formation on the surface of a heat exchanger would deteriorate its operating performances. In an ASHP unit, frost formation and accumulation on its outdoor coil surface would adversely affect its operating parameters, such as evaporating and condensing temperatures, which would in turn affect frost formation. It has been commonly acknowledged that frost formation and accumulation on outdoor coil surface has two main consequences for ASHP units. Firstly, the accumulation of large amounts of frost would deteriorate the heat transfer performance of an outdoor coil by fouling its outside surface since the frost itself had a low thermal conductivity [Stoecker 1957, Machielsen and Kerschbaumer 1989]. With a deteriorated heat transfer performance, the capacity of outdoor coil and thus the ASHP unit would decrease. To meet the specified heating requirements, its evaporating temperature must be decreased, which further reduced system efficiency. Secondly, frost impeded airflow through an outdoor coil, leading to increased fan energy consumption and a reduced airflow rate through the outdoor coil [Stoecker 1957, Barrow 1985, Seker et al. 2004b, Yao et al. 2004].

From the open literature available, much research work has been carried out to investigate the operating performance of ASHP units under frosting conditions. Domingorena and

Ball [1980] investigated the performance of a 3-ton ASHP unit in heating mode. They concluded that under frosting conditions, airflow through the outdoor coil in the ASHP unit was decreased substantially, with concurrent rapid decreases in compressor discharge and suction pressures, and refrigerant flow rate. However, He et al. [2003], Ding et al. [2004a] and Wang et al. [2011a] reported that the discharge temperatures/pressures were increased during frosting, which may be caused by different expansion devices used in experiments. Ameen [1993] pointed out that decreased refrigerant evaporating temperature and decreased refrigerant density at compressor suction during frosting would lead to a reduction in both refrigerant flow rate and compressor power input. Huang et al. [2007] tested the dynamic characteristics of an air-water heat pump unit with a multi-circuit evaporator controlled by a thermostatic expansion valve (TEV) under the frosting/defrosting conditions. The experimental results showed that airflow mal-distribution over its outdoor coil would result in intermittent or unceasing hunting during frosting. Guo et al. [2008] considered that frost growth on an outdoor coil surface of an experimental ASHP unit may be divided into three stages. In the first stage, the performance of the ASHP unit was improved due to the rough surface formed by an initial frost layer, similar to those reported by Stoecker [1957], Hosoda and Uzuhashi [1967], and Huang et al. [2008]. The initial increase in heat transfer was attributed to an increase in inlet air velocity and frost surface roughness, both of which led to an increase in the airside heat transfer coefficient, as well as an increase in heat transfer area since the nuclei of frost crystals acted like small fins. In the second stage, column-shaped ice crystals on frost surface grew in its radial rather than longitudinal direction. Therefore, the rate of increase in frost thickness was reduced or remained

unchanged as frosting went on. The heating capacity and coefficient of performance (COP) of the experimental ASHP unit were only slightly affected by frosting on outdoor coils due to a slow growth in frost thickness. During the third stage, column-shaped ice crystals on frost surface grew in its longitudinal rather than in its radial direction, thus acrose-shaped ice crystals on frost layer were formed, and the growth rate of frost thickness was increased rapidly to about 2.7 - 4.5 times of that in the second stage. Therefore, the operating performances of the ASHP unit deteriorated rapidly, and the decreasing rates of both heating capacity and COP could reach up to a level of several times of these in the second stage. The experimental results suggested that the rapid performance degradation was mainly caused by the morphological variation of frost layer during the third stage.

Many researchers have studied the degree of performance losses under frosting conditions. Miller [1984] studied the effects of frosting on COP and heating capacity of ASHP units under the frosting conditions of 4.4 °C (40 °F) to -6.7 °C (20 °F) with air relative humidity ranging between 60% and 90% using a 3-ton residential ASHP unit, where a single row spiny fin outdoor coil was used. Performance losses due to frosting were the largest when tests were conducted at between 1.7 °C and -1.1 °C (35 °F and 30 °F), with air relative humidity being greater than 70%. Approximately 10% reduction in COP and 15% reduction in heating capacity were reported under an operating condition of 80% and 90% humidity after a 60 minutes-long frosting operation. Based on the experimental study conducted by Votsis [1989], the reductions in the steady state COP varied between 10% and 27%, depending on the ambient conditions and frosting duration.

#### **2.2.4 Numerical studies on the operating performances of ASHP units under frosting conditions**

In addition to experimental studies, numerical studies on the operating performances of ASHP units under frosting conditions are also reported. It is commonly acknowledged that to analyze a frosting process is rather difficult because it is a complex unsteady heat and mass transfer problem, due to the variation in roughness of frost surface in relation to time, a very large number of variables involved, the complex surface geometry of heat exchangers and the thermodynamic properties of humid air and frost. Nonetheless, to better understand the operating characteristics of ASHP units under frosting conditions, researchers have attempted to model mathematically a frosting process.

Martinez-Frias and Aceves [1999] reported a transient frost formation model, and its integration into an existing heat pump model for predicting heat pump operating conditions and COP as a function of environmental conditions. Verma et al. [2002] developed a quasi-steady, finite-volume model for frosting on plain-fin-round-tube heat exchangers. Seker et al. [2004a, 2004b] investigated experimentally and numerically the heat and mass transfer characteristics in finned-tube heat exchangers during frosting. At the same time, Xia et al. [2004] carried out an empirical modeling study on the effects of frost accumulation on louvered-fin micro-channel heat exchangers. One of the outcomes was that bridging louver gaps by frost was a major reason for decreased airside heat transfer and therefore a capacity reduction of an outdoor coil. Meanwhile, Yao et al. [2004] reported a detailed distributed model for the outdoor coil in an ASHP water chiller/heater

unit under frosting condition. The model consisted of a frosting sub-model and a heat exchanger sub-model. Frost formation and its distribution on the surface of the outdoor coil and their impacts on the operational performance of the ASHP water heater/chiller unit were evaluated. Yang et al. [2006b] proposed a mathematical model using correlations for heat transfer coefficients and a water-vapor diffusion equation to predict the thermal performance of a finned-tube heat exchanger under frosting conditions. Tso et al. [2006a, 2006b] developed a general distributed model for two-phase flow of refrigerant coupled with a frosting model for studying the dynamic behaviors of an evaporator. The model could be used to predict liquid dry-out position, evaporator coil wall temperature distribution, the temperature of air flowing onto each row and frost height on each row, etc.

As seen, the operating performances of an ASHP unit could be deteriorated when frost is being formed and accumulated on the surface of its outdoor coil. Therefore, it is necessary to develop both measures to retard the growth of frost on outdoor coil surfaces and suitable defrosting methods to optimize the operating performances of ASHP units in terms of maintaining indoor thermal comfort and reduced energy use for defrosting.

## **2.3 Frost retarding measures and defrosting methods for ASHP units**

As discussed in Section 2.2, frost formation and accumulation on an outdoor coil surface is an undesirable phenomenon. Therefore, studies on developing frost retarding measures and defrosting methods in order to improve the operating performance of ASHP units were undertaken in the past decades. In this Section, a review of previous studies on developing frost retarding measures and defrosting methods is presented.

### **2.3.1 Changing ambient air parameters**

Previous related studies indicated that frost formation on outdoor coil surface of an ASHP unit was closely related to the ambient conditions at which the ASHP unit was operated, such as air temperature, relative humidity, and airflow rate, etc. Therefore, reducing inlet air humidity and/or increasing inlet air temperature for an outdoor coil can be effective in retarding frost formation on outdoor coil surface.

#### *Reducing inlet air humidity*

Through experimental and theoretical investigations, Xia et al. [1998] found that inlet air humidity was a key influencing factor for frosting on a finned tube outdoor coil, while inlet air temperature and inlet airflow rate also had a role to play. Similar results were also obtained in the experimental and simulation studies by Yao and Ma [2003] and Guo et al. [2006]. Kondepudi et al. [1995] experimentally studied frosting characteristics on

an ASHP unit, with and without solid desiccant placed before inlet air to the ASHP unit and found out that the use of desiccant significantly reduced frost formation rate. Wang and Liu [2005] also proposed a method of using solid desiccant to dehumidify the air before it entered an outdoor coil. Using the method, not only was air humidity reduced, but air temperature was increased by absorbing the heat from solid desiccant, so that less frost was formed on outdoor coil surface at a given frosting duration. On the other hand, due to a number of advantages including, low air pressure drop, air cleaning effects and lower regeneration temperature, liquid desiccant was also used for dehumidifying inlet air to ASHP units [Factor and Grossman 1980].

#### Preheating inlet air

Preheating inlet air to an outdoor coil is a simple but effective technique to reduce or prevent frosting. Certain heating elements can be placed in the air duct for inlet air, so that when outdoor air temperature drops below the frosting point, the heating elements are activated. To prevent frost formation, the inlet air temperature upstream of an outdoor coil must always be higher than the frosting point [Rafati Nasr et al. 2014]. Liu et al. [2007] applied heat recovery technique to an ASHP unit, so that exhausted indoor air and ambient air were mixed before entering the outdoor coil of the ASHP unit, prolonging frosting durations and reducing the rate of frost growth. Kwak and Bai [2010] used an electric heater upstream of outdoor coil of an ASHP unit. At the outdoor air condition of below 2 °C / 1 °C (dry-bulb temperature / wet-bulb temperature), the electric heater was turned on for heating the inlet air. It was shown that heating capacity was increased by

38.0% and COP by 57.0% for the ASHP unit, as compared with a conventional heat pump unit. At outdoor air condition of between 2 °C / 1 °C and 4 °C / 2 °C (dry-bulb temperature/wet-bulb temperature), the electric heater was ON/OFF controlled according to the temperature of outdoor coil. Consequently, heating capacity was increased by 9.1% and COP by 71.1%, as compared to a conventional heat pump unit. However, the disadvantage of preheating inlet air in very cold regions was the high energy use for preheating [Kragh et al. 2005]. A comparison of different frost retarding measures showed that preheating inlet air was not economical in regions with long periods of very low outdoor air temperatures [Phillips et al. 1989, Phillips et al. 1992].

#### *Increasing inlet airflow rate to an outdoor coil*

Huang et al. [1998] put forward through an experimental study that by using a variable-speed fan, appropriately increasing airflow could restrain frost growth. After analyzing the factors affecting frost growth using a special model, the method of appropriately increasing inlet airflow rate was recommended for frost retarding. Da Silva et al. [2011] conducted an experimental investigation on frost formation on a finned-tube heat evaporator considering fan characteristics. The experimental results demonstrated that airflow rate reduction was a dominant factor for the drop in evaporator's capacity and suggested that the fan-evaporator should be treated as a coupled system under frosting conditions. Later, to predict the performance of a fin-and-tube outdoor coil considering airflow reduction due to frost growth, Ye and Lee [2013] developed and experimentally validated a numerical model. The results showed that the simulated heat-transfer rates

and the accumulated frost mass agreed well with the experimental data by 7% and 9%, respectively. In practice, for better effect of frost retarding, the above air parameters can be changed altogether. Moreover, the changes in different ambient air parameters would influence differently the rate of frost retarding. An experimental investigation on the adverse effect of frost formation on a microchannel evaporator was undertaken by Moallem et al. [2013], and the experimental results indicated that air humidity impacted significantly on the rate of frost growth while air face velocity of the evaporator appeared to impact less significantly on the rate of frost growth.

### **2.3.2 Optimizing the structure of an outdoor coil**

A number of methods to retard or prevent frosting on outdoor coils in ASHP units have been developed through optimizing the structure of an outdoor coil so as to alleviate the negative impact of frosting on the operating performances of ASHP units. These methods are discussed as follows.

#### *Fin and tube pitches adjustment*

The use of an outdoor coil having wider fin spacing was recommended to slow down frost growth by Young [1980] and Watters et al. [2002]. Yan et al. [2003] conducted an experimental study on the operating performances of flat finned-tube heat exchangers under frosting conditions. Heat exchangers of single and multiple tube row(s) were tested to show the effects of various parameters on their heat transfer performances.

Experimental results showed that heat transfer rate and air pressure drop were not affected significantly by the fin pitch provided the fin spacing was large. Sommers and Jacobi [2005] found that at air-side Reynolds numbers between 500 and 1300, the air-side thermal resistance was reduced by 35% - 42% when vortex generation was used by the way of adjusting the fin structure. Therefore, a frosting process was retarded. Yang et al. [2006a] proposed optimal values of design parameters for a fin-tube heat exchanger of a household refrigerator under frosting condition to improve its thermal performance and extend its operating time, so as to retard the frosting. After optimization, the average heat transfer rate and operating time were increased by up to 6.3% and 12.9%, respectively. Lee et al. [2010] measured and analyzed the air-side heat transfer characteristics of flat finned-tube heat exchangers at different fin pitches, numbers of tube rows and tube alignment under frosting conditions. The results showed that fin pitch and staggered tube alignment had greater effects on airflow reduction.

### *Fin types*

Kondepudi and O'Neal [1990] experimentally studied the effect of different fin types (e.g. flat, wavy and louvered) on the operating performances of finned-tube heat exchangers under frosting conditions. The experimental results showed that the louvered fin type had the best thermal performance despite the presence of frost, followed by the wavy fin type and the flat fin. Yan et al. [2005] experimentally investigated the operating performances of frosted finned-tube heat exchanger with flat plate fins, one-sided louver fins and re-direction louver fins. The frost formation rate and air pressure drop rate were increased

as the relative humidity of inlet air was increased or as inlet airflow rate and the evaporating temperature of refrigerant were decreased. The amount of frost formation was the largest for heat exchangers with re-direction louver fins when other conditions being the same. Zhang and Hrnjak [2009] experimentally studied the operating performances of three types of heat exchangers with louver fin geometry under dry, wet and frost conditions: (1) parallel flow parallel fin with extruded flat tubes, (2) parallel flow serpentine fin with extruded flat tubes and (3) round tube wave plate fin. At the frosting condition, the heat exchanger with round tube wave plate fin can be used for the longest time due to its largest surface area. The increase in air-side pressure drop for the parallel flow parallel fin with extruded flat tubes heat exchanger was the lowest. Dong et al. [2013] experimentally compared the effect of using different fin types (i.e., flat, wavy and louver fins) in an outdoor coil on the periodic frosting and defrosting performances of a residential ASHP unit. The experimental results showed that the outdoor coil with flat fin demonstrated the best thermal performance in the periodic frosting/defrosting cycles of the ASHP unit, followed by the outdoor coils with wavy and louver fins, respectively.

#### *Fin surface treatment*

There were reported studies on the influence of surface treatment of outdoor coils on frosting and defrosting performances. Kuwahara et al. [1986] applied a surface-active agent to the fin surfaces of an outdoor coil to reduce water retention as the contact angle between water and coil's surface became small. Okoroafor and Newborough [2000]

found that frost growth on cold surfaces exposed to warm humid air streams could be reduced significantly by means of cross linked hydrophilic polymeric coatings. Finally, the frost thickness was decreased in the range of 10% - 30% when compared to using an uncoated metallic surface. Wu and Webb [2001] investigated the possibility of causing frost to release from a cold surface, where both hydrophilic and hydrophobic surfaces were examined. Experimental results indicated that if an outdoor coil must be operated under either freezing or non-freezing conditions, a hydrophilic coating was preferable.

Furthermore, Jhee et al. [2002] investigated the effects of treating heat exchanger surface on the frosting/defrosting behavior for a fin-tube heat exchanger experimentally. The study results revealed that a heat exchanger with a hydrophobic surface treatment was more effective in terms of higher defrosting efficiency and shortened defrosting duration, than that with a hydrophilic surface. Liu et al. [2006] reported that the use of surface hydrophilic polymer paint could retard frost formation by up to 3 hours and reduce frost thickness by at least 40%, and the frost layer formed on the coated surface was loose and could be easily removed. Cai et al. [2011] experimentally studied the frosting conditions on three kinds of surfaces: normal copper, hydrophobic coating (car wax coating) and hygroscopic coating (glycerol coating). The experimental results showed that frost growth could be restrained by using both hydrophobic coating and hygroscopic coating at the initial stage of its formation, and the thickness of hydrophilic coating was directly proportional to the frosting retarding effect.

Hence, optimizing the structure of outdoor coils by the way of adjusting fin space, using different fin types and fin surface treatment could retard frost effectively. However, this would increase the first cost of an ASHP unit.

### **2.3.3 Other frost retarding measures**

Vapor-injection technique has been marketed for use in room air conditioners since 1979 [Umezu and Suma 1984, Winandy and Lebrun 2002]. However, its applications to air conditioning received more attentions only recently, as the technique can help retard frosting for ASHP units in cold climates. Zhnder et al. [2002] tested an air-water vapor-injection heat pump, and an increase in heat output of 28% and a COP improvement of 15% compared to the tests without injection were reported at an inlet air temperature of -7 °C. Shao et al. [2002] concluded that a vapor-injection heat pump could provide enough heating capacity at an outdoor temperature of -15 °C ~ -20 °C. Nguyen et al. [2007] evaluated the thermal performances of a flash tank vapor injection (FTVI) cycle and that of a sub-cooler vapor injection (SCVI) cycle using R-407C. The heating COPs of the FTVI and the SCVI cycles were 24% and 10% higher than those of a single-stage cycle, respectively, at an ambient temperature of -7 °C. Bertsch and Groll [2008] tested a specially designed R410A air-source two-stage heat pump unit, and a heating COP of 2.1 was observed at an ambient temperature of -30 °C. Ma and Zhao [2008] carried out series of experiments on an ASHP unit with a flash-tank coupled with scroll compressor at an ambient temperature of -25 °C. Wang et al. [2009] found that a maximum COP improvement of 23% for a two-stage heat pump system was achieved at an ambient

temperature of  $-17.8\text{ }^{\circ}\text{C}$ . Heo et al. [2010] reported the COP and heating capacity of an injection cycle were enhanced by 10% and 25%, respectively, at an ambient temperature of  $-15\text{ }^{\circ}\text{C}$ .

In Japan, Aihara et al. [1997] reported the heat transfer and defrosting characteristics of a horizontal single-row array of cooled tubes immersed in a gas-solid fluidized bed. The fluidized bed produced gas-solid particle impinging jets that effectively removed frost layers on tube surface. It has been verified that frost-free running of the cooled tubes was possible under the conditions of inlet air temperature of  $-7\text{ }^{\circ}\text{C}$ , inlet air relative humidity of 80% and tube surface temperature of  $-17\text{ }^{\circ}\text{C}$ . The local contact frequency of particles onto tube surface was measured by an optical sensing system and the defrosting mechanism of impinging solid particles observed in detail with a visualization technique. Masaji [1998] developed an ASHP unit with a kerosene fired burner placed either in its indoor unit or under its outdoor coil to improve its performance at low ambient temperatures. The ASHP unit using a scroll compressor that varied the rotational speed according to the load and had liquid injected inlets was proven to work effectively either in hot summers or cold winters.

Mei et al. [2002] reported that the heating capacity of an ASHP unit could be increased, and the frost accumulation on its outdoor coil retarded by heating up the liquid refrigerant in its accumulator. By heating liquid refrigerant, the frequency of defrosting cycles was shown to be reduced by a factor of 5 in Knoxville, Tennessee, USA, and indoor supply air temperature raised by  $2 - 3\text{ }^{\circ}\text{C}$  because of the increased compressor suction pressure.

Thereafter, Byun et al. [2008] presented a method to delay frost formation in an ASHP unit by injecting a portion of high temperature refrigerant from compressor discharge into the inlet to its outdoor coil. The feasibility of using hot gas by-pass to delay frost formation was investigated experimentally and its performance compared with that of a normal 1.12 kW capacity ASHP unit without defrosting control. It was found that the use of hot gas by-pass was useful for retarding the formation and growth of frost on outdoor coil surface. The best performance was shown under a by-pass refrigerant flow rate of 0.2 kg/min (20% of the total refrigerant flow rate). During 210 min of unit's operation, the use of hot gas by-pass improved the COP and heating capacity of the ASHP unit by an average of 8.5% and 5.7%, respectively, compared to a normal ASHP unit.

Li et al. [2011] proposed a new frost-free ASHP system which was made of three subsystems: a compression refrigeration subsystem, a solution endothermic subsystem and a solution regeneration subsystem. In this new system, heat extracting process from environment included two steps: (1) extracting heat from the ambient and then to the solution; (2) releasing heat to its evaporator from the solution to avoid frosting on evaporator surface. At the same time, a theoretical model was established to analyze the operating performances of the system. The experimental results indicated that the novel system could operate more efficiently than a conventional ASHP unit in winter, and there was no need to periodically defrost. Chen et al. [2012] developed a frost-free system to be operated at below 0 °C in winter, and Ding et al. [2004a, 2004b] proposed using a by-pass solenoid valve in an ASHP unit to by-pass its thermal expansion valve when it was operating at reverse cycle defrosting mode. A new sub-cooling system employing a scroll

compressor with supplementary injections in an ASHP unit was also proposed and the relevant dynamic performances tested.

In addition, ultrasonic technology was used for retarding frost growth. Li et al. [2010] reported that the frost formation process on a flat surface was remarkably restrained due to the effect of ultrasound. Frost coverage was all less than 52% with the effect of ultrasound, compared to more than 65% without the effect of ultrasound. Wang et al. [2012c] reported that a basic ice layer on fins could not be removed with ultrasonic vibrations, but frost crystals and frost branches on the ice layer could be fractured and removed effectively. It was believed that the mechanism of ultrasonic frost suppression was mainly attributed to high frequency ultrasonic mechanical vibrations that could break up frost crystals and frost layers, then frost would fall off by gravity, but not to ultrasonic cavitation effect or heat effect.

From the above, it can be seen that the use of frost retarding measures could help prolong a frosting operation, and thus improve the COP of an ASHP unit.

#### **2.3.4 Defrosting methods**

As discussed earlier, the presence of frost on tube surface of the outdoor coil in an ASHP unit would deteriorate its operating performance, energy efficiency, reliability and life span. While the use of frost retarding measures can help delay frost formation or growth, these measures can be expensive or consume additional energy, and frost that is present

after delaying would have to be removed. Therefore, periodic defrosting becomes necessary for guaranteeing the satisfactory operation of ASHP units. In this Section, defrosting methods reviewed are all based on the assumption that no frost retarding measures are implemented during frosting.

Generally speaking, there are two types of defrosting methods. One is mechanical based by removing the frost on outdoor coil surface without any heat supplied, and the other thermal based by melting frost on outdoor coil surface using heat. For the former, Yan et al. [2003b] and Li et al. [2010] developed experimentally a ultrasonic defrosting technology. Fei and Mao [2000] proposed a new defrosting method by which frost was blown away by using compressed air. The study results indicated that the new method can remove frost in a timely manner. Therefore, this method could be applied to where compressed air was available.

Since there were a number of problems associated with the use of mechanical based defrosting method, such as complicated system and additional energy use to generate mechanical force, high first cost, etc. Therefore, less attention was paid to developing the mechanical-based defrosting methods, and more attentions were paid to thermal-based defrosting methods, including: (1) compressor shut-down defrosting, (2) electric heating defrosting, (3) hot water spray defrosting, (4) hot gas by-pass defrosting, and (5) reverse cycle defrosting.

Firstly, for compressor shut-down defrosting, ambient air is used as the heat source of defrosting. Therefore, it is normally applied to where ambient air temperature is not lower than 1 °C. When defrosting is needed, the compressor is shut down but outdoor coil air fan continues to move the ambient air at  $> 1$  °C to pass through the outdoor coil to melt the frost. Ameen et al. [1993] experimentally investigated the defrosting for a heat-pump evaporator using warm air under controlled conditions in an air-conditioned wind tunnel. The study was initiated to explore the possibility of defrosting an evaporator under frosting conditions where the heat pump unit was required to continuously provide heating. In this experimental study, a four-row straight-fin heat exchanger was used, supported from below by a load transducer to measure its weight variation during both frost accumulation and removal. The experimental results suggested that when using warm air defrosting, the rate of frost melting was influenced by air temperature, relative humidity and velocity, and the removal of residual water produced during defrosting from the evaporator surfaces was dependent on air velocity.

Secondly, electric heating defrosting usually involves electrically heating up the surface of an outdoor coil to melt off frost. For example, Kim et al. [2006], Bansal et al. [2010] and Ozkan et al. [2012] conducted comparative studies of different types of defrosting heaters applied to side-by-side refrigerators. However, no information on the frosting conditions was provided. Thereafter, Melo et al. [2013] carried out a series of experiments through a purposely-built testing apparatus. It was found that the defrosting efficiency of three types of heaters was practically the same at each operating mode. The highest efficiency of approximately 48% was obtained with a glass tube heater. A calrod heater

seemed to be mostly appropriate not only because of its efficiency, which was compatible with that of the other heaters, but also due to its low cost and easy installation. Meanwhile, Yin et al. [2012] proposed a new cold storage method based on air by-pass circulation and electric heater. Five practical cases of this new method with different defrosting heaters and air circulation modes were comparatively and experimentally studied. Experimental results showed that when using the new method, defrosting duration was shortened by 62.1%, defrosting energy consumption reduced by 61.0%, and storage temperature fluctuation decreased by 70.1%. In addition, the defrosting efficiency was increased to 77.6%, which was 2.93 times of that by using a traditional electric heating defrosting method. However, additional electrical energy was required to melt frost and an ASHP unit was out of operation during defrosting.

Thirdly, hot water spray defrosting method can be applied to where hot water for defrosting is available. However, only a limited reported studies can be identified including a patent from Tanker [1941], and Abdel-Wahed's experimental study [1983] on applying hot water spray defrosting method to a horizontal flat plate surface.

Fourthly, hot gas by-pass defrosting is largely applied to industrial ASHP units. The superheated refrigerant vapor discharged from compressor is directed into an evaporator, or outdoor coil, by-passing a condenser and an expansion device. Most likely latent heat of condensation of refrigerant vapor is used as heat source, however, sensible heat of highly superheated refrigerant vapor may also be used [Liang et al. 2005]. For most hot gas by-pass defrosting applications, hot gas was injected through a relief valve into the

suction line downstream of a suction solenoid valve which was closed during defrosting. The energy for defrosting mainly came from the compressor power consumption, so defrosting speed was slow and energy consumption was high. Moreover, it was easy for compressor to suck in liquid during a hot gas by-pass defrosting process [Krakow and Lin 1996]. On the basis of hot gas by-pass defrosting, Fu et al. [2009] divided an outdoor heat exchanger into two parts, a front part and a rear part, which were used as an evaporator and a condenser respectively during defrosting. The experimental results indicated that energy was used more efficiently, and thus defrosting duration was shorter and defrosting loss were less, than those of using reverse cycle defrosting. A novel dual hot gas by-pass defrosting method was developed to remove frost from the outdoor coil of an air-to-air heat pump [Choi et al. 2011]. Experimental results showed that the proposed method could overcome the main disadvantages for reverse cycle defrosting and hot gas by-pass defrosting, and demonstrated excellent defrosting performance for an ASHP unit during a defrosting operation. However, during a hot gas by-pass defrosting operation, defrosting duration is always very long, due to the fact that energy use for defrosting comes from the power input to the compressor, and quite amount of energy was consumed when the hot gas passing through a receiver and other system components. Moreover, the continuous decrease in discharge temperature and degree of superheat during defrosting impacted badly on the safety of compressor. Therefore, the hot gas by-pass defrosting method was limited in applications.

Lastly, for reverse cycle defrosting, the normal operation cycle during heating for an ASHP unit is reversed by using a four-way valve. During defrosting, hot gas is pumped

into an outdoor coil to melt off the frost. When the frost is melted and drained away from the coil, the ASHP unit returns to heating operation. Besides requiring a four-way valve, reverse cycle defrosting does not need more complicated or space demanding components. On the other hand, the energy used for reverse cycle defrosting comes from three sources: the power input to the compressor, the power input to the indoor air fan and the thermal energy from indoor air. The sufficient energy sources make the duration of a reverse cycle defrosting operation short. In fact, reverse cycle defrosting has been the most widely used standard defrosting method for many years, which will be further discussed in detail in Section 2.4.

#### **2.4 Operating performance of ASHP units during reverse cycle defrosting**

Currently, the most widely used standard defrosting method is reverse cycle defrosting [Ding et al. 2004a, Byun et al. 2006]. Over the years, a large number of studies have been carried out and the reviews of these studies are presented in this Section.

During a reverse cycle defrosting operation, for an ASHP unit, while most melted frost drains off from its outdoor coil's surface, some may however retain on the surface of the finned coil, which should be removed to prevent it from becoming ice when the ASHP unit returns to heating mode. Therefore, a complete defrosting process covers both melting frost and drying coil surface. As a matter of fact, not only a great deal of energy for melting frost and vaporizing melted frost off outdoor coil surface is consumed, but also the occupants' thermal comfort may be adversely affected because no heating is

provided during defrosting [Qu et al. 2010]. Therefore, shortening a defrosting period should be one of the defrosting control purposes for ASHP units. For example, Chinese Standard GB/T 7725-2004 specifies that the defrosting duration for an ASHP unit should not exceed 20% of its total working hours. On the other hand, it is noted that the research related to reverse cycle defrosting operation for ASHP units is relatively less seen comparing with that related to frosting [Yao et al. 2004]. This is because that reverse cycle defrosting is a complex process involving spatial and time variations of the temperatures of refrigerant, metal and air, as well as many other indeterminate factors resulted from transient cycling which may last for only a few minutes [Krakow et al. 1993a]. Also, an energy balance on the airside of an outdoor coil is complex due to the fact that the energy extracted from hot refrigerant gas is utilized in several different ways, e.g., heating up the evaporator coil metal surfaces, melting the frost, re-evaporating the melted frost and direct transfer to ambient air by natural convection.

#### **2.4.1 Experimental studies on ASHP units during reverse cycle defrosting**

When an ASHP unit is operated at reverse cycle defrosting mode, its outdoor coil acts as a condenser and its indoor coil as an evaporator. Also, during defrosting, the indoor air fan in an ASHP unit is normally switched off to avoid blowing cold air directly to a heated indoor space, affecting thermal comfort of occupants. Hence, the energy available from the indoor coil is basically that stored in coil metal but there is an insignificant amount of energy available from indoor air because of a negligibly small airside convective heat coefficient resulted from de-energized indoor air fan during defrosting. When there is no

more heat to be absorbed from coil metal (i.e., when coil temperature drops to a sufficiently low level), evaporating temperature, as well as the evaporating pressure, will significantly drop. Consequently, low-pressure cut-off or wet compression may take place, which may cause the ASHP unit to shut down [Miller 1987, Kondepudi and O'Neal 1990, 1991] and possibly damage the compressor. In this case, the energy to melt frost mainly comes from that stored in indoor coil metal and the input work to compressor but is not sufficient for quick defrosting. Insufficient heat available during defrosting is problematic as far as reverse cycle defrosting is concerned, with which a number of operational problems during defrosting for ASHP units are associated. These include a prolonged defrosting time and the risk of having a lower air temperature inside a heated space without heating being provided during defrosting, etc.

O'Neal et al. [1989] experimentally investigated the transient reverse cycle defrosting performance of a nominal 3-ton residential ASHP unit using a TEV. It was found that the accumulator of the ASHP unit and the TEV impacted significantly on the system's dynamic responses. The liquid levels in the accumulator varied during defrosting. The TEV appeared to work well as a defrosting expansion device because of its ability to vary orifice size in response to changing system operating conditions. On the other hand, the cycle performances during reverse cycle defrosting for ASHP units with either a scroll or a reciprocating compressor were experimentally studied and compared, in accordance with American National Standard Institute/American Society of Heating, Refrigerating and Air-conditioning Engineers (ANSI/ASHRAE) Standard 116-1983 [Payne and O'Neal 1995]. Ding et al. [2004a] utilized a solenoid valve to by-pass the TEV on an air-to-water

heat pump during the whole defrosting process to relieve shutdown caused by the low-pressure protection and to decrease the defrosting time. Huang et al. [2004] focused on the dynamic characteristics during the defrosting period, and adopted the fan pre-start method to avoid shutting down the heat pump due to high-pressure. The study results suggested that an ASHP unit using scroll compressor achieved a slightly higher integrated cyclic COP and a lower compressor discharge temperature during frosting and defrosting. Based on the tests on an air-to-water heat pump, Huang et al. [2007] pointed out that a ‘critical point’ existed during a defrosting cycle, after which operational parameters such as refrigerant temperature at the outdoor coil outlet, evaporating temperature and degree of superheat increased quickly. This was because the modes of heat transfer on the airside of the outdoor coil changed from phase-change of frost melting to air natural convection. Chen et al. [2009] investigated the effects of outdoor air parameters on reverse cycle defrosting characteristics for an ASHP unit. The experimental results showed that with an increase in outdoor air relative humidity at a constant air temperature and a constant air velocity, the total power consumption, defrosting duration and the heat taken away from an indoor space during defrosting were decreased linearly.

#### **2.4.2 Performance improvements for ASHP units during reverse cycle defrosting**

As discussed previously, defrosting an ASHP unit consumes energy and causes undesirable fluctuations of indoor air temperature and other operational problems, such as low-pressure cut-off or wet compression. Therefore, extensive research work has been carried out to improve the performance of reverse cycle defrosting of ASHP units. Young [1980] suggested that high refrigerant mass flow could be maintained by a properly sized separate defrost expansion by-pass device for a shorter defrosting duration. It was further found that an outdoor unit having a 45° slanted coil could drain off 50% more melted frost than that having a horizontal coil while still permitting a snow sheltered design and an upward directed exhaust. Fans pre-start with reverse cycle defrosting on both air to air and air to water heat pump units were found to be effective in protecting the units from being turned off owing to discharge pressure protection [Anand et al. 1989, Huang et al. 2004]. Nutter et al. [1996] studied the effects of an accumulator in suction line on frosting/defrosting performance of an ASHP unit utilizing an orifice expansion device in heating (frosting) mode and TEV in cooling (defrosting) mode. The results showed that the removal of the accumulator produced a 10% reduction in defrosting duration but a 25% reduction in the integrated cyclic COP. Wang et al. [2008] developed a new heat pump defrosting method using a refrigerant charge compensator instead of an accumulator. The test results showed an increase in refrigerant flow rate and higher suction and discharge pressures of compressor during defrosting. Liang et al. [2010] proposed a sensible heat defrosting method with a self-organizing fuzzy control system. The results of comparative tests showed that the sensible heat defrosting method could

avoid adverse shock and ‘oil rush’, which were commonly seen in conventional reverse cycle defrosting operations. Choi et al. [2011] reported a novel dual hot gas bypass defrosting method to remove frost from the outdoor coil of an air-to-air heat pump. The proposed method adopted two bypass lines of hot gas from the compressor: one was connected to the inlet of the outdoor coil, and the other to the outlet of the outdoor coil. The experimental study results revealed that, as compared to the conventional reverse cycle defrosting, the new method was 13% better on energy efficiency, with however slightly longer (126%) defrosting duration.

On the other hand, thermal energy storage (TES) technology has played an important role in energy management, and has been used extensively in building HVAC systems. When compared to sensible heat energy storage, latent heat energy storage requires a smaller amount of mass of storage medium for a given amount of energy to be stored. A further advantage of latent heat storage is that heat storage and delivery normally occur over a fairly narrow temperature range (the transition zone) which corresponds to the phase transition temperature of a phase change material (PCM). The operating temperature span of latent heat storage systems can, therefore, be quite narrow [Paris et al. 1993]. Based on these advantages, the technology of latent heat thermal energy storage has been developed rapidly over recent decades. Moreover, the compactness of a PCM storage system allows a greater flexibility in choosing a location for installing a storage system.

In general, PCMs can be classified into organic type such as paraffin, and inorganic type such as hydrated salts and binary mixture. Inorganic PCMs have been widely used

currently because of their high thermal conductivity and excellent chemical stability. The selection criteria of PCMs were previously discussed [Sharma and Sagara 2005, Pasupathy et al. 2008]. TES for HVAC applications can involve storage at various temperatures associated with heating and cooling processes [ASHRAE 2007]. For example, high temperature storage is typically associated with the use of solar energy collectors [Rabin et al. 1995, Esen and Ayhan 1996, Bajnoczy et al. 1999], waste heat utilization [Gu et al. 2004], heat pump applications, and low temperature storage with the use of ice storage system [Masoero 1984, Matsuki et al. 1999, Ismail et al. 2001] and free cooling [Vakilaltojjar and Saman 2001, Arkar et al. 2007], etc.

To improve the reverse cycle defrosting performance of ASHP units, the technologies of TES and PCM found their applications in recently years because of their energy storage advantages. Chen et al. [2006] used DX40 as a thermal storage material, which was of inorganic type with a melting point of 42 - 44 °C, as a heat source for defrosting. Hu et al. [2011] used  $\text{CaCl}_2 \cdot 6\text{H}_2\text{O}$  as PCM, which was also of inorganic type with a melting point of 29 °C in their experimental study on defrosting performance for an experimental ASHP unit. The experimental results suggested that the use of PCM was able to help shorten the defrosting time by 3 min or 38%, and minimize the risk of shutting down the ASHP unit due to low suction pressure through increasing compressor's suction pressure by about 200 kPa, when compared to the use of the traditional standard reverse cycle hot gas defrosting method. In addition, the mean indoor coil surface temperature during defrosting was about 25 K higher than that when the traditional standard reverse cycle hot gas defrosting method was used. Furthermore, Qu et al. [2010] reported that using a

TES based defrosting method could help achieve improved indoor thermal comfort, with a shorter defrosting period and a higher indoor supply air temperature during reverse cycle defrosting.

### **2.4.3 Studies on multi-circuit outdoor coil of ASHP units during reverse cycle defrosting**

For an outdoor coil used in an ASHP unit, on its refrigerant side, multiple parallel circuits are commonly used for minimized refrigerant pressure drop and enhanced heat transfer efficiency. On its airside, however, there is usually no segmentation corresponding to the number of refrigerant circuits. Aganda et al. [2000a] compared the predicted and experimental heat transfer performance of a finned tube outdoor coil, which is a single-circuit, multi-pass finned tube heat exchanger. In addition, Aganda et al. [2000b] found that airflow mal-distribution reduced the performance of an evaporator circuit, as compared to uniform air flow passing through the outdoor coil. Circuits at the edges of the coil, where air velocity was low, did not perform well. With refrigerant flow controlled by one thermostatic expansion valve, the worst performing circuit affected the performance of the whole outdoor coil, by as much as 35%. Kim et al. [2009a] presented a hybrid-individual degree of superheat control method for refrigerant flow balancing in a multi-circuit evaporator: upstream versus downstream flow control. Small balancing valves were used in each circuit along with a primary expansion device to control the overall degree of superheat. A simulation model was also developed to consider evaporator flow mal-distributions for a 10.55 kW residential R410A heat pump and then

validated by comparing predicted with measured results. Simulation results showed that there were significant benefits in controlling degree of superheat at each circuit of the evaporator through the hybrid-individual control method. Furthermore, the upstream refrigerant flow control consistently outperformed the downstream refrigerant flow control, and recovered most of the loss in cooling capacity and COP due to non-uniform airflow distribution. Later, Kim et al. [2009b] utilized the model to further evaluate the effects of uneven air and refrigerant flow distributions and the benefits of upstream hybrid control in response to these effects.

While multi-circuit outdoor coils have been commonly employed in ASHP units, very limited reported studies on defrosting characteristics over the surface of multi-circuit outdoor coils may be identified in the open literature. For a multi-circuit outdoor coil in an ASHP unit, uneven defrosting over the outdoor coil surface was reported. For example, the outdoor coil in an experimental residential ASHP unit, as reported by O'Neal et al. [1989], had four parallel refrigerant circuits. Noticeable differences in the surface temperatures at the exit of the four circuits during a reverse cycle defrosting operation were reported. The rates of increase in the surface temperatures at the exits of the up circuit(s) were much quicker than that of the down circuit(s). Termination of defrost was triggered when the surface temperature at the exit of the lowest circuit reached 18.3 °C (65 °F). However at the same time, the surface temperature at the exit of the top circuit already reached about 37.7 °C (100 °F). Similar results can also be seen in the experimental study on an outdoor coil having six rows and fourteen circuits during hot gas by-pass defrosting conducted by Stoecker et al. [1983]. Furthermore, in the study

reported by Wang et al. [2008], it was shown that at six minutes into defrosting, the surfaces of down refrigerant circuit(s) in a multi-circuit outdoor coil were still covered by frost while that of up circuits were already free of frost.

Although other factors may lead to uneven defrosting on the surface of a vertical multi-circuit outdoor coil, the fact that melted frost flowing downwards due to gravity was considered as a major cause for uneven defrosting. However, few studies on the effects of downwards flowing of melted frost over multi-circuit outdoor coil surface on reverse cycle defrosting performance may be identified in open literature, except that Qu et al. [2012a] suggested that downwards flowing of melted frost over a multi-circuit outdoor coil in an ASHP unit during reverse cycle defrosting could affect the defrosting performance, by using more energy for defrosting and prolonging a defrosting process. This was because the downwards flowing of melted frost helped form or reinforce a water layer between the frost and the coil surface, which introduced a thermal resistance [Payne and O'Neal 1995], and thus reduced the heat transfer between them. However, no detailed quantitative analysis of these negative effects was carried out and thus reported.

#### **2.4.4 Numerical studies on the operating performances of ASHP units during reverse cycle defrosting**

One key feature when modeling a defrosting process is that it is at least somewhat stochastic. During a defrosting operation, the frost on the surface of an outdoor coil will not necessarily be melted uniformly throughout the surface. The frost over some parts of the coil surface remains attached to the coil surfaces until it is completely melted and sublimated while the frost at other locations may be partially melted, and then detaches from the coil surface, falling down to the coil surface at a lower level or to a drainage tray.

From the open literature available, modeling a defrosting process has attracted lots of research attentions. Early modeling work focused mainly on outdoor coils of simple geometry, such as finite slabs [Goodman and Shea 1960], horizontal flat plate [Abdel-Wahed et al. 1983], or flat plate cooler [Sherif and Sherif 1992]. Thereafter, a number of studies on modeling a defrosting process in ASHP units were carried out. Noticeably, Krakow et al. [1992a, 1992b] developed a reverse cycle defrosting model for an outdoor coil. In this model, the process of frost melting on the surface of an outdoor coil was idealized by subdividing it into four stages: pre-heating, melting, vaporizing and dry heating, as illustrated in Fig. 2.1. A number of heat and mass transfer parameters required for simulating defrosting performance, e.g., the maximum mass of surface water, free-convection air film conductance, air/water film conductance and surface water vaporization coefficient, were however experimentally determined.

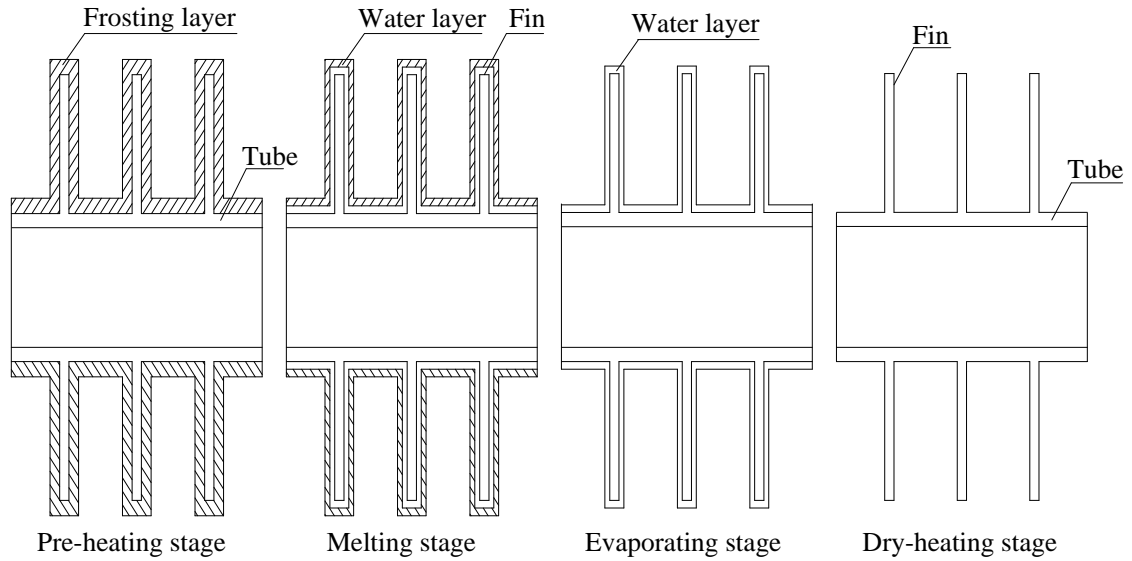


Fig. 2.1 Schematic diagram illustrating reverse cycle defrosting of an outdoor coil cell  
[Krakow et al. 1992a, 1992b]

Later, Krakow et al. [1993a, 1993b] presented an idealized reverse cycle defrosting model for an ASHP unit with a receiver. On the basis of the above mentioned model, a validated defrosting model for an ASHP unit using capillary tube was developed by Liu et al. [2003]. Distributed modeling was used for both evaporator and condenser because of their importance during reverse cycle defrosting. Sherif and Hertz [1998] presented a semi-empirical model for electric defrosting of a cylindrical coil cooler. In this model, it was assumed that the heat provided by an electric-heater was taken away by both frost layer and refrigerant vapor, but the ratio between the two was arbitrarily chosen. Al-Mutawa and Sherif [1998a, 1998b] developed an analytical model of a cylindrical coil cooler to predict the evaporation, sublimation and melting rates during hot gas by-pass defrosting. In this model, a moving boundary technique was used and the defrosting process was divided into two stages, pre-melting and melting. Alebrahim and Sherif [2002] reported

an electric defrosting model for a finned-tube outdoor coil using the enthalpy method to predict defrosting duration and frost surface temperature profiles. Hoffenbecker et al. [2005] reported the development of a transient model for predicting the heat and mass transfer during a hot gas by-pass defrosting process on an industrial air-cooling evaporator. The model focused on both the energy distribution during defrosting and the optimization of hot gas temperature. Dopazo et al. [2010] developed a detailed transient simulation model of hot gas by-pass defrosting in an air-cooled evaporator. In this model, a defrosting process was subdivided into six stages: preheating, tube frost melting, fin frost melting, air presence, retained water vaporizing and dry-heating. Although the above mentioned defrosting models were developed and used in studying defrosting performance, none of them in fact considered the effects of downwards flowing of the melted frost due to gravity along the surface of an outdoor coil on defrosting performance, by either assuming a stable water layer or no water retention on coil surface.

Recently, Qu et al. [2012b] reported on a modeling analysis where a semi-empirical model for the defrosting on the airside of a four-circuit outdoor coil in an ASHP unit was developed. In this model, the negative effects of melted frost on defrosting performance were quantitatively studied. It was further predicted that if the melted frost could be drained away locally, the defrosting efficiency for the ASHP unit could be increased by up to 18.3%. Similar results were also reported by Dong et al. [2012] in a study on the energy consumptions for vaporizing the melted frost and heating ambient air during reverse cycle defrosting in an ASHP unit. However, in Qu's model [Qu et al. 2012b], the energy used to heat the metal in an outdoor coil during reverse cycle defrosting was

neglected. In fact, this part of energy consumption accounted for as much as 16.5% of the total defrosting energy use during reverse cycle defrosting [Dong et al. 2012].

## **2.5 Control methods to start and end a defrosting operation**

As mentioned, frosting would seriously affect the operating performance of an ASHP unit by reducing its COP and output heating capacity. Hence, periodic defrosting is necessary. However, proper defrosting initiation and termination control can impact energy efficiency and system reliability [Votsis et al. 1989, Hewitt and Huang 2008], relevant research work on selecting suitable control parameters for defrost initiation and termination has therefore been carried out and reported.

### **2.5.1 Defrosting initiation**

There are mainly two types of control method to start a defrosting operation: time-based defrosting and demand defrosting.

For the former, defrosting in ASHP unit is controlled by a pre-set time cycle. For the reasons of simplicity and low-cost, many of the earlier ASHP units employed a simple timer to control a defrosting cycle. Usually, for every 60 to 90 minutes of frosting time, a defrosting operation would be initiated. Performances of these earlier ASHP units could well suffer from some unnecessary defrosting operations, resulting in a degraded operational efficiency.

For the later, demand defrosting control, firstly proposed by Eckman [1987], has been applied to initiating a defrosting cycle in an ASHP unit for decades. For defrosting refrigerated display cabinets, Eckman considered that time-based defrosting may cause a number of unnecessary defrosting cycles which reduced the energy efficiency of the refrigeration systems for the cabinets and the accuracy of temperature control of the cabinets. A demand defrosting control method which defrosted the display cabinet when sufficient frost was formed to adversely affect the operating performance of the display cabinet would lead to: (1) better temperature control, (2) increased product quality and life, (3) reduced product losses, and (4) significant energy savings. Therefore, when applying this control method, an ASHP unit would start defrosting only when an adequate frost buildup was detected. Therefore, it was important to accurately detect the presence and growth of frost.

A number of demand defrosting control techniques have been developed over the years which included: measuring the thermal conductivity of ice [Llewelyn 1984], sensing the temperature difference between the air and evaporator surface [Ciricillo 1985], air pressure differential across an evaporator [Heinzen 1988], and fan power sensing [Muller 1975]. Recent defrosting methods developed included defrosting initiation by measuring the ice thickness through using holographic interferometry technique [Hao et al. 2002], measuring the frost surface temperature by infrared thermometer [Iragorrry and Tao 2005], sensing refrigerant flow instability [Lawrence and Evans 2008], using photo-coupler [Byun et al. 2006, Xiao et al. 2009, Xiao et al. 2010, Wang et al. 2013a], photo-optical

systems [Woodley 1989] or fiber-optic sensors [Paone and Rossi 1991] as a frost sensing device, applying neural networks to modeling the amount of frost on coil surface [Datta and Tassou 1997, 2002].

Allard and Heinzen [1988] reported an adaptive defrosting method, which could initiate a defrosting cycle only when needed, thus saving energy by eliminating unnecessary defrosting cycles but yet maintaining the operating efficiency of an ASHP unit. It was accomplished by automatically adjusting the frost accumulation period to achieve an optimal predetermined defrosting time. The optimal defrosting time was previously determined for a particular ASHP unit and was programmed into the control method. The next frost accumulation time period was determined based on the optimal defrosting time, the previous frost accumulation time, and the previous actual defrosting duration. Huang et al. [2008] conducted a numerical study concerning the effect of frost thickness on the heat transfer in a four-row plate finned-tube exchanger. The study results revealed that the heat exchanger should go through defrosting when half of a single flow channel area was blocked by frost.

Often, defrosting operations were undertaken at wrong occasions. Therefore, Wang et al. [2011b] discussed “Mal-defrost phenomena” where defrosting operations were carried out a long time after a “critical” level of frost has been reached, or when they were not necessary. Different defrosting control strategies and the possible causes for mal-defrosting phenomena were analyzed. Field investigations on the characteristics for an ASHP unit under two typical mal-defrost phenomena were carried out. Later, to quantify

the performance drop in an ASHP unit operated in moderate climate conditions for a special mal-defrost phenomenon, a field test was conducted by Wang et al. [2013b] for 8 days at the start of a heating season in Beijing, China. The mal-defrost phenomenon was found with more than 60% frosted area of the outdoor heat exchanger after the system running 5 days. During this frosting period, the system COP was significantly degraded, only 2.3 under an environment temperature of 7.9 °C. Comparing the test data before and after frosting, it was found that the mal-defrost phenomenon decreased the system COP by up to 40.4% and the heating capacity by up to 43.4%.

### **2.5.2 Defrosting termination**

With respects to defrosting termination, related research is much less seen. It should be noted that for defrosting on ASHP unit, a complete defrosting process covers both melting frost and drying coil surface. Otherwise, once the ASHP unit returning to heating operation, retained melted frost on outdoor coil surface would become ice. This may change the structure of a frost layer, increase the density and enhance thermal conductivity of the frost layer [Lee and Ro 2001].

In practical applications, a reverse cycle defrosting operation can be terminated based on surface temperature of an outdoor coil, pressure difference across an outdoor coil, or time. Terminating a defrosting operation based on the surface temperature of an outdoor coil is currently the mostly used method. A temperature sensor is usually placed on the lowest liquid-line circuit of a vertically installed multi-circuit outdoor coil. A reverse cycle defrosting operation will be terminated once a preset temperature is reached. However, different temperature settings have been used and reported, from 12 °C [Ding et al. 2004a] to 50 °C [Hu 2010], as listed in the Table 2.1.

Table 2.1 Temperature settings to end a reverse cycle defrosting operation for ASHP units

Year	Literature	Circuit number	Temperature (°C)	Facility capacity (kW)
1995	Payne and O'Neal	4	26.7	10.6 (Cooling)
2003	Liu et al.	4	30	0.88 (Compressor)
2004	Huang et al.	/	22	50 (Cooling)
2004	Ding et al.	2	12	8.82 (Cooling)
2005	Cho et al.	/	20	/
2007	Huang et al.	12	24	55 (Cooling)
2009	Huang et al.	12	10	55 (Cooling)
2011	Hu	2	50	2.5 (Cooling)
2011	Choi et al.	12	20	16 (Cooling)
2012	Dong et al.	2	33	3.514 (Heating)
2012	Dong et al.	2	26	3.62 (Heating)
2012	Qu et al.	4	24	6.8 (Heating)
2013	Wang et al.	4	15	55-350 (Heating)

## 2.6 Conclusions

The development of air conditioning and heat pump technology is a natural consequence to both pursuing high quality living and working environments, and at the same time addressing the issue of sustainability. ASHP units have been widely used for space cooling in summer and space heating in winter for many years, due to their distinguished advantages of energy saving and environmental protection. However, when an ASHP unit operates in space heating mode in winter time, frost can be formed and accumulated on the surface of its outdoor coil when its temperature is below 0 °C and lower than the dew point of ambient air. Frosting deteriorates the operation and energy efficiency, and reduces the output heating capacity of the ASHP unit. Therefore periodic defrosting becomes necessary. Currently, the most widely used standard defrosting method for ASHP units is reverse cycle defrosting. Defrosting helps an ASHP unit return to its rated performance, although the process itself consumes energy, causing undesirable fluctuations of indoor air temperature and other operational problems.

Extensive related studies on the performance of ASHP units under frosting or defrosting condition have been undertaken. From the open literature available, the research work related to reverse cycle defrosting performance of ASHP units was relatively less seen comparing with that related to frosting. This was because that reverse cycle defrosting was a complex process involving spatial and time variations as well as many other indeterminate factors resulted from transient cycling which may last for only a few minutes. Both experimental and numerical approaches were adopted in these studies to

investigate the operating performances of ASHP units under both frosting and defrosting conditions. Various measures to address the problems associated with the frosting and defrosting operations of ASHP units have been considered. However, there are still a number of issues where further extensive research work is required, as follows:

- As presented in Sections 2.4.3 and 2.4.4, although limited previous experimental and simulation studies on understanding the uneven defrosting for an ASHP unit with a vertically installed multi-circuit outdoor coil during reverse cycle defrosting have been conducted and reported, the research work on quantifying the negative effects of downwards flowing of melted frost due to gravity along the surface of its outdoor coil on defrosting performance cannot be identified. Therefore, experimental studies on quantifying the negative effects of melted frost should be carried out with a specially-made outdoor coil that can be used to quantify the negative effects.
- A limited number of modeling studies on operating performance during reverse cycle defrosting have been carried. However, previous modeling studies on developing mathematical models that can be used to quantify the negative effects of alleviating the downwards flowing of melted frost on outdoor coil surface on defrosting performances cannot be identified. Therefore, such models should be developed and validated using the experimental data obtained.
- Although uneven defrosting over the surface of a vertical multi-circuit outdoor

coil was observed, for existing ASHP units previous studies on developed methods to alleviate the negative effects of uneven defrosting cannot be identified in open literature. This suggested the need to develop suitable methods to alleviate the negative effects.

The literature review presented in this part has identified a number of important areas where further in-depth research work is required, as summarized above. There are the expected suggests of the investigations to be carried out in this project reported in this thesis.

## **Chapter 3**

### **Proposition**

#### **3.1 Background**

It has been clearly demonstrated from the literature review presented in Chapter 2 that ASHP units have been widely used worldwide as an energy efficient and environmental friendly means for building thermal environmental control. However, when an ASHP unit operates in heating mode, frost can be accumulated on the surface of its outdoor coil. Frosting deteriorates its operation and energy efficiency, and therefore periodic defrosting becomes necessary. Currently, the most widely used standard defrosting method for ASHP units is reverse cycle defrosting. Defrosting helps an ASHP unit return to its rated performance, at the expense of consuming energy and causing undesirable fluctuations of indoor air temperature and other operational problems for the ASHP unit.

The previous related studies available in the open literature concentrated on studying the operating performances of ASHP units under both frosting and defrosting conditions, and various possible measures to address the problems associated with the frosting and defrosting operations of ASHP units. However, uneven defrosting over the entire airside surface of a vertically installed multi-circuit outdoor coil was observed and reported during reverse cycle defrosting for ASHP units. Uneven defrosting could lead to a prolonged defrosting duration and a lower defrosting efficiency. Although other factors

may lead to uneven defrosting on the surface of a vertical multi-circuit outdoor coil, the fact that melted frost flowing downwards due to gravity was considered as a major cause for uneven defrosting. Therefore, it is necessary to experimentally study the negative impacts of downwards flowing of melted frost over the surface of a vertical multi-circuit outdoor coil on defrosting performance for an ASHP unit, by comparing the measured defrosting performances with and without the melted frost downwards flowing from up circuit(s) to down circuit(s) in an experimental multi-circuit outdoor coil. On the other hand, to enable further quantitatively analyzing the effects of locally draining away the melted frost on reverse cycle defrosting performance of an ASHP unit, and to develop methods to alleviate the negative effects of uneven defrosting on defrosting performance of an existing ASHP unit, modeling studies should also be carried out.

### **3.2 Project title**

The thesis focuses on the following three major issues related to reverse cycle defrosting for ASHP units: (1) experimentally studying the negative effects of downwards flowing of the melted frost on reverse cycle defrosting performance for an experimental ASHP unit having a vertically installed experimental three-circuit outdoor coil; (2) developing empirical mathematical models for the defrosting performance for the experimental ASHP unit with and without local drainage of the melted frost from its vertically installed three-circuit outdoor coil; and (3) exploring a method of potentially alleviating the negative effects of downwards flowing of melted frost over the experimental three-circuit outdoor coil and thus improving the defrosting performance for an existing ASHP unit

having a vertical multi-circuit outdoor coil based on the models developed. The research project reported in this thesis is therefore entitled “An experimental and numerical study on improving defrosting performances for an air source heat pump unit having a multi-circuit outdoor coil”.

### **3.3 Aims and objectives**

The objectives of the research work reported in this thesis are as follows:

- 1) To experimentally study the impacts of allowing melted frost to flow freely downwards due to gravity along the surface of the vertical experimental three-circuit outdoor coil on the defrosting performances in the experimental ASHP unit during reverse cycle defrosting;
- 2) To carry out a modeling study on defrosting performance for the experimental ASHP unit with local drainage of the melted frost from its experimental three-circuit outdoor coil. The models will be validated using the experimental data collected.
- 3) To undertake a modeling study on alleviating uneven defrosting for the experimental three-circuit outdoor coil during reverse cycle defrosting, using the models developed.

### **3.4 Research methodologies**

Both experimental and numerical approaches will be adopted in the project. A specially-made experimental ASHP setup will be established, consisting of the experimental ASHP unit having the vertically installed experimental three-circuit outdoor coil, an environmental chamber including one simulated heated indoor space and one simulated frosting outdoor space. The experimental three-circuit outdoor coil will be specially made, where water collecting trays will be placed between circuits to facilitate local drainage of melted frost during reverse cycle defrosting. The experimental ASHP setup will be detailed in Chapter 4.

In the experimental study, three experimental cases, with different arrangements of water collecting trays placed between or under circuit(s), will be designed. The temperatures of tube surface at the exits of each refrigerant circuit, coil fin surface at the center of each circuit, and the melted frost collected will be measured. Since placing a water collecting tray directly under a circuit would stop the melted frost from flowing into the circuit(s) underneath, the effects of downwards flowing of melted frost over a vertical multi-circuit outdoor coil surface in an ASHP unit on defrosting performance during reverse cycle defrosting can therefore be experimentally investigated. The experimental cases and study results will be presented in Chapter 5.

In developing mathematical models, the fundamentals of heat and mass transfers will be applied, to be supplemented by experimental data, where appropriate. This will make the

models to be developed semi-empirical. It is expected that two semi-empirical mathematical models, corresponding to two settings of with and without the use of water collecting trays between circuits, will be developed.

Finally, when studying alleviating the negative effects for existing ASHP units, modeling approach will be adopted as a starting point to save time and cost. The semi-empirical models developed and validated can be used as a model tool and study results are to be reported in Chapter 7.

The experimental ASHP setup will be built up in the HVAC Laboratory in the Department of Building Services Engineering, The Hong Kong Polytechnic University.

## **Chapter 4**

# **An Experimental Setup for an Experimental ASHP Unit Having a Multi-circuit Outdoor Coil**

### **4.1 Introduction**

An experimental setup for an experimental ASHP unit having a multi-circuit outdoor coil was established in the HVAC Laboratory of The Department of Building Services Engineering, The Hong Kong Polytechnic University. The primary purpose of having such an experimental setup was to facilitate carrying out the research work related to studying the negative effects of downwards flowing of melted frost on the surface of a multi-circuit outdoor coil in an ASHP unit on defrosting performance during reverse cycle defrosting and developing the measures to alleviate the negative effects for improved defrosting performance for ASHP units.

The experimental setup consisted of an experimental ASHP unit, an environmental chamber including one simulated heated indoor space and one simulated frosting outdoor space. A computerized data measuring, logging and control system was built into the experimental setup. A vertically installed three-circuit outdoor coil, which was a key component to the successful study on the negative effects of melted frost flowing downwards along the surface of a multi-circuit outdoor coil in an ASHP unit during reverse cycle defrosting, was specially made as part of the experimental ASHP unit.

This Chapter firstly describes the experimental setup and its major components in detail. This is followed by reporting the computerized measuring devices and data acquisition system. Finally, the method of evaluating the mass of accumulated frost on an outdoor coil surface is given.

## **4.2 Detailed descriptions of the experimental setup**

Fig. 4.1 shows the schematic diagram of the experimental setup. The experimental ASHP unit was modified from a commercially available standard ASHP unit and was installed inside the existing environmental chamber. The environmental chamber was divided into a heated indoor space and a frosting outdoor space, where simulated indoor and outdoor conditions in terms of air temperature and humidity necessary for testing the defrosting performance of the experimental ASHP unit can be maintained. The indoor coil of the experimental ASHP unit was installed inside the heated indoor space and a specially-made three-circuit outdoor coil inside the frosting outdoor space. In addition, although not shown in Fig. 4.1, necessary outdoor airflow ductwork was also included in the experimental setup.

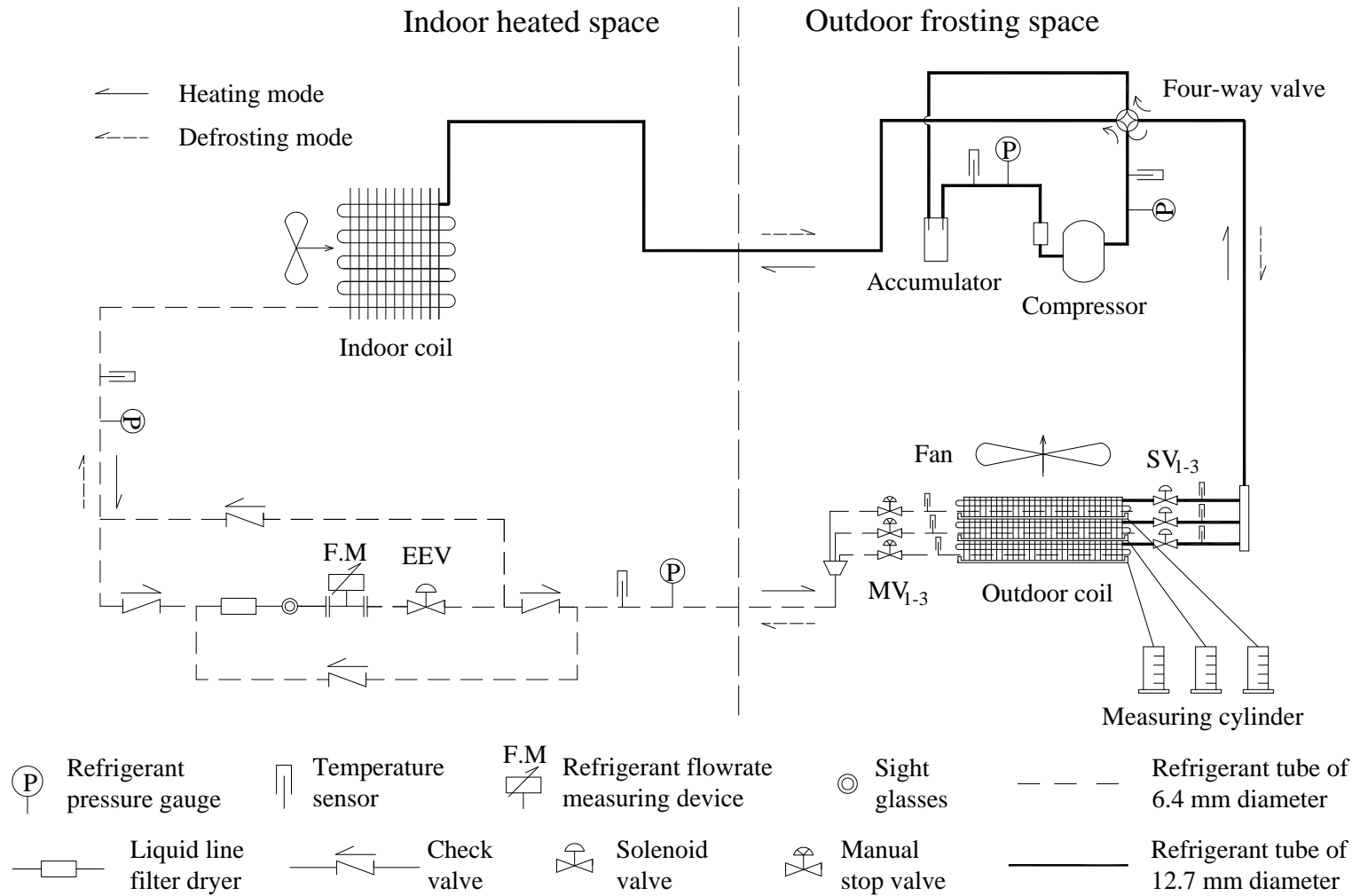


Fig. 4.1 Schematics of the experimental setup for an experimental ASHP unit installed in an environmental chamber

#### **4.2.1 The experimental ASHP unit**

The experimental ASHP unit was retrofitted from a nominal 6.5 kW heating capacity split-type residential ASHP unit. The major components in the ASHP unit included a variable-speed rotor compressor, an electronic expansion valve (EEV), the specially-made vertically installed three-circuit outdoor coil and an indoor coil. The specifications of the ASHP unit excluding the outdoor coil are given in Table 4.1, with further details for the outdoor coil given in Section 4.2.2. The compressor was of swing type and equipped with a suction line accumulator to minimize liquid flow to the compressor during start up and transient operation periods. The refrigerant used was R22. Other necessary accessories and control devices, such as a sight glass, a filter, an accumulator and safety devices, were provided to ensure the normal and safe operation of the experimental ASHP unit.

The EEV used in the experimental ASHP unit was controlled by a built-in degree of superheat controller (Model No.: LS-IC003C), with a total of 480-pulses of valve opening positioning. The port diameter of the EEV was 1.4 mm. It was used to maintain a desired degree of refrigerant superheat at the evaporator exit.

Table 4.1 Specifications of the experimental ASHP unit excluding the outdoor coil

Parameters	Values/ details
<i>Compressor</i>	
Compressor type	Swing
Rated heating capacity (kW)	6.5
Rated input power (kW)	1.84
Refrigerant	R22
<i>EEV</i>	
Port diameter (mm)	1.4
Pulse Range (Pulse)	0~480
Rated Capacity (kW)	5.3
<i>Indoor coil</i>	
Tube length (mm)	875
Tube external diameter (mm)	7.9
Tube spacing (mm)	12
Fin thickness (mm)	0.16
Fin pitch (mm)	1.2
Number of tube rows	2
Number of circuits	4
Air flow rate (m <sup>3</sup> /h)	1050
Tube material	Copper
Fin material	Aluminum
Fin type	Louver

#### 4.2.2 The specially-made vertically-installed outdoor coil and its airside details

The outdoor coil used in the experimental ASHP unit, where frosting and defrosting took place, was specially designed and made for the study reported in this thesis, as shown in Fig. 4.2. There were three individual and parallel refrigerant circuits and the airside surface areas corresponding to each of the three circuits were equal. The outdoor coil was vertically installed, and in each circuit a solenoid valve and a manual stop valve were available.

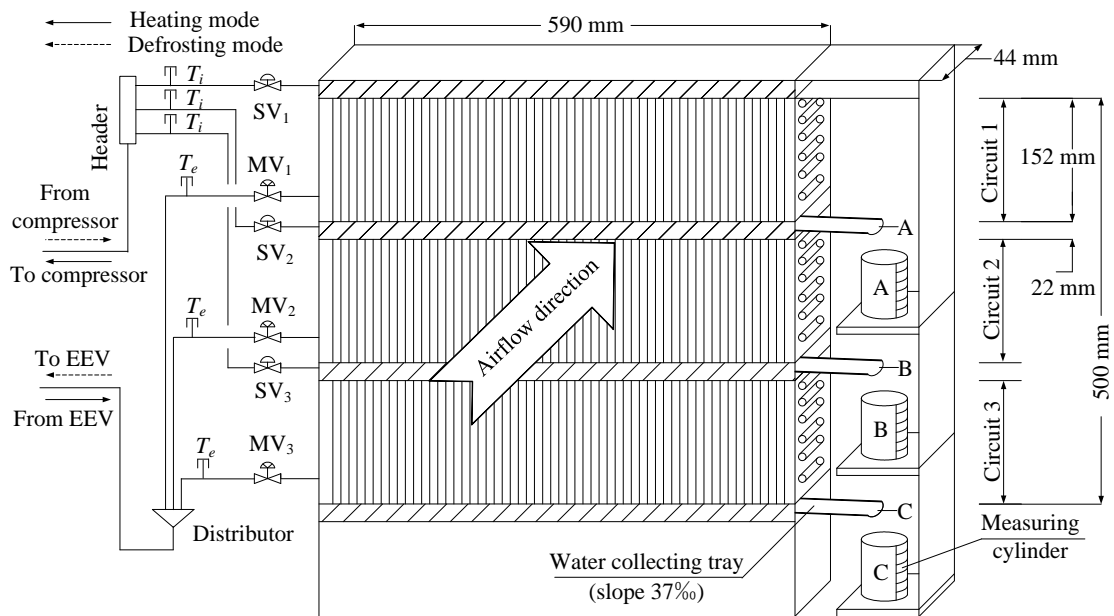


Fig. 4.2 Details of the three-parallel refrigerant circuit outdoor coil and locations of solenoid valves and manual stop valves

As seen in Fig. 4.2, three water collecting trays made of PVC, Trays A to C, were added to the outdoor coil. They can be placed under each circuit of the outdoor coil when

necessary. In this way, the downwards flowing of melted frost would be restricted within a circuit. Furthermore, three water collecting cylinders, A to C, were connected to these trays, so that melted frost from each circuit during defrosting may be collected and weighted. The technical specifications of the three-parallel refrigerant circuit outdoor coil are shown in Table 4.2.

Table 4.2 Specifications of the vertically installed outdoor coil

Item	Parameters	Values
1	Height (mm)	500
2	Width (mm)	590
3	Fin height (mm)	152.4
4	Fin width (mm)	44
5	Fin thickness (mm)	0.115
6	Fin pitch (mm)	2.1
7	Tube external diameter (mm)	10
8	Tube thickness (mm)	0.5
9	Tube spacing (mm)	20
10	Number of tube rows	2
11	Number of circuits	3
12	Circuit pitch (mm)	22
13	Tube material	Copper
14	Fin material	Aluminum
15	Fin type	Plate
16	Water collecting tray material	PVC

### 4.2.3 Environmental chamber

The experimental ASHP unit was installed in the existing environmental chamber having a simulated heated indoor space and a simulated frosting outdoor space. The two spaces were separated by a thermally insulated partition. The sizes of both indoor and outdoor spaces were each measured at 3.9 m (L) × 3.8 m (W) × 2.8 m (H). The existing chamber in the experimental setup had a separate direct expansion (DX) air conditioning (A/C) system and sensible and latent load generating units (LGUs), so that suitable testing conditions in both indoor and outdoor spaces may be maintained, as illustrated in Fig. 4.3.

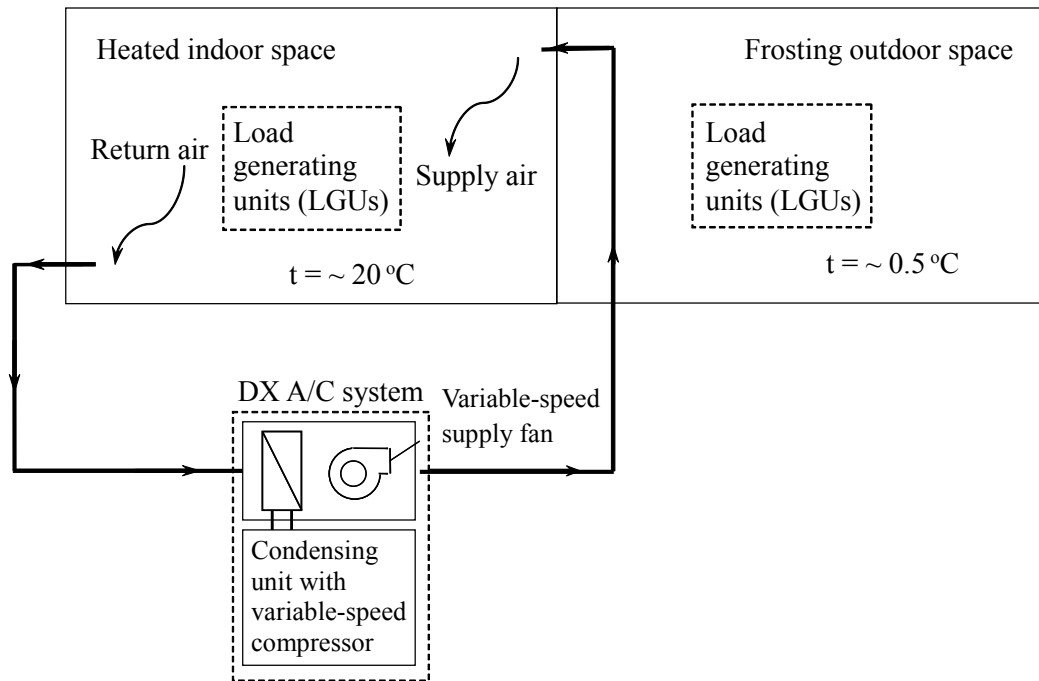


Fig. 4.3 The schematic diagram of the environmental chamber

The DX A/C system mainly included a variable-speed rotor compressor, an EEV, an air cooled tube-plate-finned condenser and a high-efficiency louver-fin-and-tube DX

evaporator, a supply fan, etc. The nominal output cooling capacity from the DX A/C system was 9.9 kW, but the actual output cooling capacity could be modulated from 15% to 110% of the nominal capacity. Both supply air fan and compressor were driven by variable-frequency drives. The working fluid of the DX A/C system was refrigerant R22. The sensible and latent heating capacities of the LGUs were 12 kW and 4.8 kW, respectively. Their heat and moisture generation rates regulated by Solid State Relay may be varied manually or automatically with a pre-set pattern through operator's programming. Test conditions in both the indoor space and the outdoor space were monitored with air temperature and humidity measuring sensors located in the rooms. During normal heating (or frosting) operation, the frosting environment in the outdoor space was maintained by running the experimental ASHP unit and LGUs together while the heated environment in the indoor space jointly by the experimental ASHP unit, the DX A/C system and LGUs.

### **4.3 Computerized instrumentation and data acquisition system (DAS)**

The computerized instrumentation for the experimental setup is also shown in both Fig. 4.1 and Fig. 4.2. The experimental setup was fully instrumented for measuring all of its operating parameters, which may be classified into three types, temperature, pressure and flow rate. Since all measurements were computerized, all sensors and measuring devices were able to output direct current signal of 4-20 mA or 1-5 V, which were transferred to a data acquisition system (DAS) for logging and recording.

### 4.3.1 Sensors/measuring devices for temperatures, pressures and flow rates

Fig. 4.4 shows the airside details of the three-circuit outdoor coil in the experimental ASHP unit installed in the frosting outdoor space. Air dry-bulb temperatures upstream of the outdoor coil were measured at 6 points using pre-calibrated K-type thermocouples and air wet-bulb temperatures also at 6 points using temperature sensors (PT100, Class A). The average values from these measurements were used as the inlet air dry-bulb temperature and wet-bulb temperature in the follow-up calculation. On the other hand, air temperature and humidity downstream of the outdoor coil were measured by a hygrosensor located inside an air duct 900 mm downstream of the outdoor coil. Furthermore, the air flow rate passing through the outdoor coil was measured using a flow hood which had a 16-point velocity grid located at the center of a 400×400 mm air duct of 600 mm long, as shown in Fig. 4.4.

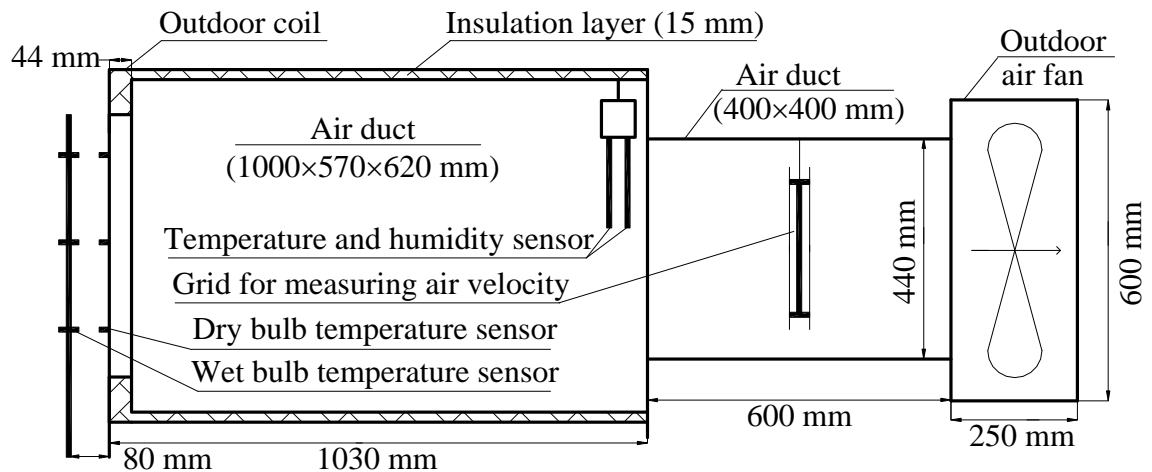


Fig. 4.4 The airside details of the experimental outdoor coil in the experimental ASHP unit installed in the frosting outdoor space

Pre-calibrated K-type thermocouples were also used for measuring the temperatures of tube/coil and fin surfaces of the outdoor coil. Six were for measuring the refrigerant tube surface temperatures at both the inlets ( $T_i$  in Fig. 4.2) and exits ( $T_e$  in Fig. 4.2) of the three refrigerant circuits. Three were affixed on the fin surface at the center of each circuit. Furthermore, three thermocouples were placed inside the cylinders to measure the temperatures of melted frost. For the experimental ASHP unit, refrigerant pressures were measured using pressure transmitters and refrigerant mass flow rate by a variable area flow meter.

Table 4.3 summarizes the measuring accuracy for various sensors/instruments used in the experimental ASHP unit, and the calculated relative standard errors for the two calculated parameters of total energy used during defrosting and defrosting efficiency, respectively.

Table 4.3 Measurement/calculation errors of system parameters

No.	Parameters	Measurement/ calculation errors
1	Air dry-bulb temperature upstream of the outdoor coil (K-type thermocouple)	$\pm 1\text{ }^{\circ}\text{C}$
2	Air wet-bulb temperature upstream of the outdoor coil (PT100, Class A)	$\pm 0.1\text{ }^{\circ}\text{C}$
3	Air temperature downstream of the outdoor coil (hygrosensor)	$\pm 0.2\text{ }^{\circ}\text{C}$
4	Air relative humidity downstream of the outdoor coil (hygrosensor)	$\pm 1.0\text{ }\%$
5	Air flow rate passing through the outdoor coil (flow hood)	$\pm 3\text{ }\%$
6	Temperatures of tube/coil and fin surfaces of the outdoor coil (K-type thermocouple)	$\pm 1\text{ }^{\circ}\text{C}$
7	Refrigerant pressure (pressure transmitters)	$\pm 0.3\text{ }\%$
8	Refrigerant mass flow rate (variable area flow meter)	$\pm 1.6\text{ }\%$
9	Mass of melted frost collected (weighting scale)	$\pm 0.1\text{ g}$
10	Temperature of melted frost (K-type thermocouple)	$\pm 1\text{ }^{\circ}\text{C}$
11	Total energy used for defrosting (calculated)	$\pm 1\%$
12	Defrosting efficiency (calculated)	$\pm 0.15\%$

### 4.3.2 The DAS

A DAS was used in this experimental setup. It provided up to 66 channels for measuring/monitoring various operating parameters of the setup. The direct current signal from various measuring devices/sensors could be scaled into their real physical values of the measured parameters using a data logging and control supervisory program. The DAS collected and recorded all the measured data throughout both frosting and defrosting periods at an interval of 5 s. In addition, during defrosting, photos for surface conditions of the outdoor coil were taken at an interval of 10 s.

### 4.4 Evaluating the mass of accumulated frost on outdoor coil surface

With the availability of the above instrumentation on the airside of the outdoor coil, the air parameters up-stream and down-stream of the outdoor coil, such as air temperatures and moisture contents, may be real time measured and the mass of frost accumulated during the period of  $\Delta t$  can be evaluated by Eq. (4.1) [Guo et al. 2008]:

$$\Delta M_f = \frac{m_{o,a} \Delta t}{1 + w_i} (w_{o,i} - w_{o,e}) \quad (4.1)$$

where  $m_{o,a}$  is the mass flow rate of the air across the outdoor coil,  $w_{o,i}$  and  $w_{o,e}$  are the air moisture contents at the inlet and the exit of the outdoor coil, respectively, which can be obtained by:

$$w = \frac{622\phi p_{asw}}{(101.325 - \phi p_{asw})} \quad (4.2)$$

where  $\phi$  is the measured air relative humidity,  $p_{asw}$  the saturated water vapor pressure as a function of measured dry-bulb temperature,  $t_{adb}$ .  $p_{asw}$  can be estimated by the following equations:

when  $t_{adb}$  is between -100 °C and 0 °C [13]:

$$p_{asw} = \frac{e^{-5.67 \times 10^3 T_{adb}^{-1} + 6.39 - 9.68 \times 10^{-3} T_{adb} + 6.22 \times 10^{-7} T_{adb}^2 + 2.07 \times 10^{-9} T_{adb}^3 - 9.48 \times 10^{-13} T_{adb}^4 + 4.16 \times \ln(T_{adb})}}{1000} \quad (4.3a)$$

when  $t_{adb}$  is between 0 °C and 200 °C [13]:

$$p_{asw} = \frac{e^{-5.800 \times 10^3 T_{adb}^{-1} + 1.391 - 0.0486 T_{adb} + 0.418 \times 10^{-4} T_{adb}^2 - 0.145 \times 10^{-7} T_{adb}^3 + 6.546 \times \ln(T_{adb})}}{1000} \quad (4.3b)$$

where  $T_{adb}$  is the absolute air temperature, to be evaluated by:

$$T_{adb} = 273 + t_{adb} \quad (4.4)$$

In this study reported in this thesis,  $\Delta t$  was set at 5 s, same as the time interval used for data logging. Hence, the actual total amount of frost formed on the outdoor coil surface,  $M_f$ , could be real time evaluated by summing up  $\Delta M_f$ , displayed and recorded using the

data logging supervisory program.

#### **4.5 Conclusions**

To facilitate the intended research work reported in this thesis, an experimental ASHP setup was established. The experimental setup mainly included the experimental ASHP unit, the existing environmental chamber and the instrumentation including the DAS.

The experimental ASHP setup was fully instrumented using high quality sensors/measuring devices. Totally thirty-nine operating parameters in the setup could be real-time measured, monitored, recorded and processed by the data logging and control supervisory programs.

The availability of the experimental setup was expected to be extremely useful in studying the negative effects of downwards flowing of melted frost on the surface of a multi-circuit outdoor coil in an ASHP unit on defrosting performance during reverse cycle defrosting, and developing the measures to alleviate the negative effects for improved defrosting performance for ASHP units.

Photos showing the details of the experimental setup are in Appendix A.

## **Chapter 5**

### **An Experimental Study on Improving Defrosting Performances for an ASHP Unit Having a Multi-circuit Outdoor Coil**

#### **5.1 Introduction**

Since the oil crisis in the early 1970s, there has been much research effort in developing smaller, quieter and higher efficiency heat pump systems. One obvious advantage for using a heat pump unit is that it can provide heating or cooling from one single machine without any major modification [Byun et al. 2006]. ASHP units used as cooling or heating sources for building heating, ventilation and air conditioning installations have found increasingly wide applications over the recent decades in many parts of the world [Wang et al. 2012a, Mohanraj et al. 2012].

It is noted that an outdoor coil in an ASHP unit is usually of multi-circuit structure in order to minimize its refrigerant pressure loss and enhance its heat transfer [Choi et al. 2011, Qu et al. 2012, Lin et al. 2013]. Also an outdoor coil is usually installed vertically for floor space saving. However, as revealed in the literature presented in Chapter 2, allowing the melted frost to flow downwards on the surface of a vertical outdoor coil due to gravity would adversely affect the defrosting performances of an ASHP unit. For example, it was reported [Qu et al. 2012a] that when defrosting at the top circuits was ended, the bottom ones were still covered with frost. One important reason for this was

believed to be the existence of melted frost flowing from top to bottom due to gravity. While few studies about the effects of downwards flowing of melted frost due to gravity over a vertical multi-circuit outdoor coil on defrosting performance may be identified in open literature, a previous related study [Qu et al. 2012a] has suggested that downwards flowing of melted frost over a vertical multi-circuit outdoor coil during reverse cycle defrosting could adversely affect the defrosting performance of an ASHP unit, by using more energy for defrosting and prolonging a defrosting process. This was because the downwards flowing of melted frost helped form or reinforce a water layer between the frost and coil surface, introducing an additional layer of thermal resistance [Payne and O'Neal 1995], thus reducing the heat transfer between the two. Furthermore, more residual water could be left on the surface of bottom circuits and thus more energy needed to dry the residual water on the bottom circuits. However, no detailed quantitative analysis of these negative effects was carried out and reported.

Therefore, an experimental study on the effects of downwards flowing of melted frost due to gravity over the experimental vertical three-circuit outdoor coil surface on the defrosting performance of the experimental ASHP unit during reverse cycle defrosting has been carried out and the study results are reported in this Chapter. Experimental procedures and conditions are firstly presented. This is followed by reporting experimental results. Finally, based on the experimental results, a quantitative analysis on the impacts of the downwards flowing of the melted frost due to gravity on defrosting performance is reported.

## **5.2 Experimentation**

### **5.2.1 Experimental ASHP unit**

All the experimental work reported in this Chapter was carried out using the experimental ASHP setup whose schematic diagram is shown in Fig. 4.1 in Chapter 4. All measurement/calculation errors of system parameters are already summarized in the Table 4.3.

### **5.2.2 Experimental procedures and conditions**

Prior to defrosting operation, the experimental ASHP unit was operated in the heating (frosting) mode for 1 hour, at an outdoor frosting ambient temperature of  $0.5 \pm 0.2$  °C (dry-bulb temperature) and  $90 \pm 3\%$  relative humidity, which was jointly maintained by the use of both experimental ASHP unit and the LGUs placed in the outdoor frosting space.

Before defrosting was started, the compressor was firstly switched off. One minute after compressor shutdown, the four-way valve was switched to defrosting mode. Four seconds later, the compressor was powered on again, and a defrosting operation was started. Defrosting operation was manually terminated when the tube surface temperature of the lowest refrigerant circuit (Circuit 3) in the outdoor coil reached 24 °C [Krakow et al. 1993a, Ding et al. 2004a, Hu et al. 2011, Qu et al. 2012a, Rahman and Jacobi 2012, Wang

et al. 2013a]. The outdoor air fan during defrosting was turned off, but the indoor air fan remained operation at a lower speed. During frosting, air temperature inside the heated indoor space was maintained at 20 °C, which was jointly maintained by the use of both experimental ASHP unit and the existing air conditioning system. The experimental conditions are summarized in Table 5.1.

Table 5.1 Experimental conditions

Item	Parameters	Values
1	Air temperature in indoor heated space (°C)	20
2	Air temperature in outdoor frosting space (°C)	0.5 ± 0.2
3	Air relative humidity in outdoor frosting space (%)	90 ± 3
4	Face velocity of outdoor coil (m/s)	1.2 <sup>a</sup>
5	Face velocity of indoor coil at defrosting mode (m/s)	2.31
6	Face velocity of indoor coil at heating (frosting) mode (m/s)	3.68
7	Heating (frosting) operation duration (min)	60

<sup>a</sup> The value at the beginning of a heating (frosting) operation. During heating (frosting), the face velocity was decreased due to frost growth.

Series of experimental work using the experimental ASHP unit have been carried out to study the effects of downwards flowing of the melted frost over the outdoor coil surface due to gravity on defrosting performance. In order to obtain meaningful experimental results, it was necessary to ensure that frost accumulated on the surface of the three circuits was even. Therefore, a series of trial-and-error manually adjusting the degree of

opening of the stop valves was carried out to adjust the refrigerant flow into each circuit. Consequently, a set of fixed degree of valve openings was obtained, so that the amount of frost accumulation on the three circuits was close to each other (difference < 10%). Experimental work was then carried out at three experimental cases, as detailed in Table 5.2, so that the effects of downwards flowing of melted frost on defrosting performance can be comparatively and quantitatively analyzed.

Table 5.2 Three experimental cases

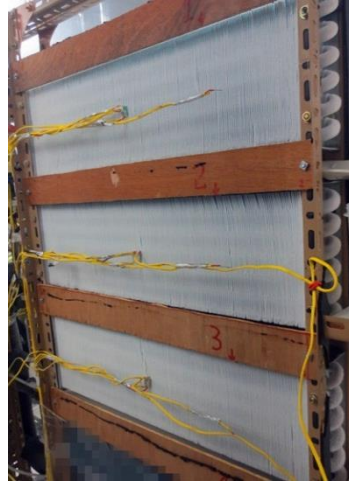
Case	No. of water collecting trays installed	Positions of water collecting trays	Experimental results shown in
1	1 (Tray C)	Under Circuit 3	Figs. 5.1, 5.2, 5.5, 5.7
2	2 (Trays A, C)	Under Circuit 1 and 3	Figs. 5.1, 5.3, 5.6, 5.8
3	3 (Trays A, B, C)	Under each circuit	Figs. 5.1, 5.4, 5.7, 5.8

### 5.3 Experimental results

Fig. 5.1 presents twelve photographs showing the defrosting process on the airside of the three circuits of the experimental outdoor coil, with photos (a1) to (a4) for Case 1, photos (b1) to (b4) for Case 2, and photos (c1) to (c4) for Case 3, respectively.



a1 (Case 1)

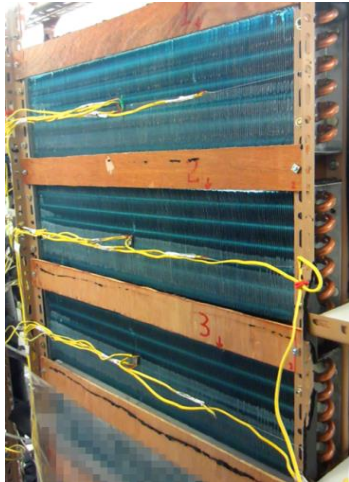


b1 (Case 2)

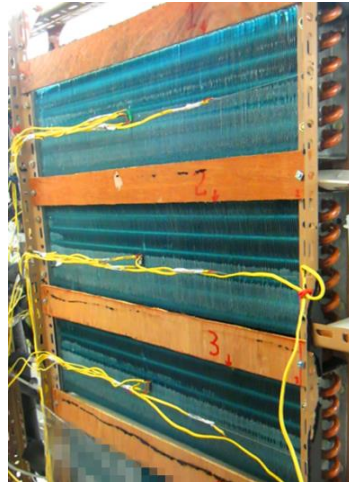


c1 (Case 3)

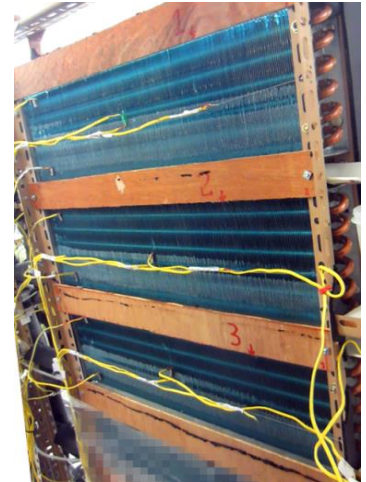
0 s (starting of the defrosting)



a2 (Case 1)



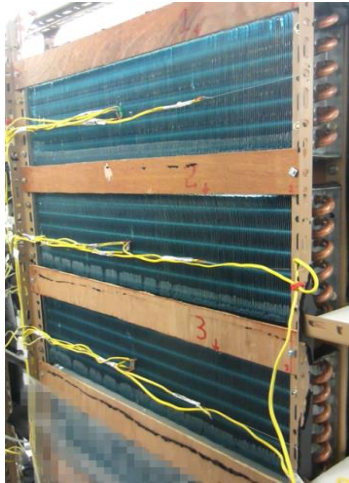
b2 (Case 2)



c2 (Case 3)

100 s into defrosting operation

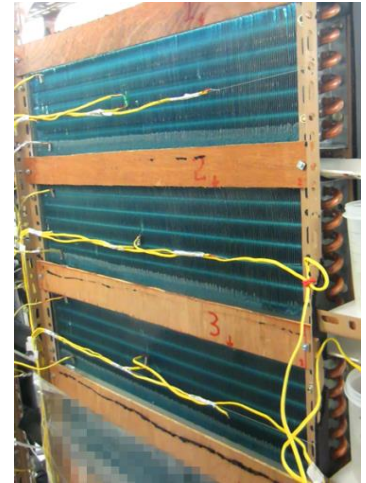
Fig. 5.1 Airside surface conditions of the outdoor coil during defrosting in the three cases (twelve photographs)



a3 (Case 1)



b3 (Case 2)

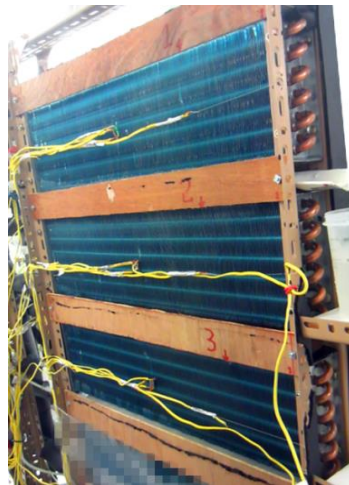


c3 (Case 3)

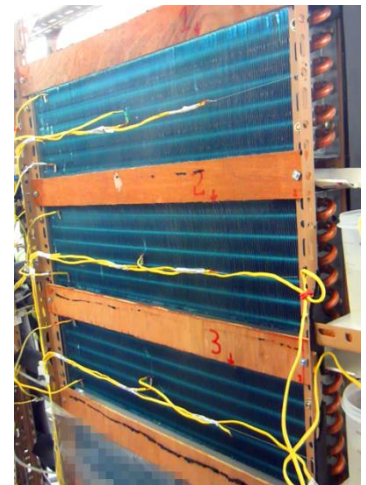
130 s into defrosting operation



a4 (Case 1)



b4 (Case 2)



c4 (Case 3)

150 s into defrosting operation

Fig. 5.1 (Cond.) Airside surface conditions of the outdoor coil during defrosting in the three cases (twelve photographs)

As observed from Fig. 5.1 (a1), Fig. 5.1 (b1) and Fig. 5.1 (c1), the surface conditions at the start of defrosting for the three cases were virtually the same. From Fig. 5.1 (a2), Fig. 5.1 (b2) and Fig. 5.1 (c2), it can be seen that frost melting was all started at 100 s into defrosting, and no melted frost flowing downwards may be observed at this stage. Furthermore, as seen from Fig. 5.1 (a3), at 130 s into defrosting operation, in Case 1, frost melting on the surface of Circuit 1 was quicker than that on the surface of Circuit 2, while melted frost flowed downwards from Circuit 1 to Circuit 2. On the other hand, frost melting on the surface of Circuit 3 was later than that on the surface of Circuit 2, because the melting frost flowing downwards to Circuit 3 was more than that to Circuit 2. However, as seen from Fig. 5.1 (b3) for Case 2 and Fig. 5.1 (c3) for Case 3, the state of frost melting on the two up-circuits was basically the same. The melted frost from Circuit 1 was taken away by the collecting tray before it reached Circuit 2. Finally, the airside conditions of the outdoor coil at 150 s into defrosting operation at the three experimental cases are shown in Fig. 5.1 (a4), Fig. 5.1 (b4), and Fig. 5.1 (c4), respectively. It can be seen from Fig. 5.1 (a4) that with only one tray, while the airside of Circuit 1 was already free of frost, there was still frost on the surface of lower part of Circuit 2 and Circuit 3 waiting to be melted. Also as seen from Fig. 5.1 (b4) that with two collecting trays installed under Circuit 1 and Circuit 3, there was nearly no frost left on the two up circuits, while clearly there was some frost left on the Circuit 3. However, as seen from Fig. 5.1 (c4) that with three collecting trays installed, the frost on the three circuits all disappeared. Therefore, defrosting was quicker and more even with trays installed. From the above twelve photos, the negative effects of downwards flowing of melted frost over the

experimental three-circuit vertical outdoor coil due to gravity on defrosting performance during reverse cycle defrosting can be visually observed.

The measured operating performances of the experimental ASHP unit during defrosting, corresponding to the three experimental cases, are presented in Figs. 5.2 - 5.7. In all these figures, for their time (horizontal) axis, 80 s is the chosen starting time in order to clearly show the temperature rise during defrosting. Figs. 5.2 - 5.4 present the measured tube surface temperatures at the exits of the three refrigerant circuits during defrosting. Figs. 5.5 - 5.7 show the measured fin temperatures at the center point of the three circuits. It is noted that the variation trends of these temperatures are similar to those reported by O'Neal et al. [1989].

It can be seen from Fig. 5.2 that in Case 1, the temperatures remained around 0 °C during the first 100 s, and started to rise steadily thereafter. As already shown in Fig. 5.1 (a2), Fig. 5.1 (b2) and Fig. 5.1 (c2), frost on the surface of Circuit 3 began melting at 100 s into defrosting operation, and thereafter, the tube surface temperatures increased steadily from 0 °C to 24 °C. The tube surface temperatures of the three circuits reached 24 °C at 172 s, 182 s and 186 s, respectively. In Case 2, as shown in Fig. 5.3, the time for the surface temperature at the exit of two up-circuits reached 24 °C was nearly the same at 174 s, and that for Circuit 3 was a little longer at 180 s. However, as shown in Fig. 5.4 , in Case 3, the surface temperatures at the exits of the three circuits reached 24 °C almost at the same time, at 167 s, 166 s, and 168 s, respectively. The time differences of 6 s and 18 s in Case 2 and Case 3 compared to that in Case 1 clearly showed that it would take

longer time for the bottom circuit to reach 24 °C when fewer trays were installed, so that a defrosting operating was prolonged, and more energy consumed.

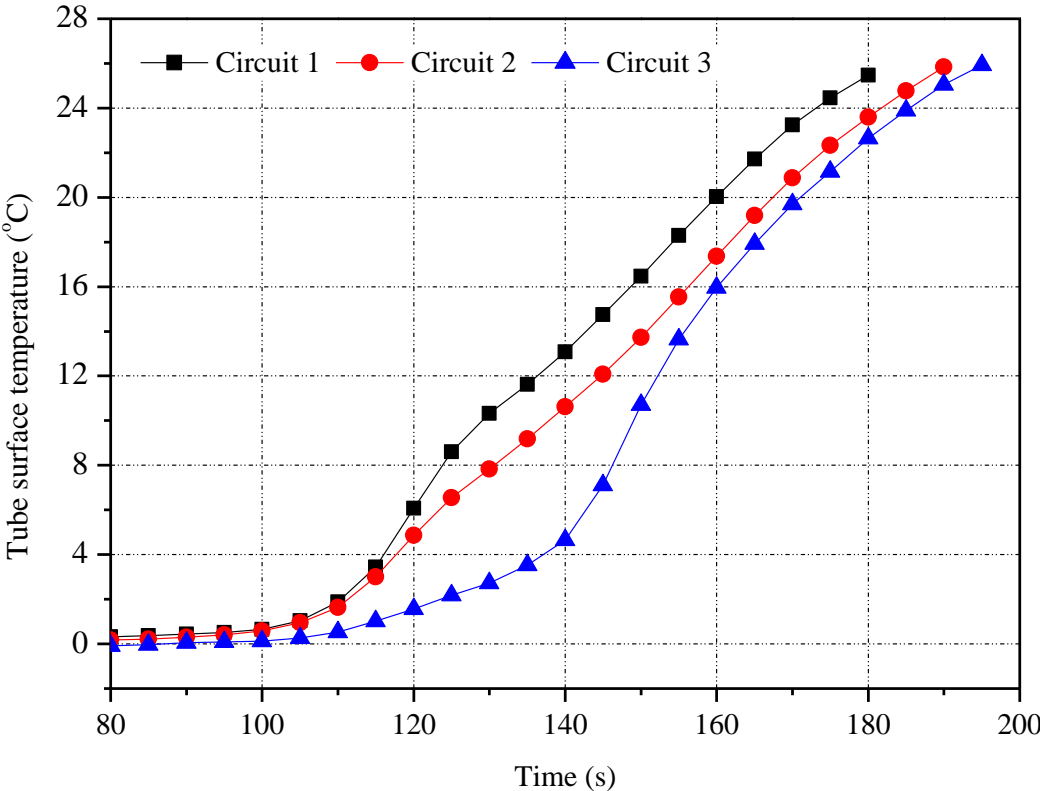


Fig. 5.2 Measured tube surface temperatures at the exits of the three refrigerant circuits during defrosting (Case 1)

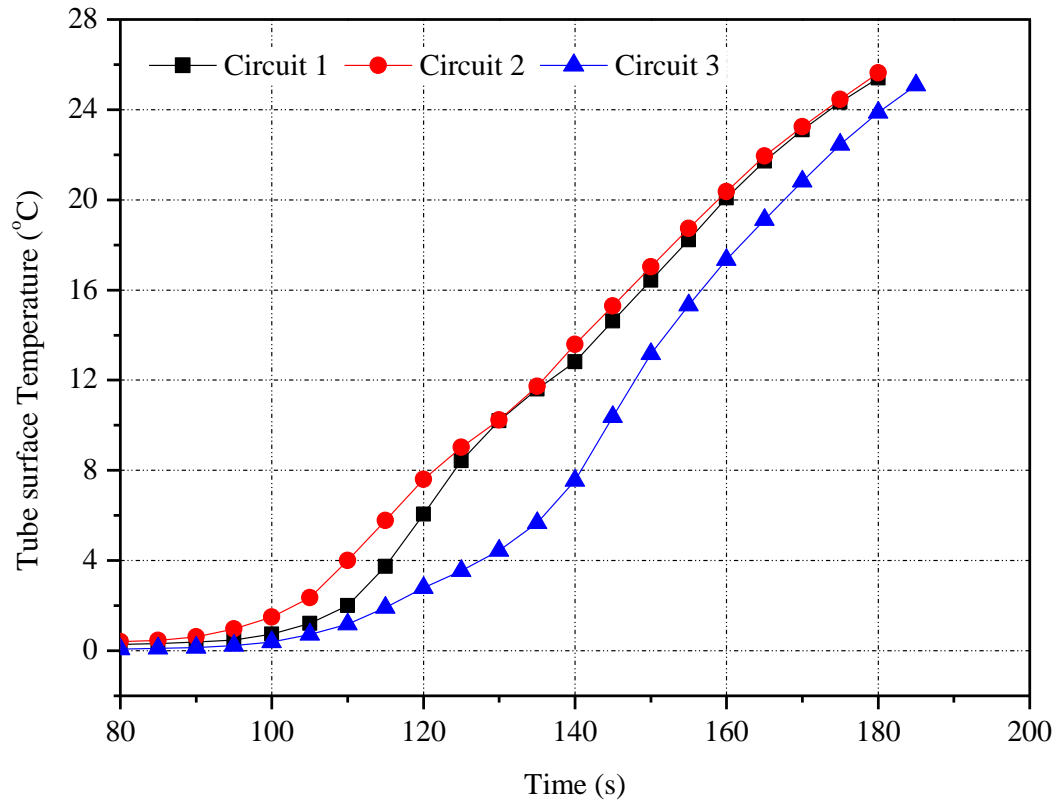


Fig. 5.3 Measured tube surface temperatures at the exits of the three refrigerant circuits during defrosting (Case 2)

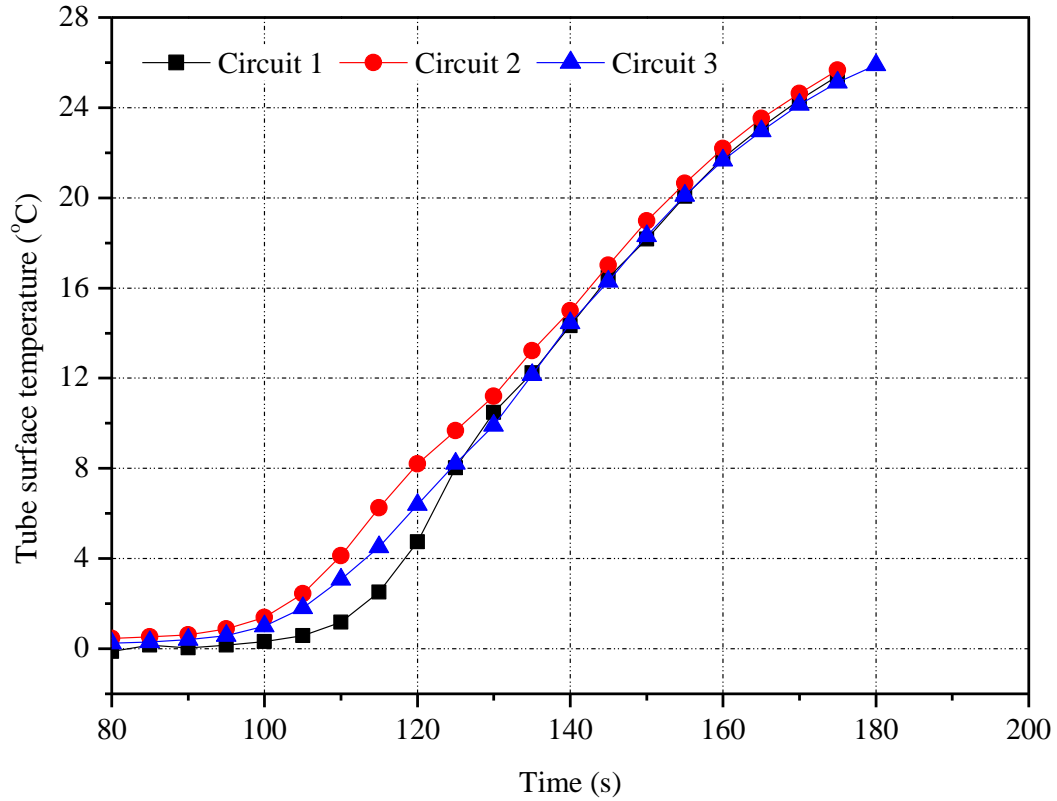


Fig. 5.4 Measured tube surface temperatures at the exits of the three refrigerant circuits during defrosting (Case 3)

Figs. 5.5 - 5.7 show the variations of the measured fin surface temperatures at the center point of each circuit in the three experimental cases. Unlike tube surface temperatures, fin surface temperatures remained at 0 °C at the first 110 s into defrosting. The rise in fin temperature was later than that in tube surface temperature. This was because the tube was in direct contact with hot refrigerant, but the fin was indirectly in contact with refrigerant via tube. As seen in Fig. 5.5, in Case 1, it took 75 s, 80 s and 85 s for the fin temperatures to reach 24 °C in the three circuits, respectively. Again, it took a longer time for the fin temperature in the bottom circuit to reach 24 °C, which could be also attributed to the downwards flowing of melted frost from up circuit(s).

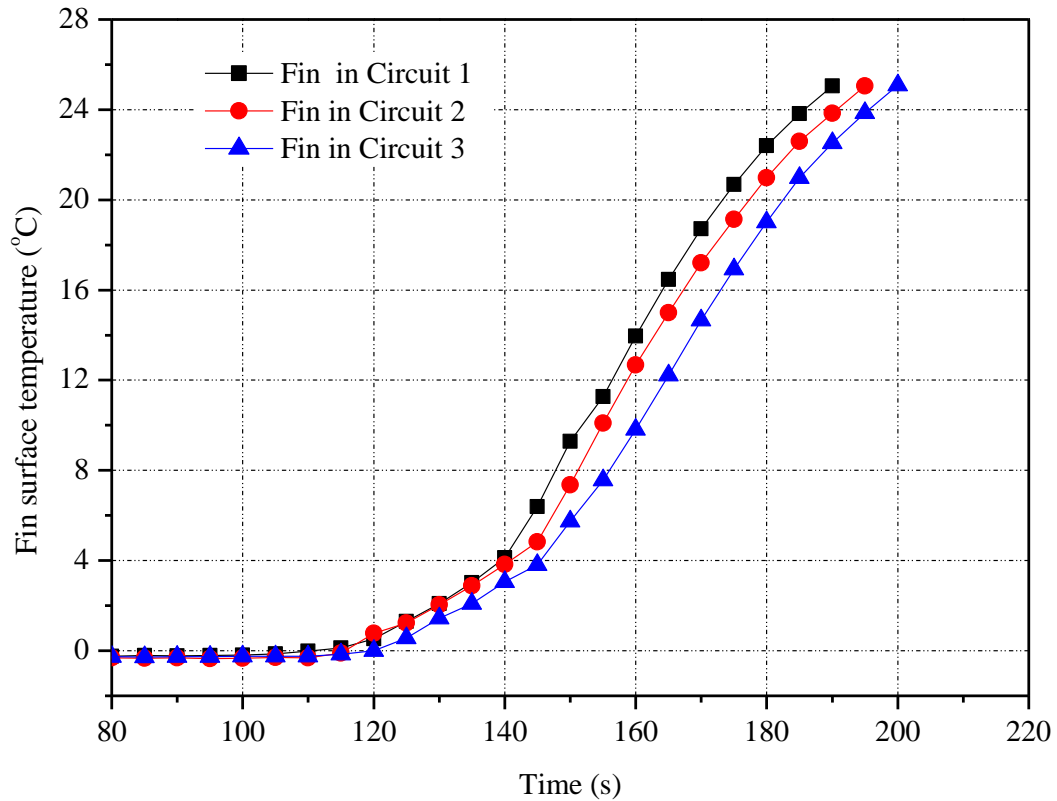


Fig. 5.5 Measured fin temperatures at the center of the three refrigerant circuits during defrosting (Case 1)

In Fig. 5.6, the variations of measured fin temperatures in Case 2 are shown. Unlike those shown in Fig. 5.5, fin temperatures at the up two circuits reached 24 °C almost at the same time at 185 s, as the downwards flowing of melted frost from Circuit 1 to Circuit 2 was stopped by the presence of the collecting trays, but the fin temperature of Circuit 3 reached 24 °C at about 7 s later, at 192 s. When the melted frost from each circuit was taken away by the collecting trays before downwards flowing to lower circuits in Case 3, as shown in Fig. 5.7, the time durations for fin temperatures at three circuits reached 24 °C were very close to each other, at 177 s, 179 s, and 175 s, respectively. Furthermore, as more water collecting trays installed, the duration for the fin temperature in Circuit 3 to

reach 24 °C gradually became smaller. Therefore, the negative effects of downwards flowing of melted frost over a vertical multi-circuit outdoor coil on defrosting performance of an ASHP unit during reverse cycle defrosting are further shown.

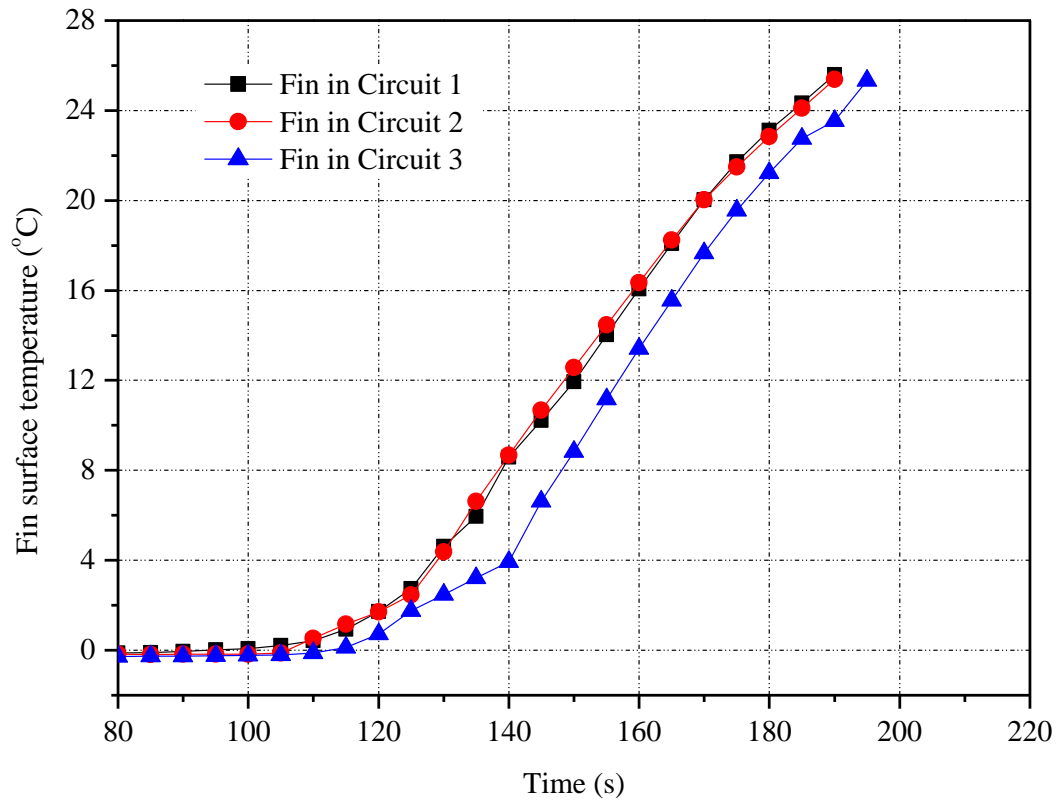


Fig. 5.6 Measured fin temperatures at the center of the three refrigerant circuits during defrosting (Case 2)

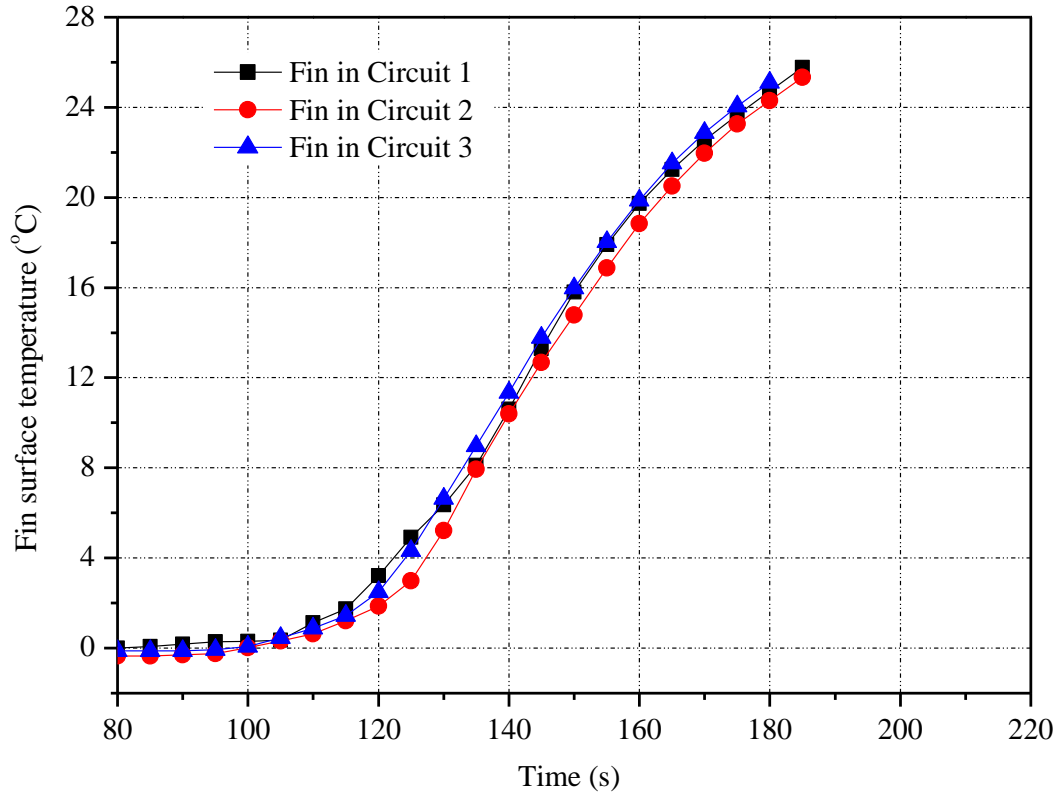


Fig. 5.7 Measured fin temperatures at the center of the three refrigerant circuits during defrosting (Case 3)

Fig. 5.8 presents the variations of measured melted frost temperatures in the water collecting cylinders in the three cases. The temperature of melted frost in Cylinder C, in Case 1, rose from 0.3 °C at 130 s to about 1.6 °C at 195 s. In Case 2, the temperature of melted frost in Cylinder A, collected from Circuit 1, was around 0 °C at 130 s to 150 s into the defrosting operation and rose to about 0.15 °C at 195 s. The temperature of melted frost from Circuit 3 in Cylinder C increased from 0.4 °C at 130 s to 1.2 °C at 195 s. However, in Case 3, the temperatures of the melted frost in the three Cylinders, i.e., A, B and C, all rose slowly from about 0 °C to less than 0.2 °C at 195 s. The temperature of the melted frost in Case 1 was always higher than that in Case 3, because the melted frost

flowing path was shortened so that the heat transfer between fins and melted frost was decreased. On the other hand, in Case 2, the flowing path of the melted frost collected in the Cylinder A was half of that in Cylinder C, so that its temperature was always lower. These, therefore, further confirmed the negative effects of downwards flowing of melted frost due to gravity during reverse cycle defrosting on defrosting performance.

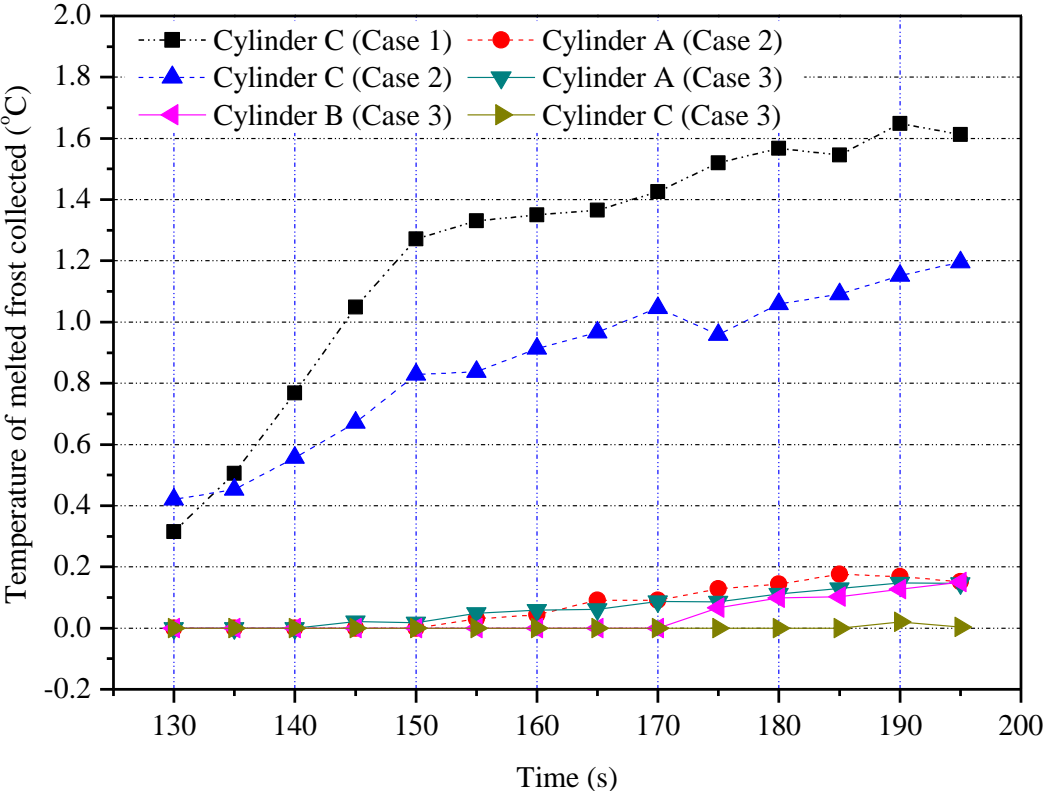


Fig. 5.8 Temperatures of melted frost collected in the water collecting cylinders in the three cases

Moreover, the total amount of melted frost collected in Case 1 was 921 g, 22 g less than that collected in Case 2, and 48 g less than that collected in Case 3. The net differences

of 22 grams and 48 grams were considered to have been evaporated. This was because the melted frost flowing down was heated by the upper part of lower circuit(s) which was warmer as the hot refrigerant flowed from top to bottom within the circuit during defrosting. This explained why less melted frost was collected with upper collecting trays.

Furthermore, downwards flowing of the melted frost not only delayed a defrosting process, but also led to energy waste. The energy used for reverse cycle defrosting comes from three sources: the power input to the compressor, the power input to the indoor air fan and the thermal energy from indoor air. The total energy used for defrosting was 727 kJ in Case 1, but 652 kJ in Case 3, or 10.4% less. In Case 2, the total energy consumed was at 683 kJ, or 6.05% less than that in Case 1.

Defrosting efficiency can be used to evaluate the performance of a defrosting operation. It is defined as the ratio of the actual amount of energy consumption required to both melt the accumulated frost and vaporize the retained melted frost to the total amount of energy available from an outdoor coil during an entire defrosting operation, as follows:

$$\eta_d = \frac{E_m + E_v}{Q_{com} + Q_{fan} + Q_{air}} \quad (5.1)$$

where  $E_m$  and  $E_v$  are the total heat used for melting frost and vaporizing the retained water, respectively, and they are evaluated by:

$$E_m = M_f L_{sf} \quad (5.2)$$

$$E_v = M_v L_v \quad (5.3)$$

where  $M_f$  and  $M_v$  are the total mass of the frost formed on the outdoor coil and the mass of vaporized melted frost, respectively, and  $L_{sf}$  and  $L_v$  latent heat of frost melting and latent heat of evaporation of water, respectively. Also in Equation (5.1),  $Q_{com}$ ,  $Q_{fan}$  and  $Q_{air}$  are the energy consumptions by compressor and supply fan, and the thermal energy from indoor air during defrosting, respectively.

In this experimental study, the defrosting efficiencies calculated for the three cases were 43.5%, 50.6% and 56.7%, respectively. Therefore, allowing melted frost freely flowing down due to gravity would lead to more energy consumption during defrosting. There can be two reasons for more energy use: a) evaporating some of the melted frost as mentioned earlier; b) when a defrosting process was prolonged, the fin surface in an up circuit(s) could be dry already, while that in a down circuit(s) was still wet, if not still covered with frost. Therefore, thermal energy would be used for just heating ambient cold air, which was highly undesirable.

## **5.4 Conclusions**

The experimental results and corresponding quantitative analysis reported in this Chapter demonstrated the negative effects of allowing melted frost to flow downwards due to gravity over the airside surface of an experimental vertical three-circuit outdoor coil in an ASHP unit on defrosting performance during reverse cycle defrosting: a longer defrosting duration and more energy consumption. Furthermore, the study results also suggested that the use of water collecting trays was effective in mitigating the negative effects. Therefore, to have a further better understanding of heat and mass transfer mechanisms when the melted frost from upper circuits flows over the frosted surface of lower circuits in a vertical multi-circuit outdoor coil, a related mathematical modeling study on defrosting performance for the experimental ASHP unit with local drainage of melted frost from its three-circuit outdoor coil out has been carried out, and the study results are reported in Chapter 6.

## **Chapter 6**

# **A Semi-empirical Mathematical Modeling Study on Improving Defrosting Performances for an ASHP Unit Having a Multi-circuit Outdoor Coil**

### **6.1 Introduction**

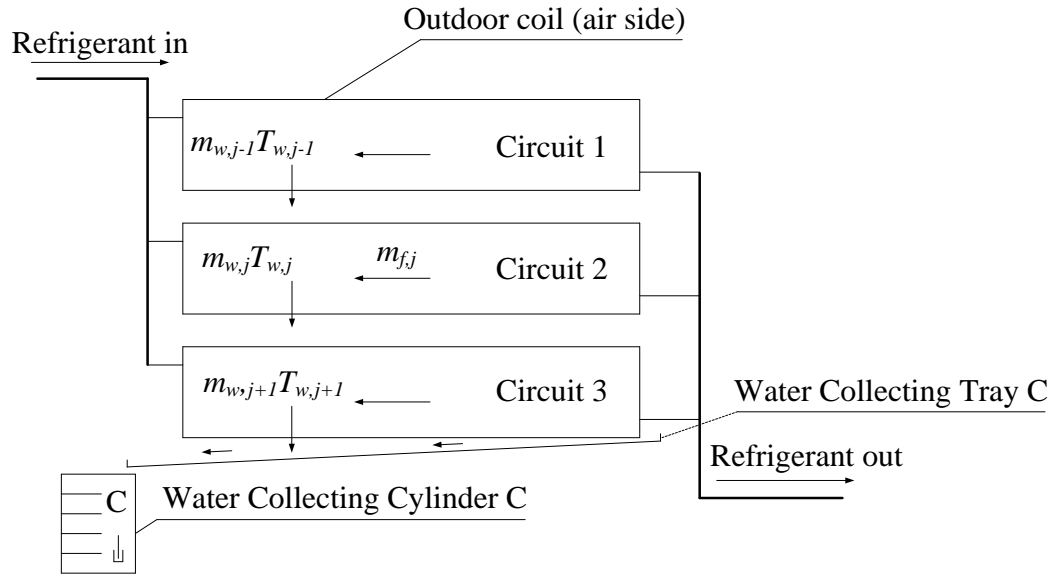
In Chapter 5, the experimental study on the defrosting performance where the melted frost was drained away locally during reverse cycle defrosting in an ASHP unit is reported. In the experimental study, a specially-made experimental three-circuit outdoor coil was used by placing water collecting trays under each circuit. Comparative experiments with and without the use of water collecting trays between circuits were carried out and experimental results suggested that the use of the water collecting trays helped shorten the defrosting duration by 9.2% and reduce the defrosting energy use by 10.4%.

To enable further quantitative analysis on the effects of locally draining away the melted frost on reverse cycle defrosting performance in an ASHP unit, a related mathematical modeling study on defrosting performance with local drainage using water collecting trays was considered necessary. Therefore, a modeling study of the defrosting process taking place in the specially-made three-circuit experimental outdoor coil, at two experimental settings of with and without the use of water collecting trays between circuits was carried out and the study results are reported in this Chapter. Two semi-

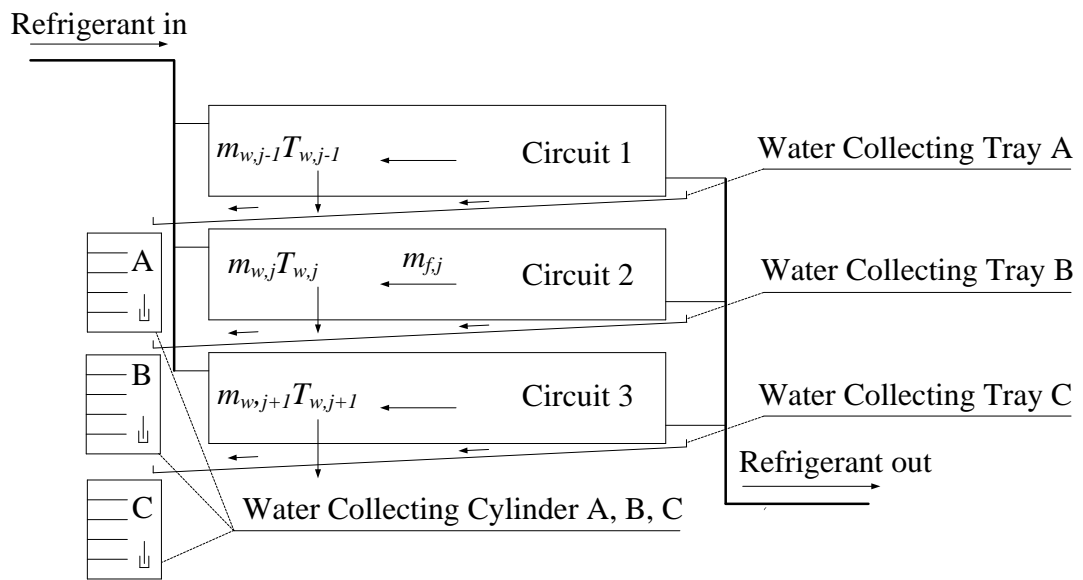
empirical mathematical models, corresponding to the two settings, were developed. In this Chapter, firstly the detailed development of the two semi-empirical models is presented. This is followed by reporting the experimental validations of the two models using the experimental data reported in Chapter 5. Finally, detailed discussions on the potential uses of the two models developed and the limitations of the modeling work reported are included.

## **6.2 Development of the semi-empirical mathematical models**

As shown in Fig. 6.1 and Table 6.1, two semi-empirical models were developed based on if water collecting trays were installed between circuits. Model 1 was developed for the condition when only one water collecting tray (Tray C) was installed under the lowest circuit, and connected to a water collecting cylinder (Cylinder C), i.e., no water trays were installed between circuits. However, Model 2 was for the condition when three water collecting trays (A, B and C) were each placed under Circuits 1 to 3, and connected to three cylinders (A, B, C), respectively. When developing the two mathematical models, the entire airside of the tailor-made three-circuit outdoor coil surface was divided into three control volumes, respectively, corresponding to the three circuits shown in Fig. 6.1. For each control volume, lumped parameter modeling approach was applied.



Model 1



Model 2

⊥ Thermal-couple

Fig. 6.1 Conceptual models for the airside of the three-circuit outdoor coil in the experimental ASHP unit

Table 6.1 Two semi-empirical models

	No. of water collecting trays installed	Positions of water collecting trays	Modeling results shown in
Model 1	1 (Tray C)	Under Circuit 3	Figs. 6.1 - 6.7
Model 2	3 (Trays A, B, C)	Under each circuit	Figs. 6.1 - 6.5, 6.8 - 6.11

In the modeling study reported in this Chapter, unlike the models developed in previous studies [Krakow et al. 1992a, Krakow et al. 1992b, Qu et al. 2012b], a defrosting process on the airside of the outdoor coil was divided into four stages: (1) preheating, (2) frost melting without water flowing away from a circuit, (3) frost melting with water flowing away from a circuit, and (4) water layer vaporizing. Such a way of staging a defrosting process could enable a proper account for the flow of the melted frost into, or away from a control volume according to the use of water collecting trays in the experimental three-circuit outdoor coil.

Under the assumption of four stages of defrosting, a defrosting process began with preheating. In this stage, all the melted frost could be held on finned coil surface due to surface tension. When the frost in direct contact with the surface of tubes and fins was melted, a thin water layer was formed. At the end of the first stage, the thin water layer covered the entire air side surface of outdoor coil. However, the water layer was not in contact with ambient air within the entire first stage. In the second stage, as the heat was transferred from warmer water layer to frost, the thickness of frost layer was decreased

and that of water layer increased, so that water layer started to be in contact with air of low temperature. However, there was no melted frost flowing away from a circuit, as the mass of the melted frost held did not reach its maximum that could be held by surface tension [Krakow et al. 1992b]. The third stage began with the start of downwards flowing of the melted frost, as the force of gravity was larger than surface tension. In Model 1, the melted frost downwards flowed from an up-control volume into a down-control volume due to gravity during this stage. However, in Model 2, the melted frost did flow out of a control volume but did not flow into a down-control volume as it was taken away by the water collecting trays installed between the circuits, and was then collected by respective cylinders.

Finally, at the beginning of the fourth stage, or water layer vaporizing stage, the entire outdoor coil surface was free of frost but covered by the retained water. When the tube surface temperature at the exit of the lowest refrigerant circuit (Circuit 3 in this study) in the outdoor coil reached 24 °C [Qu et al. 2010, Qu et al. 2012a, Qu et al. 2012b] defrosting was terminated.

### **6.2.1 Assumptions and calculation conditions**

The two semi-empirical models were developed based on fundamentals of energy and mass conservation, heat and mass transfer within each of the control volumes at each stage of the defrosting process, and using also some of the experimental data obtained previously. When establishing the two models, the followings were assumed:

- i. The convective heat transfer between frost and ambient air in the first two stages was neglected. Therefore, the mass loss of frost due to sublimation during these two stages was neglected.
- ii. The thermal conductivities of tubes and fins were much higher than those of frost and retained water, and hence their heat transfer resistances neglected.
- iii. The mass flow rate of refrigerant was evenly distributed into the three refrigerant circuits during defrosting, and the frost was assumed to be uniformly accumulated over the coil surface before starting defrosting.
- iv. The movement of the melted frost layer was considered to be a flowing boundary. Because the velocity of the water flow was very small as observed during experiments, the melted frost layer flowed in laminar regime.
- v. During the third stage, the retained water in each control volume was in a dynamic equilibrium, i.e., the difference between the mass of water entering a control volume and that flowing away from the control volume was equal to the rate of frost melting within the control volume.
- vi. During defrosting, the melted frost infiltrated into the porous structure of frost. The contact area between the frost and melted frost would increase as water

flowed downwards, suggesting that the flow resistance was increased downwards along the surface of outdoor coil. Therefore, the velocity of water layer in each control volume was decreased from top to bottom.

- vii. During defrosting, there was no frost chip or debris flowing into a down circuit or a water collecting tray(s).
- viii. During defrosting, the mass of melted frost left on water collecting trays or vaporized from water collecting trays and cylinders was neglected.
- ix. In the process of the melted frost falling into a down circuit or a water collecting tray, the heat dissipated from the melted frost to ambient air was negligible because the falling distance was small.

Furthermore, the following experimental data, presented in Chapter 5, were also used in assisting the development of the two semi-empirical models:

- a) The total mass of the frost was experimentally obtained at 1050 g, thus following Assumption (iii), the mass of frost formed on the surface of each circuit,  $M_{f,j} (j = 1-3)$ , was  $1050 / 3$  g, or 350 g.
- b) At 40 s into defrosting, the preheating stage (first stage) was over.

- c) At 90 s into defrosting, the frost melting without water flowing away from a circuit stage (second stage) was over.
  
- d) The following experimentally measure refrigerant flow rate, tube surface temperatures at inlets and outlets of each circuit, temperature of ambient air surrounding the outdoor coil, and compressor discharge pressure during defrosting were used as the inputs to the models developed.

## **6.2.2 Model development**

As mentioned, two semi-empirical models were developed, for the two settings of with and without the use of water collecting trays between circuits. The use of trays would stop the melted frost from flowing into the circuits (or control volumes) underneath in Stage 3. Therefore, the two models were identical for Stages 1, 2 and 4, with only the modeling work in Stage 3 being different. In this section, for simplicity, the complete development of Model 1 is firstly presented. For Model 2, only the modeling work in Stage 3 is reported.

### **6.2.2.1 Model 1 development (all four stages)**

The model was developed by applying the energy and mass conservation in each of the three control volumes, at each of the fourth defrosting stages.

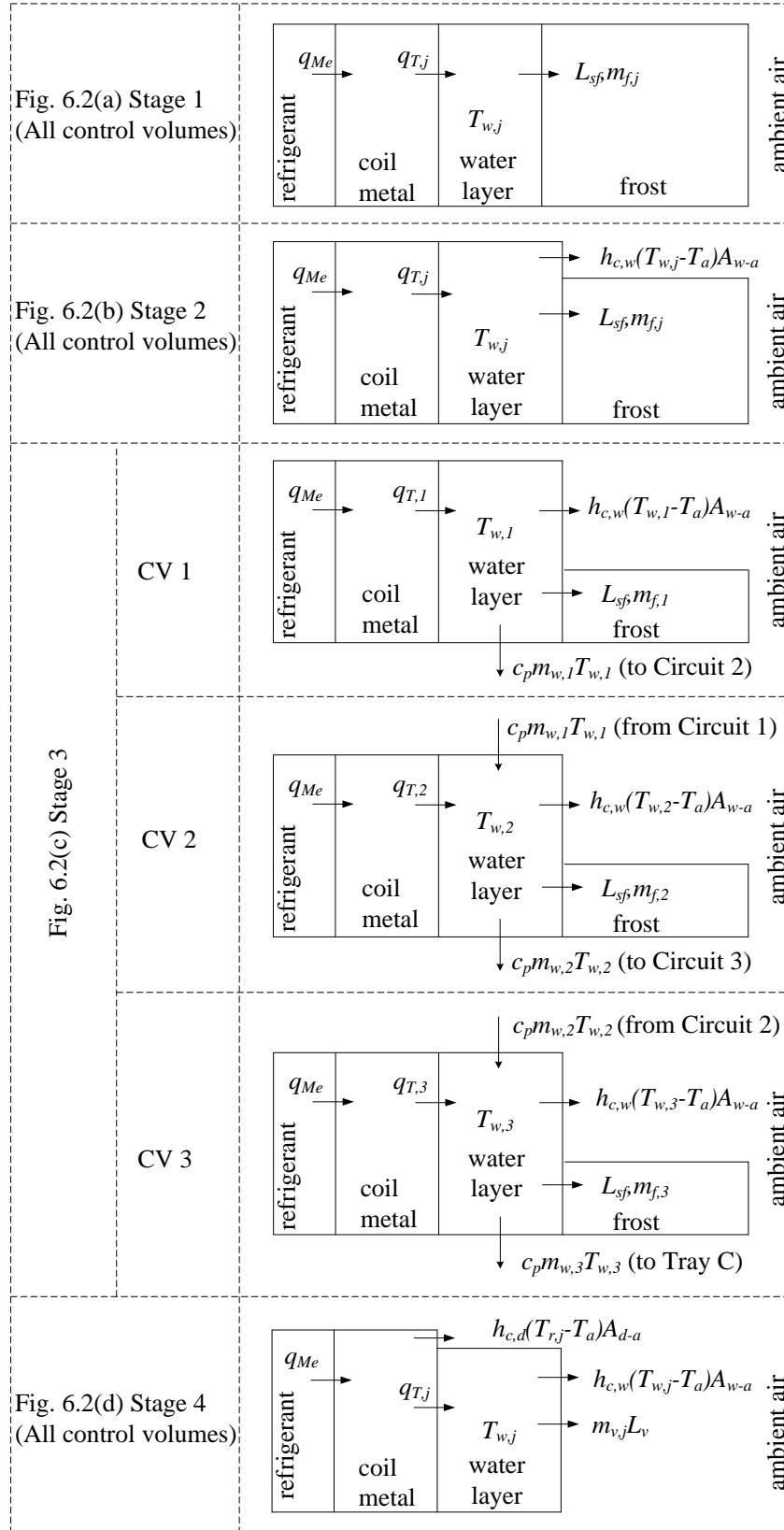


Fig. 6.2 Schematics of mass and energy flows in the four defrosting stages for Model 1

First stage: preheating

As shown in Fig. 6.2(a), energy and mass conservation in Control Volume  $j$  yielded:

$$q_j \Delta t = L_{sf} m_{f,j} \Delta t + c_p \Delta (M_{w,j} T_{w,j}) + q_{Me} \Delta t \quad (j=1-3) \quad (6.1)$$

As  $\Delta t \rightarrow 0$ , Eq. (6.1) can be written as

$$q_j = L_{sf} m_{f,j} + c_p \frac{d(M_{w,j} T_{w,j})}{dt} + q_{Me} \quad (j=1-3) \quad (6.2)$$

where  $M_{w,j}$  is the accumulated mass of the retained melted frost in the Control Volume  $j$ :

$$M_{w,j} = \int_0^t m_{f,j} dt \quad (j=1-3) \quad (6.3)$$

where  $t$  is the ending time of Stage 1 defrosting,  $T_{w,j}$  temperature of the melted frost on the surface of Circuit  $j$  (as shown in Fig. 6.1).

On the other hand, the heat transferred from the water layer to frost layer for frost melting was:

$$h_w(T_{w,j} - T_{tp})A_0 = L_{s,f}m_{f,j} \quad (j=1-3) \quad (6.4)$$

where  $T_{tp}$  is the triple point of water,  $A_0$  the equivalent airside surface area of a refrigerant circuit.

Also in Eq. (6.4),  $h_w$ , the average coefficient of convective heat transfer caused by water flow inside a control volume, was evaluated by:

$$h_w = \int_{jH}^{(j+1)H} h_{w,x} dx / H \quad (j=1-3) \quad (6.5)$$

where the convective heat transfer coefficient due to water flow downwards was evaluated by [Hoffenbecker et al. 2005]:

$$h_{w,x} = 0.332 \frac{\lambda}{x} \text{Re}_x^{\frac{1}{2}} \text{Pr}^{\frac{1}{3}} \quad (6.6)$$

To evaluate  $h_{w,x}$ , it was necessary to evaluate the velocity of water layer in each control volume, which, based on Assumption (vi), would decrease from top to bottom within a circuit, and could be estimated by [Qu et al. 2012b]:

$$v_j = \frac{H}{t_{d,1}} 0.85^{j-1} \quad (j=1-3) \quad (6.7)$$

where  $t_{d,1}$  is defrosting duration in Circuit 1, and an experimentally obtained value 168 s was used for  $t_{d,1}$ .  $H$  is the height of a refrigerant circuit.

Furthermore,  $q_{Me}$  is the energy used to heat the metal of outdoor coil and can be evaluated by [Dong et al. 2012]:

$$q_{Me} = c_{PMe} \times (m_{Cu} + m_{Al}) \frac{\Delta T_{Me}}{\Delta t} \quad (6.8)$$

where  $\Delta T_{Me}$  is the average temperature difference of outdoor coil metal and was evaluated by [Dong et al. 2012]:

$$\Delta T_{Me} = T_t - T_0 \quad (6.9)$$

$$T_0 = \frac{1}{2}(T_{in,0} + T_{e,0}) \quad (6.10)$$

$$T_t = \frac{1}{2}(T_{in,t} + T_{e,t}) \quad (6.11)$$

where  $T_0$  and  $T_t$  are the average temperatures of outdoor coil metal at the start and end of a defrosting process and,  $T_{in}$  and  $T_e$  the inlet and outlet tube surface temperatures of

outdoor coil. In Eq. (6.8),  $c_{PMe}$  is the average specific heat of metal (copper and aluminum) and can be evaluated by:

$$c_{PMe} = \frac{m_{Cu}c_{Cu} + m_{Al}c_{Al}}{m_{Cu} + m_{Al}} \quad (6.12)$$

Meanwhile, the heat transfer in Control Volume  $j$  can be expressed as [Qu et al. 2012b],

$$q_j = \frac{T_{r,j} - T_{ICW,j}}{R_r} A_t \quad (6.13)$$

where  $T_{ICW}$  is the temperature at the interface between coil surface and water layer,  $T_{r,j}$  the average temperature of refrigerant in Circuit  $j$ . The relationship between  $T_{ICW}$  and  $T_{w,j}$  in this stage was [Qu et al. 2012b]:

$$T_{w,j} = \frac{T_{ICW,j} + T_{tp}}{2} \quad (j=1-3) \quad (6.14)$$

As the heat transfer resistances of tubes and fins were neglected (Assumption (ii)), the thermal resistance of refrigerant,  $R_r$ , was evaluated by an empirical experimental correlation for the refrigerant side mean heat transfer coefficient,  $h_{TPM}$  [Shah 1979]:

$$R_r = \frac{1}{h_{TPM}} \quad (6.15)$$

During defrosting, two different heat transfer regions existed in the refrigerant side of the outdoor coil, namely (1) a superheated region and (2) a two-phase region. In the superheated region, the convective heat transfer coefficient of refrigerant,  $h_{r,sh}$ , was evaluated by the standard Dittus-Boelter correlation [Dittus and Boelter 1985]:

$$h_{r,sh} = 0.023 \text{Re}_{sh}^{0.8} \text{Pr}_{sh}^{0.3} \frac{\lambda_{sh}}{d_i}, \quad \text{for } \frac{L}{d_i} \geq 10, \text{Re}_{sh} \geq 10^4, \text{Pr}_{sh} = 0.7 \sim 160 \quad (6.16)$$

where  $\lambda_{sh}$  is thermal conductivity of refrigerant in the superheated region,  $d_i$  the inner diameter of refrigerant tube, and  $L$  the tube length of a refrigerant circuit.

The convective heat transfer coefficient of refrigerant in the two-phase region,  $h_{r,tp}$ , was evaluated using the liquid refrigerant heat transfer coefficient,  $h_{r,L}$ , which was evaluated by [Shah 1979]:

$$h_{r,tp} = h_{r,L} \left[ (1-x)^{0.8} + \frac{3.8x^{0.76}(1-x)^{0.04}}{P_{re}^{0.38}} \right] \quad (6.17)$$

$$h_{r,L} = 0.023 \text{Re}_L^{0.8} \text{Pr}_L^{0.3} \frac{\lambda_L}{d_i} \quad (6.18)$$

where  $x$  is the thermodynamic vapor quality,  $\lambda_L$  thermal conductivity of liquid refrigerant, and  $P_{re}$  the reduced pressure, determined by [Shah 1979]:

$$P_{re} = \frac{P}{P_c} \quad (6.19)$$

where  $P$  is the actual compressor discharge pressure.  $P_c$  is the critical pressure for R22, and a value of 4.99 MPa was used.

Since the boundary of the two-phase region was moving during defrosting,  $h_{TPM}$ , a mean heat transfer coefficient of refrigerant in Eq. (6.15) was evaluated by Shah [1979] as:

$$h_{TPM} = h_{r,L} \left( 0.55 + \frac{2.09}{P_{re}^{0.38}} \right) \quad (6.20)$$

In Eq. (6.13),  $A_i$  is the total refrigerant tube surface area of each circuit,

$$A_i = \frac{A_{tube}}{3} \quad (6.21)$$

where  $A_{tube}$  is the total refrigerant tube surface area of the entire three-circuit outdoor coil.

Moreover, in Eqs. (6.2) and (6.13),  $q_j$  can also be evaluated by [Qu et al. 2012b, Ye and Lee 2013]:

$$q_j = m_{r,j} (h_{r,in} - h_{r,e}) \quad (j=1-3) \quad (6.22)$$

where  $m_{r,j}$  is the mass flow rate of refrigerant in Control Volume  $j$ . Enthalpies of refrigerant at both inlet and outlet of each circuit,  $h_{r,in}$  and  $h_{r,e}$ , were evaluated from the measured inlet and outlet refrigerant temperatures and the measured compressor discharge pressure.

Second stage: frost melting without water flowing away from a circuit

As shown in Fig. 6.2(b), energy conservation in Control Volume  $j$ , taking into account the convective heat transfer between water layer and ambient air, required:

$$q_j = L_{sf} m_{f,j} + c_p \frac{d(M_{w,j} T_{w,j})}{dt} + h_{c,w} (T_{w,j} - T_a) A_{f-a} + q_{Me} \quad (j=1-3) \quad (6.23)$$

where  $h_{c,w} (T_{w,j} - T_a) A_{f-a}$  is the heat transferred to ambient air from the effective airside surface area,  $A_{f-a}$ , which was covered by only the melted frost in Control Volume  $j$ . In the second and third stages,  $A_{f-a}$ , was evaluated by [Hu et al. 2011, Krakow et al. 1992b]:

$$A_{f-a} = A_0 \left( \frac{\int_0^t m_{f,j} dt}{M_{f,j}} \right)^{1.5} \quad (j=1-3) \quad (6.24)$$

Since the outdoor fan was turned off during the entire defrosting process, natural convection was the most important form to transfer the heat from the outdoor coil or the retained water to ambient air. The Nusselt Number and the corresponding coefficients of natural convective heat transfer were used [Jaluria 1980]:

$$Nu_L = \frac{h_c H}{\lambda_a} = 0.13(Gr Pr)^{\frac{1}{3}}, \quad \text{for } 10^9 < GrPr < 10^{13} \quad (6.25)$$

where

$$Gr = \frac{g\beta(T_w - T_a)}{\nu^2} H^3 \quad (6.26)$$

Furthermore, the heat transferred from the water layer to frost layer for melting the frost and to ambient air was:

$$h_w(T_{w,j} - T_{ip})A_0 = L_{sf}m_{f,j} + h_{c,w}(T_{w,j} - T_a)A_{f-a} \quad (j=1-3) \quad (6.27)$$

Third stage: frost melting with water flowing away from a circuit

Unlike in Stages 1, 2 or 4, as shown in Fig. 6.2(c), in this stage, there were differences for the energy and mass flows in the three control volumes, as the melted frost started to flow away from a circuit. For Circuit 1, no melted frost flowed into it as it was at the highest level, but the melted frost in this circuit flowed down into Circuit 2. For Circuit 2, the melted frost in this circuit flowed into Circuit 3. Finally, the melted frost in Circuit 3 flowed into water collecting Tray C and was collected by Cylinder C as shown in Fig. 6.1.

As shown in Fig. 6.2(c1), energy conservation in Control Volume 1 (Circuit 1) yielded:

$$q_1 = L_{sf}m_{f,1} + c_p M_{w,\max} \frac{dT_{w,1}}{dt} + c_p m_{w,1} T_{w,1} + h_{c,w} (T_{w,1} - T_a) A_{f-a} + q_{Me} \quad (6.28)$$

where  $M_{w,\max}$  is the maximum of the melted frost held on the surface of a refrigerant circuit.

Mass conservation in this control volume was:

$$m_{w,1} = m_{f,1} \quad (6.29)$$

For the other two control volumes, as shown in Figs. 6.2(c2) and 6.2(c3), energy conservation yielded:

$$q_j + c_p m_{w,j-1} T_{w,j-1} = L_{sf} m_{f,j} + c_p M_{w,\max} \frac{dT_{w,j}}{dt} + c_p m_{w,j} T_{w,j} + h_{c,w} (T_{w,j} - T_a) A_{f-a} + q_{Me}$$

(j=2,3) (6.30)

Mass conservation was:

$$m_{w,j} = m_{f,j} + m_{w,j-1} \quad (j=2,3) \quad (6.31)$$

Fourth stage: water layer vaporizing

In this stage, the surface of outdoor coil was free of frost, and the vaporization of the retained water took place. As illustrated in Fig. 6.2(d), energy conservation in Control Volume  $j$  yielded:

$$q_j = c_p \frac{d(M_{w,j} T_{w,j})}{dt} + h_{c,w} (T_{w,j} - T_a) A_{w-a} + h_{c,d} (T_{r,j} - T_a) A_{d-a} + m_{v,j} L_v + q_{Me}$$

(j=1-3) (6.32)

where  $h_{c,w} (T_{w,j} - T_a) A_{w-a}$  is the heat transferred to low temperature ambient air from water layer in Control Volume  $j$ , and  $h_{c,d} (T_{r,j} - T_a) A_{d-a}$  the heat transferred to ambient air from high temperature dry coil surface in Control Volume  $j$ .

Mass conservation in Control Volume  $j$  was:

$$M_{w,j} = M_{w,\max} - \int_0^t m_{v,j} dt \quad (j=1-3) \quad (6.33)$$

where  $m_{v,j}$  is the mass flow rate of the retained water vaporized from Circuit  $j$  and was proportional to the difference in vapor pressure between the exposed water surface and ambient air, as described by Mills [1999], expressed as:

$$m_{v,j} = h_D A_{w-a} (\rho_{vsj} - \rho_{va}) \quad (j=1-3) \quad (6.34)$$

In Eqs. (6.32) and (6.34),  $A_{w-a}$  is the effective wetted airside surface area of a refrigerant circuit. As the vaporizing process went on, the area was diminishing. The relationship between the effective wetted airside surface area and the equivalent airside surface area of a refrigerant circuit was [Hu et al. 2011, Krakow et al. 1992b]:

$$A_{w-a} = A_0 \left( \frac{M_{w,j}}{M_{w,\max}} \right)^{1.5} \quad (6.35)$$

Then, the effective dry airside surface area of a refrigerant circuit in this stage,  $A_{d-a}$ , was:

$$A_{d-a} = A_0 - A_{w-a} \quad (6.36)$$

Moreover, the coefficient of convective mass transfer,  $h_D$ , was related to the coefficient

of natural convective heat transfer,  $h_c$ , according to the Lewis Analogy [Threlkeld 1970, Padki et al. 1989]:

$$h_D = \frac{h_c}{c_p \rho_a (Le)^{\frac{2}{3}}} \quad (6.37)$$

where  $Le$  is the Lewis Number for air and water vapor mixtures and a fixed value of 0.845 was used in this study [Qu et al. 2012b].

#### **6.2.2.2 Model 2 development (only Stage 3)**

Schematics of mass and energy flows in defrosting Stages 1, 2 and 4 for Model 2 are the same as those for Model 1 shown in Fig. 6.2, except that in Stage 3 in Model 2, which is shown in Fig. 6.3. Hence, for Model 2, all the equations for Stages 1, 2 and 4 were identical to those in Model 1, except those for Stage 3.

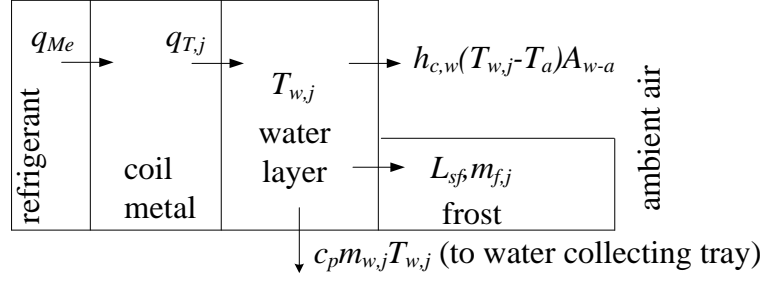


Fig. 6.3 Schematics of mass and energy flows in Stage 3 of defrosting for Model 2

In Stage 3, energy conservation in Control Volume  $j$  yielded:

$$q_j = L_{sf} m_{f,j} + c_p M_{w,\max} \frac{dT_{w,j}}{dt} + c_p m_{w,j} T_{w,j} + h_{c,w} (T_{w,j} - T_a) A_{f-a} + q_{Me} \quad (j=1-3) \quad (6.38)$$

where  $M_{w,\max}$  is the maximum of the melted frost held on the surface of Circuit  $j$ .

Mass conservation in Control Volume  $j$  was:

$$m_{w,j} = m_{f,j} \quad (j=1-3) \quad (6.39)$$

### 6.2.2.3 Modeling a water collecting tray and a water collecting cylinder

As part of the entire setup of the three-circuit outdoor coil, a mathematical sub-model for the heat and mass flows on a water collecting tray and a water collecting cylinder was also developed, and used together with the two Models. As seen from Fig. 6.1, for Model

1, the melted frost flowing away from the three circuits was collected by Cylinder C via Collecting Tray C. However, for Model 2, the melted frost flowing away from Circuits 1 to 3 was collected, by Cylinders A, B and C, via Collecting Trays A, B and C, respectively. As shown in Fig. 6.4, there were three steps for the process of the mass and energy flows in a water collecting tray during defrosting. Step 1 started during Stage 3 defrosting and the melted frost started to flow away from a refrigerant circuit and into a water collecting tray.

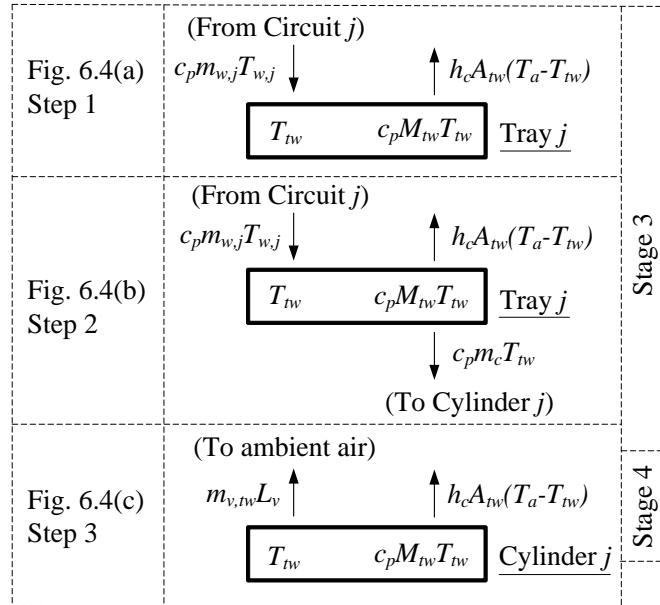


Fig. 6.4 Schematics of mass and energy flows in a water collecting tray and a water collecting cylinder during defrosting

The energy conservation of the melted frost collected on the tray in Step 1 required:

$$c_p m_{w,j} T_{w,j} = c_p \frac{d(M_{tw} T_{tw})}{dt} - h_c A_{tw} (T_a - T_{tw})$$

$$(j = 3 \text{ for Model 1 and } j = 1-3 \text{ for Model 2}) \quad (6.40)$$

where  $M_{tw}$  is the accumulated mass of the retained melted frost in the water collecting tray, which can be evaluated using Eq. (6.3). In addition,  $T_{w,j}$  is the temperature of the retained water on the surface of tubes and fins of each circuit (as shown in Fig. 6.1), and could be evaluated using Eqs. (6.28) and (6.30).  $T_{tw}$  is the temperature of the melted frost collected,  $T_a$  the temperature of ambient air during defrosting.

As the time went by, more and more water would be accumulated on the tray. When the melted frost started to flow away from the tray and into its connecting cylinder, Step 1 was ended and Step 2 started. As shown in Fig. 6.4(b), energy conservation in Step 2 yielded:

$$c_p m_{w,j} T_{w,j} = c_p M_{tw,\max} \frac{dT_{tw}}{dt} + c_p m_{w,j} T_{tw} - h_c A_{tw} (T_a - T_{tw})$$

$$(j = 3 \text{ for Model 1 and } j = 1-3 \text{ for Model 2}) \quad (6.41)$$

where  $M_{tw,\max}$  is the maximum mass of the retained water that can be held on the collecting tray.

When there was no more melted frost flowing away from the water collecting tray, Step 2 was ended and Step 3 commenced. As shown in Fig. 6.4(c), energy conservation for the collected melted frost in the cylinder in Step 3 required:

$$c_p \frac{d(M_{tw} T_{tw})}{dt} = m_{v,tw} L_v + h_c A_{tw} (T_a - T_{tw}) \quad (6.42)$$

where  $m_{v,tw}$  is the rate of vaporization for the melted frost vaporized from the cylinder.

As shown in Fig. 6.4(c), Step 3 started during Stage 3 defrosting, and ended after Stage 4 defrosting was over. Eqs. (6.40) - (6.42) are the governing equations for evaluating the temperatures of the melted frost collected in the collecting cylinder.

#### 6.2.2.4 The method of solving the two models

When solving the two semi-empirical models, Euler's method [Gerald and Wheatley 2003] was applied to solving all the differential Eqs. (6.2) - (6.4), (6.13), (6.22), (6.23), (6.27) - (6.33) and (6.38) - (6.42). The mass flow rate and temperature of the melted frost flowing away from a upper control volume were regarded as the same as those of the melted frost entering an adjacent lower control volume. Moreover, based on the Assumption (ix), the thermal properties of the retained water leaving the control volume were regarded as those of the melted frost collected in the respective water collecting cylinders. Fig. 6.5 shows the computational algorithm for the four defrosting stages for the two models.

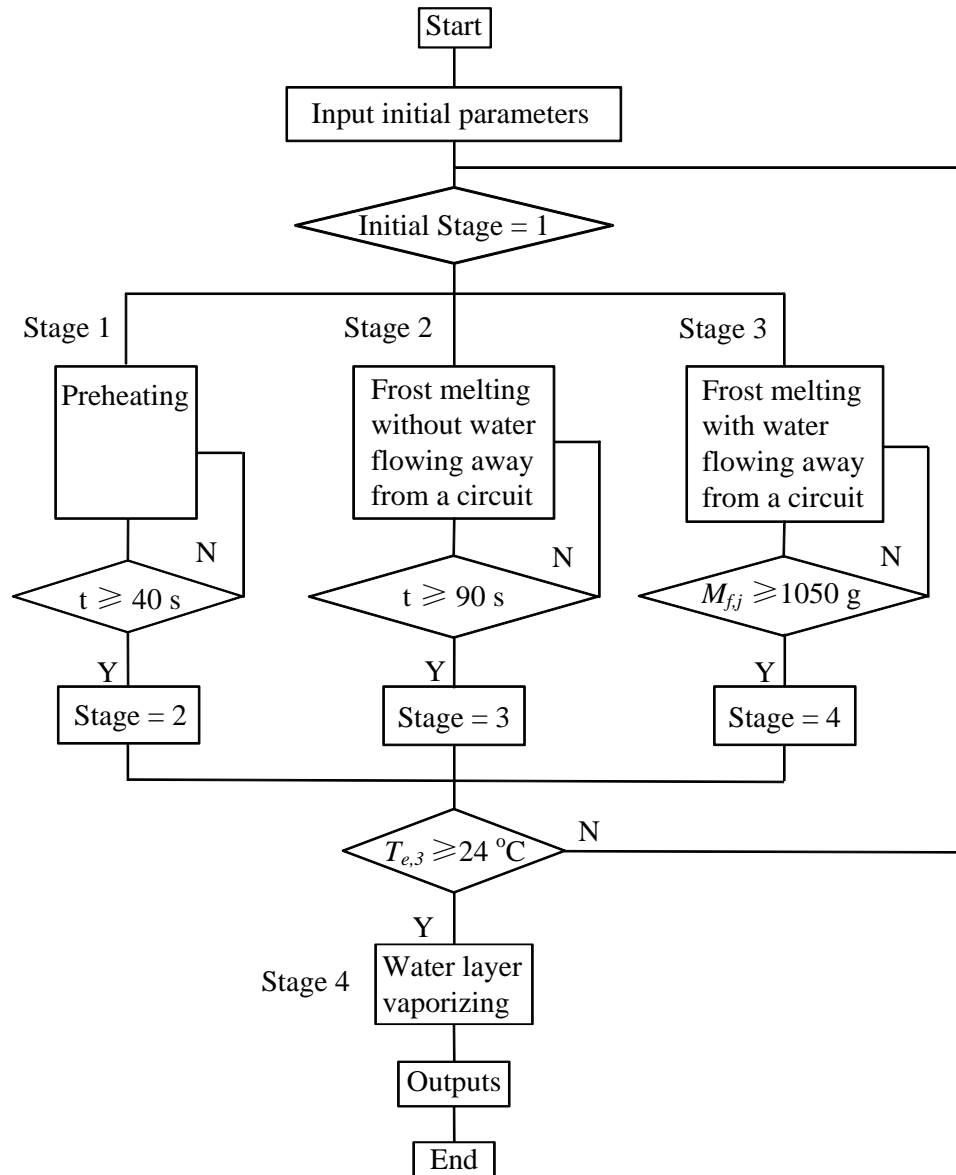


Fig. 6.5 The computational algorithm for the four defrosting stages in two models

### **6.3 Experimental validation of the two models**

The validation of the two empirical models developed was carried out by comparing the experimental data presented in Chapter 5 and the predicted data using the models for the key operating parameters of the experimental ASHP unit.

#### **6.3.1 Validation of Model 1**

Model 1 was validated by comparing the predicted defrosting duration, tube surface temperatures at exit of each circuit, temperature variations of the melted frost collected in Cylinder C and the total mass of the melted frost collected with the corresponding experimental data presented in Chapter 5.

Both measured and predicted tube surface temperatures at the exit of each circuit are shown in Fig. 6.6. Model 1 predicted that, at 186 s into defrosting process, the surface temperature at the exit of Circuit 3 reached 24 °C, the same as the experimental defrosting duration as reported. As seen from the diagram, the curves representing the predicted and the measured tube surface temperatures at the exits of the three circuits agreed very well during the entire defrosting process. Compared with the measured data, the maximum deviations of predicted results for Circuits 1-3 were -1.8 °C, -1.2 °C, and 2.4 °C respectively. The average deviations between measured and predicted results for Circuits 1-3 were -0.2 °C, 0 °C and 0.4 °C, respectively.

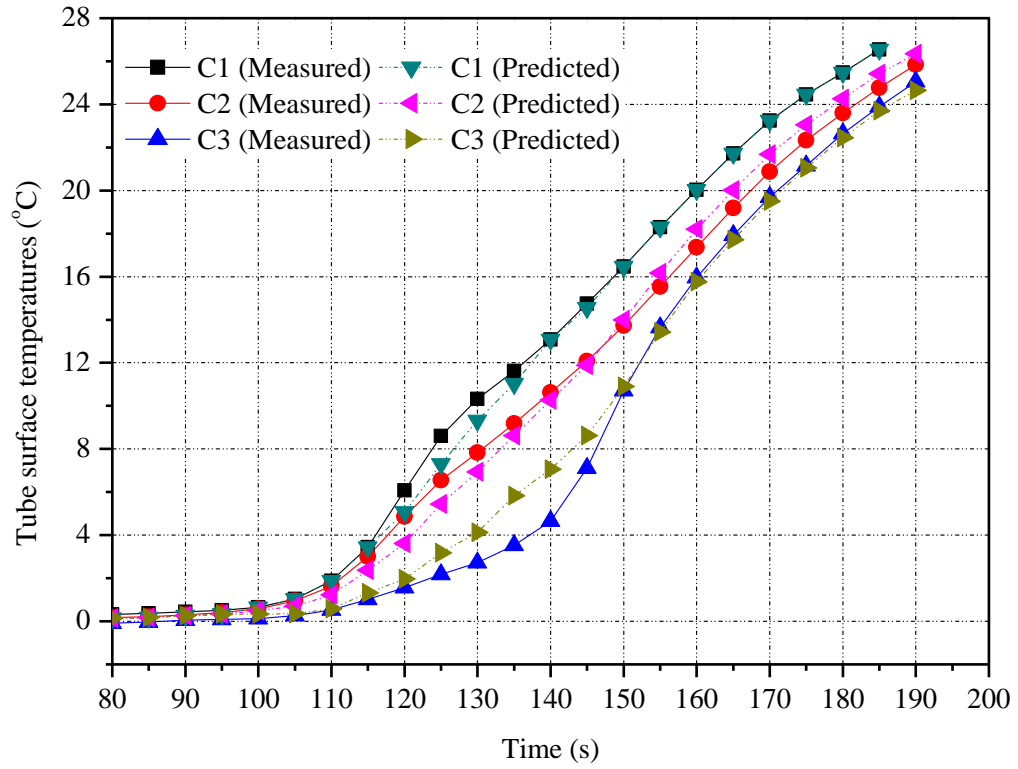


Fig. 6.6 Comparison between the measured and predicted tube surface temperatures at the exit of each circuit (Model 1)

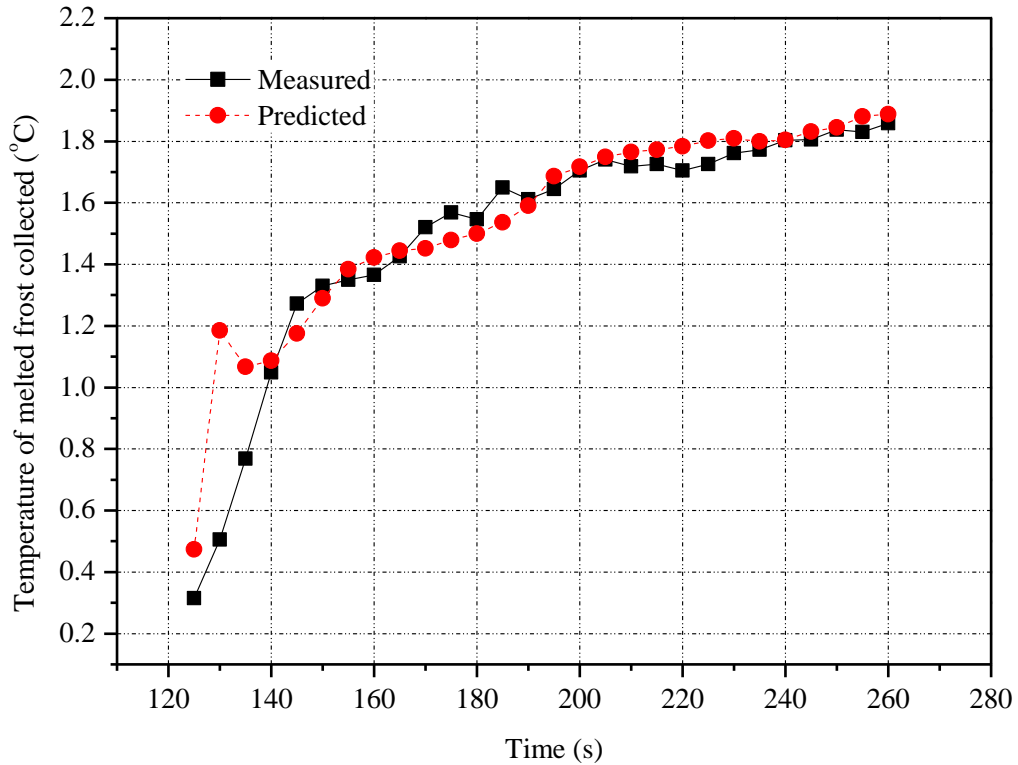


Fig. 6.7 Comparison between the measured and predicted temperatures of melted frost collected in Cylinder C (Model 1)

Fig. 6.7 shows the measured and predicted temperatures of the melted frost collected in Cylinder C. As seen in Fig. 6.7, the predicted temperature of the melted frost collected using the model developed agreed reasonably well with the experimental data. The maximum and average deviations between the measured and the predicted results were 0.68 °C and 0.05 °C, respectively.

Furthermore, as reported in Chapter 5, the experimental total mass of melted frost collected in Cylinder C was 931 g. Using Model 1, the predicted total melted frost mass was 933 g, with only 0.2% difference.

### 6.3.2 Validation of Model 2

Model 2 was validated by comparing the following four operating parameters: defrosting duration; tube surface temperatures at exit of each circuit; temperature variations of the melted frost collected in three water collecting cylinders and the mass of the melted frost collected in each cylinder.

The measured and predicted refrigerant tube surface temperatures at the exit of three circuits are shown in Fig. 6.8. Model 2 predicted that, at 168 s into defrosting process, the surface temperature at the exit of each circuit reached 24 °C, which was the same as the experimental results reported in Chapter 5. Overall, the curves representing the measured and predicted data agreed well during the entire defrosting process. Compared with the measured data, the maximum deviations of predicted results for Circuits 1-3 were 2.5 °C, -1.8 °C, and -1.2 °C respectively. The average deviations between measured and predicted results for Circuits 1 - 3 were 0.7 °C, -0.6 °C and -0.1°C, respectively.

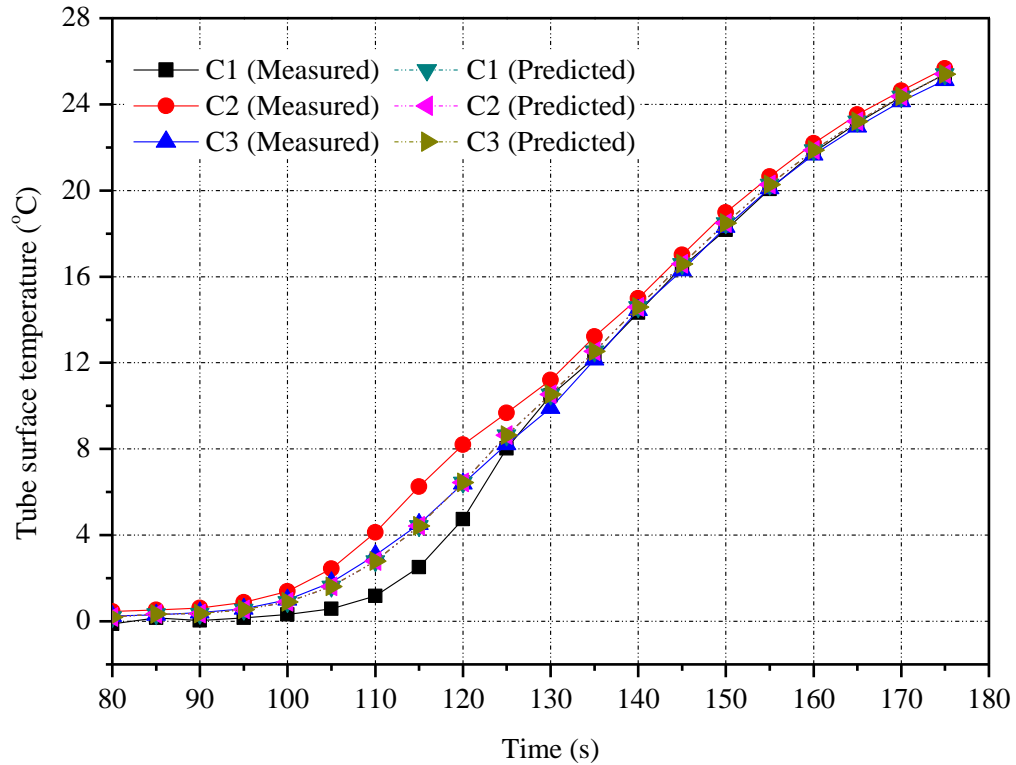


Fig. 6.8 Comparison between the measured and predicted tube surface temperatures at exits of the three circuits (Model 2)

Moreover, Figs. 6.9 - 6.11 show the measured and predicted temperatures of the melted frost collected in each of the three water collecting cylinders. Fig. 6.9 shows the measured and predicted temperatures of the melted frost collected in Cylinder A during defrosting. As seen, the predicted temperature of the melted frost collected in the cylinder agreed well with the experimental results. For melted frost collected in Cylinders B and C, their predicted and measured temperatures also agreed reasonably well, as shown in Figs. 6.10 and 6.11, respectively. Compared with the measured data, the maximum deviations of predicted results for melted frost collected in Cylinders A, B and C were 0.084 °C, 0.085 °C, and 0.068 °C respectively. The average deviations between measured and predicted results were 0.002 °C, 0.002 °C and 0.010°C, respectively.

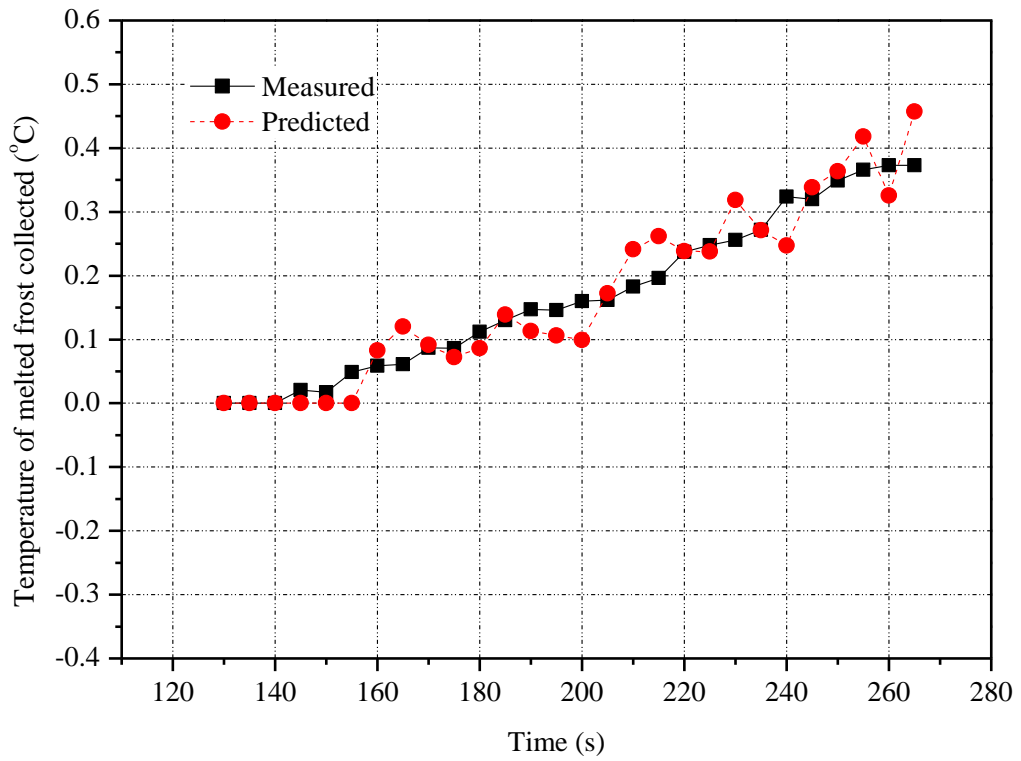


Fig. 6.9 Comparison between the measured and predicted temperatures of melted frost collected in Cylinder A (Model 2)

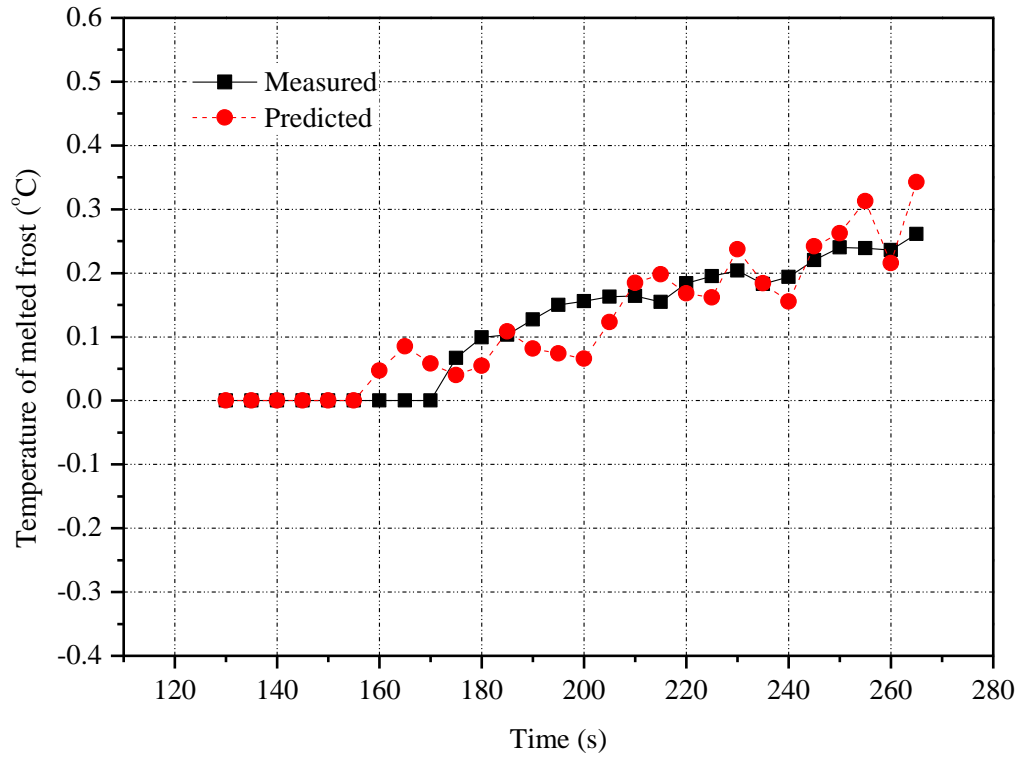


Fig. 6.10 Comparison between the measured and predicted temperatures of melted frost collected in Cylinder B (Model 2)

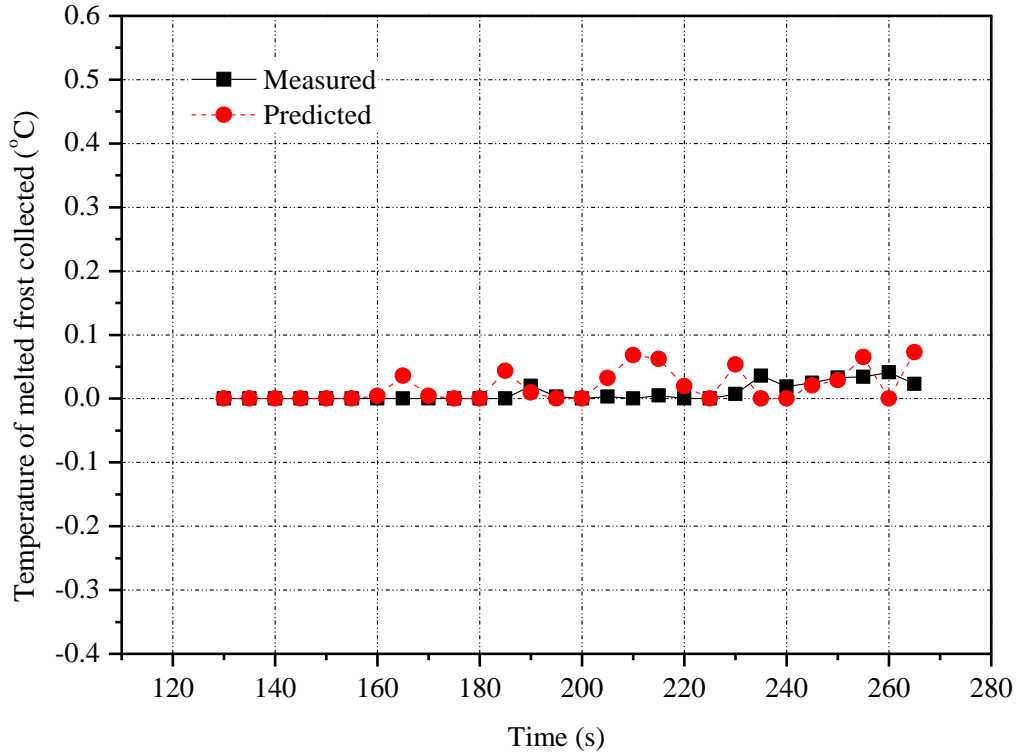


Fig. 6.11 Comparison between the measured and predicted temperatures of melted frost collected in Cylinder C (Model 2)

Furthermore, using Model 2, the predicted mass of the melted frost collected in Cylinders A, B, and C were all at 327 g. As reported separately in Chapter 5, their corresponding experimental values were 317 g, 328 g and 324 g, respectively. Therefore, the largest difference was only at 3% for Cylinder A.

From the comparisons presented above, it was considered that the two empirical models were experimentally validated, and the validated models can be further used to quantitatively analyze the defrosting performances of an ASHP unit as discussed in Section 6.4.

## **6.4 Discussions**

### **6.4.1 Potential uses of the two models developed**

The two experimentally validated semi-empirical models can have a number of potential applications. Firstly, they can be used to quantitatively analyze not only the negative effects of melted frost downwards flowing due to gravity, but also the impacts of locally draining away the melted frost using water collecting trays on reverse cycle defrosting performance in an ASHP unit. Secondly, the two models can be used to optimize the design of an outdoor coil, and positioning water collecting trays. Thirdly, a number of operating parameters for an ASHP unit, which are difficult to measure experimentally, could be predicted. For example, frost melting rate and the temperature of retained water over the surface of outdoor coil. Fourthly, with the validated models, energy consumptions on melting frost, vaporizing the melted frost, heating low temperature ambient air, and heating the outdoor coil metal during a reverse cycle defrosting process could be evaluated. Finally, the models can be used to assist exploring novel operational and control strategies for better defrosting performances of a multi-circuit outdoor coil during reverse cycle defrosting.

#### **6.4.2 Limitations of the modeling work**

Although the two models were developed based on energy and mass flows conservations, there existed a few limitations. Those included the nine assumptions listed in Section 6.2.1, which were necessary in model developments, but introduced errors to the models. However, there errors were still within acceptable levels. Moreover, certain empirical formulas were used, such as the Eq. (6.20), which had their limitations. Furthermore, experimental data were also used in assisting the model developments, thereby making the two models empirical. Therefore, appropriate modifications might have to be introduced when the models are to be used for studying ASHP units with different configurations or operating conditions. Nonetheless, the models developed could adequately describe the defrosting performance for the experimental ASHP unit with local drainage of the melted frost from its outdoor coil.

## **6.5 Conclusions**

Following on the experimental study on draining away locally the melted frost for an experimental ASHP unit having three refrigerant circuits using water collecting trays between circuits reported in Chapter 5, a modeling study on the defrosting process taking place at the specially made three-circuit outdoor coil, at the two experimental settings of with and without the use of water collecting trays between circuits was carried out and is reported in this Chapter. Two empirical models, corresponding to the two settings, were therefore developed and validated. The validated models could adequately describe the defrosting performance for the experimental ASHP unit with local drainage of the melted frost from its outdoor coil.

As briefly mentioned in Section 6.4.1, the models developed can have a number of potential applications. Therefore, in the next Chapter, a modeling study on alleviating uneven defrosting for the experimental three-circuit outdoor coil using the model developed is presented.

Programs of Model 1 in this Chapter, written in Matlab R2012a, are listed in Appendix B.

## **Chapter 7**

# **A Modeling Study on Alleviating Uneven Defrosting for the Experimental Three-circuit Outdoor Coil during Reverse Cycle Defrosting**

### **7.1 Introduction**

In Chapter 5, the experimental study on the defrosting performance of the experimental ASHP unit when the melted frost was drained away locally from its specially-made three-circuit outdoor coil was carried out and reported. In addition, to enable further quantitative analysis on the effects of locally draining away the melted frost on reverse cycle defrosting performance in the experimental ASHP unit with the three-circuit outdoor coil, two semi-empirical mathematical models, corresponding to the two experimental settings were developed, and experimentally validated, and are reported in Chapter 6. The validated models could be used to adequately describe the defrosting performance for the experimental ASHP unit with local drainage of the melted frost from its outdoor coil, and their potential applications are briefly discussed in Section 6.4.1.

While the outcomes from the studies reported in the last two Chapters demonstrated the effectiveness of locally draining away the melted frost from a vertically installed multi-circuit outdoor coil, for existing ASHP units, however, it is hardly possible to install water collecting trays between circuits. Nonetheless, for existing ASHP units, it is still possible

to vary the heat input to each refrigerant circuit through varying refrigerant supply to each circuit. This is because uneven defrosting was fundamentally caused by different thermal loads imposed to each circuit due to the downwards flowing of the melted frost on the surface of a multi-circuit outdoor coil, when the supply of refrigerant or heat to each circuit was the same. Consequently, if the heat to be supplied to each circuit may be varied according to the actual defrosting thermal load each circuit is to deal with, then the problem of uneven defrosting may be alleviated. Modulating valves installed at an inlet refrigerant pipe to each circuit may be deployed to vary the refrigerant flow thus heat input to each circuit.

In this Chapter, using one of the developed empirical models reported in Chapter 6, a modeling study on varying heat (via refrigerant flow) supply to each refrigerant circuit in the specially-made experimental three-circuit outdoor coil to alleviate uneven defrosting is reported. Firstly, the methodology and three study cases are explained. Secondly, the results of the modeling study on defrosting durations and energy use in the three study cases are presented. Finally, a conclusion is given.

## **7.2 Methodology and study cases**

The modeling study reported in this Chapter was carried out using the previously developed and validated semi-empirical mathematical model at the experimental setting of without the use of water collecting trays between circuits, which is reported in Chapter 6. In this Section, the three study cases are firstly detailed. This is followed by presenting the assumptions used for the three study cases.

### **7.2.1 The three study cases**

When an ASHP unit operates at defrosting mode, usually the refrigerant discharged from compressor is equally distributed into each circuit of multi-circuit outdoor coil. However, as the melted frost flows downwards along the surface of outdoor coil due to gravity, the heating load for each refrigerant circuit becomes different. In this modeling study, therefore, to alleviate the uneven defrosting due to the downwards flowing of melted frost for the experimental three-circuit vertical outdoor coil during reverse cycle defrosting, three study cases were included where different openings of modulating valves were applied so as to vary the heat supply to each of the three circuits. Table 7.1 details the opening of valves and other operational changes in the three cases, which are respectively explained as follows:

Table 7.1 Valves opening of modulating and other operational changes in the three study cases

Case No.	Opening of modulating valve	Other operational changes
Case 1	The opening values of three valves on each circuit, from top to bottom, were fixed at 92.5%, 97.8% and 100%, respectively.	None
Case 2	Fully open all valves at the start of defrosting, and fully close the modulating valve on Circuit 1 when its tube surface temperature at exit reaches 24 °C.	None
Case 3	Fully open all valves at the start of defrosting, and fully close the modulating valve on Circuit 1 when its tube surface temperature at exit reaches 24 °C.	Keep the refrigerant flows to Circuit 2 and Circuit 3 unchanged by reducing compressor speed to 66.7% of the original speed when the modulating valve on Circuit 1 is closed.

## Case 1

In the experimental study reported in Chapter 5, the defrosting durations for the 3 circuits, from top to bottom, were 172 s, 182 s, and 186 s, respectively, when the supplies of the refrigerant mass to the three circuits were the same, as shown in Fig. 7.1. In other words, the defrosting durations for the top and the middle circuits were 92.5% and 97.8%, respectively, of that for the bottom circuit. Study Case 1 was then designed, where the modulating valve for the bottom circuit was fully opened and the openings of the modulating valve for the top and middle circuits were set at 92.5% and 97.8% of full opening, respectively. In this way, the heat supplies to the three circuits via the supply of refrigerant during defrosting were no longer the same, and the assumed refrigerant mass flow rates to each circuit during defrosting are shown in Fig. 7.2.

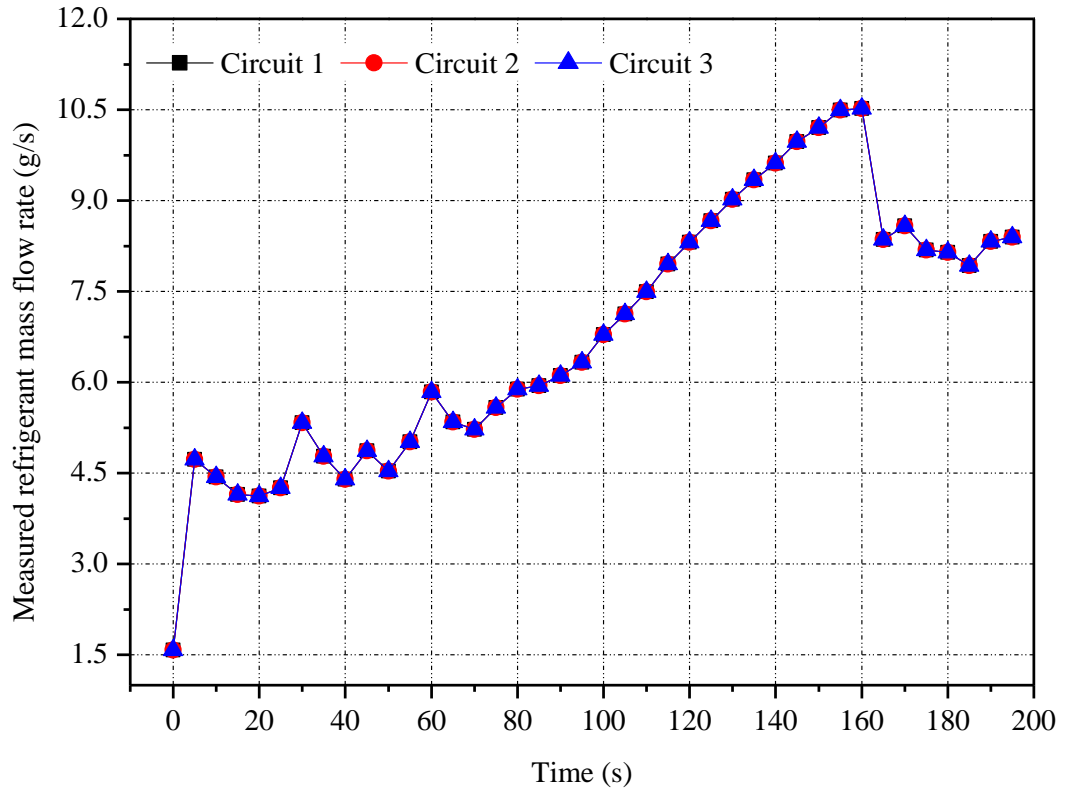


Fig. 7.1 Measured refrigerant mass flow rate

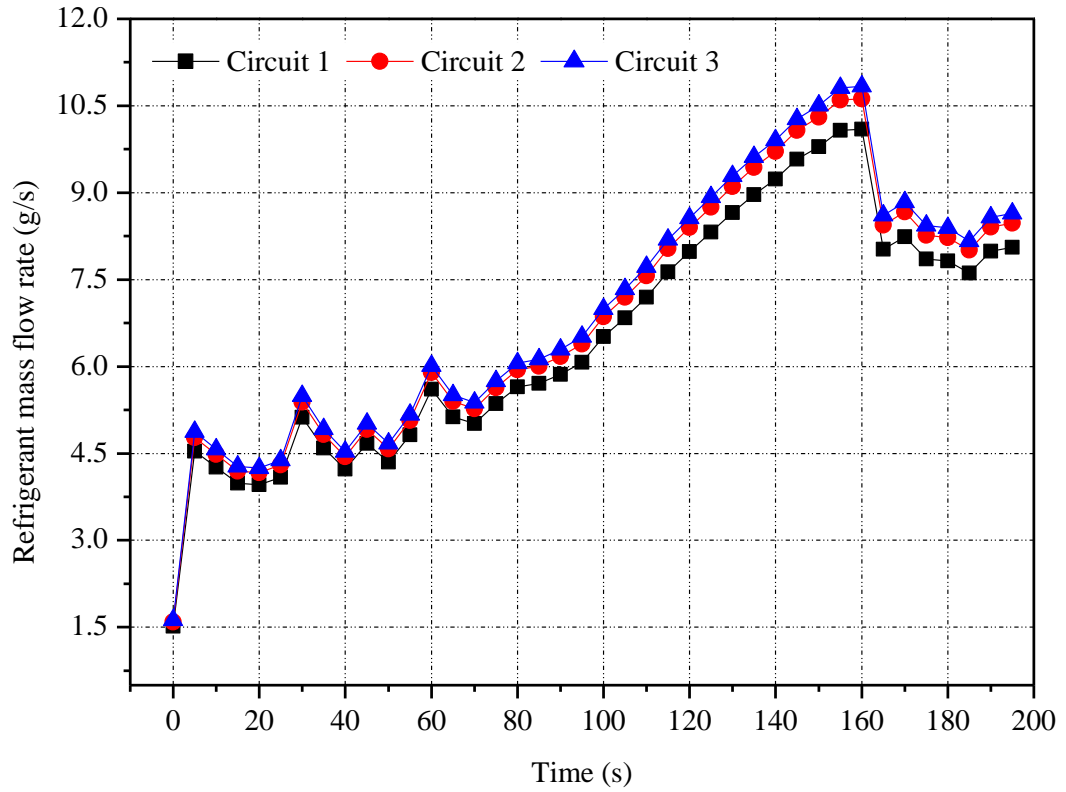


Fig. 7.2 Assumed refrigerant mass flow rates to three circuits in Study Case 1

## Case 2

The results from the experimental study reported in Chapter 5 also revealed that the defrosting duration for Circuit 1 was the shortest. Hence, it was also possible to vary the heat input to the three refrigerant circuits by fully closing the modulating valve on Circuit 1 when its tube surface temperature at exit reached 24 °C [Qu et al. 2012a, 2012b]. Therefore, in Study Case 2, it was designed that the three valves on the three circuits were fully open at the start of defrosting. When the tube surface temperature at exit on Circuit 1 reached 24 °C, its modulating valve would be fully closed. Consequently, more refrigerant would flow into the other two refrigerant circuits to speed up their defrosting. Fig. 7.3 shows the assumed refrigerant mass flow rates to each circuit during defrosting in Case 2.

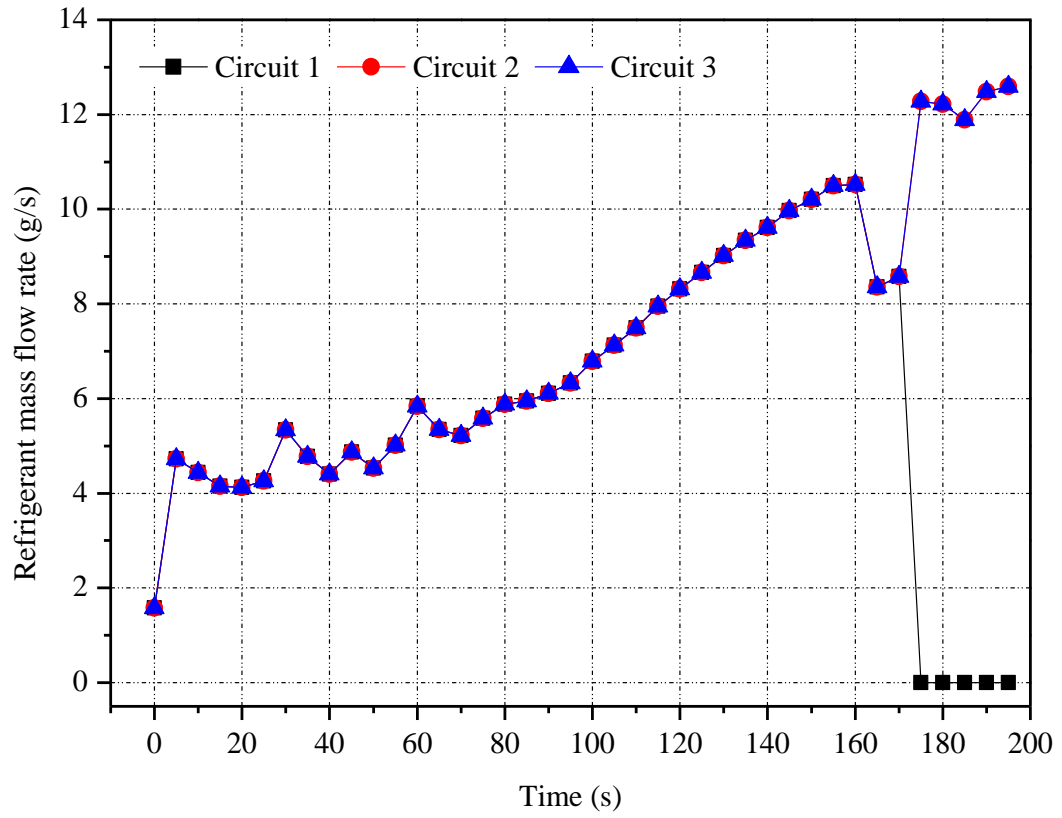


Fig. 7.3 Assumed refrigerant mass flow rates to three circuits in Study Case 2

### Case 3

In Study Case 2, when the modulating valve on Circuit 1 was closed, the refrigerant flow rates to the other two circuits were increased. To possibly reduce defrosting energy consumption, however, it was possible to decrease compressor speed so that the refrigerant flow rates to Circuit 2 and Circuit 3 remained unchanged. Therefore, in Study Case 3, it was designed that the three modulating valves on the three circuits were fully open at the start of defrosting. When the tube surface temperature at the exit on Circuit 1 reached 24 °C, its modulating valve would also be fully closed, same as that in Study Case 2. However, compressor speed was also reduced by 1/3 at the same time. The assumed refrigerant mass flow rates to each circuit during defrosting in Study Case 3 are shown in Fig. 7.4.

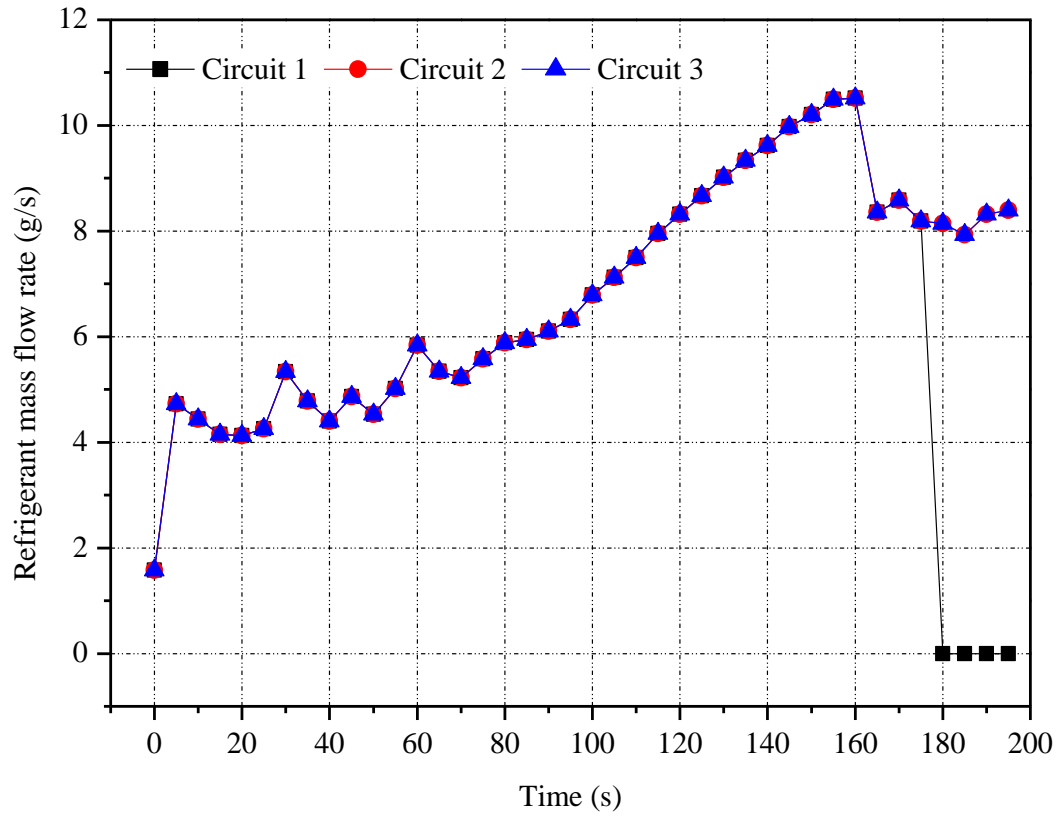


Fig. 7.4 Assumed refrigerant mass flow rates to three circuits in Study Case 3

### 7.2.2 The assumptions used in the modeling study

The following were assumed:

- i). In the three study cases, the refrigerant mass flow rate passing through a modulating valve to each circuit during defrosting was assumed to be positively correlated to the respective percentage openings of the three modulating valves, under a constant total refrigerant flow rate. For example, when the percentage openings of valves are 50% for the valve on Circuit 1, 100% for the valves on Circuit 2 and Circuit 3, respectively, the ratio of the three valves' openings is 1:2:2, and thus the percentage shares of the total refrigerant mass flow rate passing through the three modulating valves are 20%, 40%, and 40%, respectively. The assumed refrigerant mass flow rates to each circuit during defrosting in Case 1 shown in Fig. 7.2 were derived following this assumption;
- ii). In Case 2, the total refrigerant mass flow was evenly distributed to the other two refrigerant circuits during defrosting after the modulating valve on Circuit 1 was closed. As a result, the refrigerant mass flow rate to Circuit 2 and Circuit 3 was each increased by 50%;
- iii). In Case 3, as the modulating valve on Circuit 1 was closed, the refrigerant mass flow in Circuit 2 and Circuit 3 remained unchanged, as a result of compressor speed reduction by 33%;

- iv). When the tube surface temperature at the exit of a refrigerant circuit reached 24 °C, the defrosting operation on that circuit was considered ended;
- v). The defrosting duration for the ASHP unit was the same as that of Circuit 3.

### **7.3 Modeling results**

Using the validated empirical model at the setting of without the use of water collecting trays, as reported in Chapter 6, a modeling study for the three study cases was undertaken and the study results are shown in Figs. 7.5 - 7.7 for the three study cases. In addition, to illustrate the effectiveness of varying heat supply to respective refrigerant circuit, the results of the experimental study reported in Chapter 5, and modeling study for the setting of without the use of water collecting trays between circuits reported in Chapter 6, are also presented in Figs. 7.8 to 7.9 for comparison purposes. In Figs. 7.5 - 7.9, for their time (horizontal) axis, although defrosting starts at 0 s, 80 s is the chosen time point for these figures in order to more clearly show the temperature rise during defrosting. Further, Table 7.2 summarizes the defrosting durations in the three study cases and in the previous experimental and simulation studies. In addition, for the results presented here for the three study cases, the time difference in defrosting duration between Circuit 1 and Circuit 3,  $\Delta t$ , was used as a parameter to indicate the degree of uneven defrosting.

#### Case 1

Fig. 7.5 shows the variations of the predicted tube surface temperatures at the exit of each circuit in Study Case 1. It can be seen that the defrosting durations for Circuit 2 and Circuit 3 were shortened, but that for Circuit 1 was slightly extended, as compared to the experimental and simulation results shown in Figs. 7.8 and 7.9. This was because the refrigerant supply to each circuit was no longer the same. Following the Assumption i) specified in Section 7.2.2, as shown in Fig. 7.2, the refrigerant mass flow rate during defrosting in Circuit 1 is decreased, and that in Circuit 3 increased, as compared to the experimental data shown in Fig. 7.1. The simulation results suggested that the defrosting durations were 178 s for Circuit 1 and Circuit 2, and 183 s for Circuit 3, respectively. Compared to the results from the reported experimental and modeling studies, the defrosting duration for Circuit 3 or the ASHP unit was decreased by 3 s, or  $\sim 1.6\%$ . Also, as seen,  $\Delta t$  was 5 s, which is much shorter than the experimental value of 13 s, suggesting that the uneven defrosting was significantly alleviated.

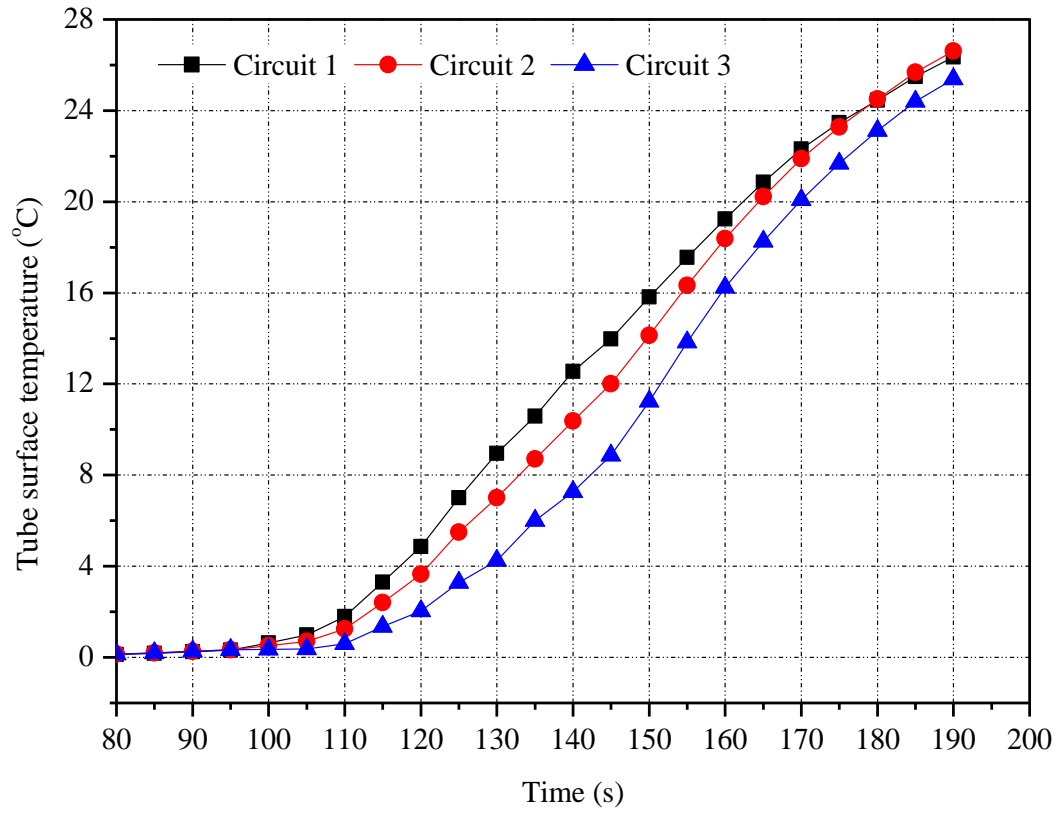


Fig. 7.5 Predicted tube surface temperatures at circuit exits (Case 1)

## Case 2

Fig. 7.6 shows the variations of the predicted tube surface temperatures at the exit of each circuit in Study Case 2. When the tube surface temperature at the exit of Circuit 1 reached 24 °C at 173 s into defrosting, its modulating valve was closed, so that, the refrigerant supply to Circuit 1 was reduced to 0 g/s. At the same time, since the compressor speed remained unchanged, the refrigerant supplies to Circuit 2 and Circuit 3 were consequently increased, as shown in Fig. 7.3. As a result of the increase in refrigerant mass flow rate, it can be seen from Fig. 7.6 that the tube surface temperatures were increased for Circuit 2 and Circuit 3, but decreased for Circuit 1 after closing valve. The simulation results demonstrated that the defrosting for durations were 173 s for Circuit 1, 176 s for Circuit 2, and 179 s for Circuit 3, respectively. Compared to the results of the reported experimental and modeling studies, the defrosting duration for Circuit 3 or the ASHP unit was decreased by 7 s, or about 3.8%. The value of  $\Delta t$  was 6 s, also suggesting the alleviated uneven defrosting.

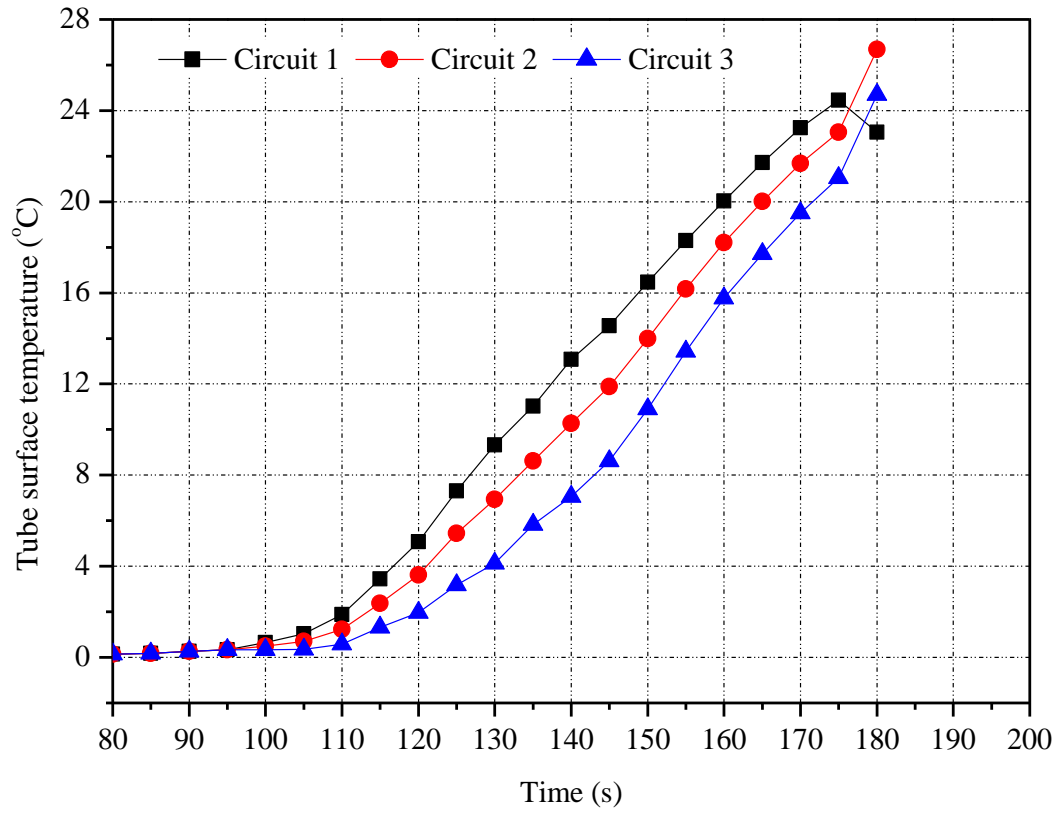


Fig. 7.6 Predicted tube surface temperatures at circuit exits (Case 2)

### Case 3

Fig. 7.7 shows the variations of the predicted tube surface temperatures at the exit of each circuit in Study Case 3. As shown in Fig. 7.4, when the modulating valve on Circuit 1 was closed at 172 s into defrosting, its refrigerant mass flow rate was reduced to 0 g/s. For the other two circuits, the refrigerant mass flow rates remained unchanged after compressor speed was reduced by 1/3. As seen, the surface temperature for Circuit 1 was reduced after closing the valve, but those for Circuit 2 and Circuit 3 continued their increasing trend. The simulation results showed that the defrosting durations were 172 s for Circuit 1, 182 s for Circuit 2, and 186 s for Circuit 3, respectively. Unlike the other two study cases, the defrosting duration for Circuit 3 or the ASHP unit was not changed, when compared with the results of the reported studies. However,  $\Delta t$  was slightly increased by 1 s to 14 s, suggesting that the problem of uneven defrosting remained.

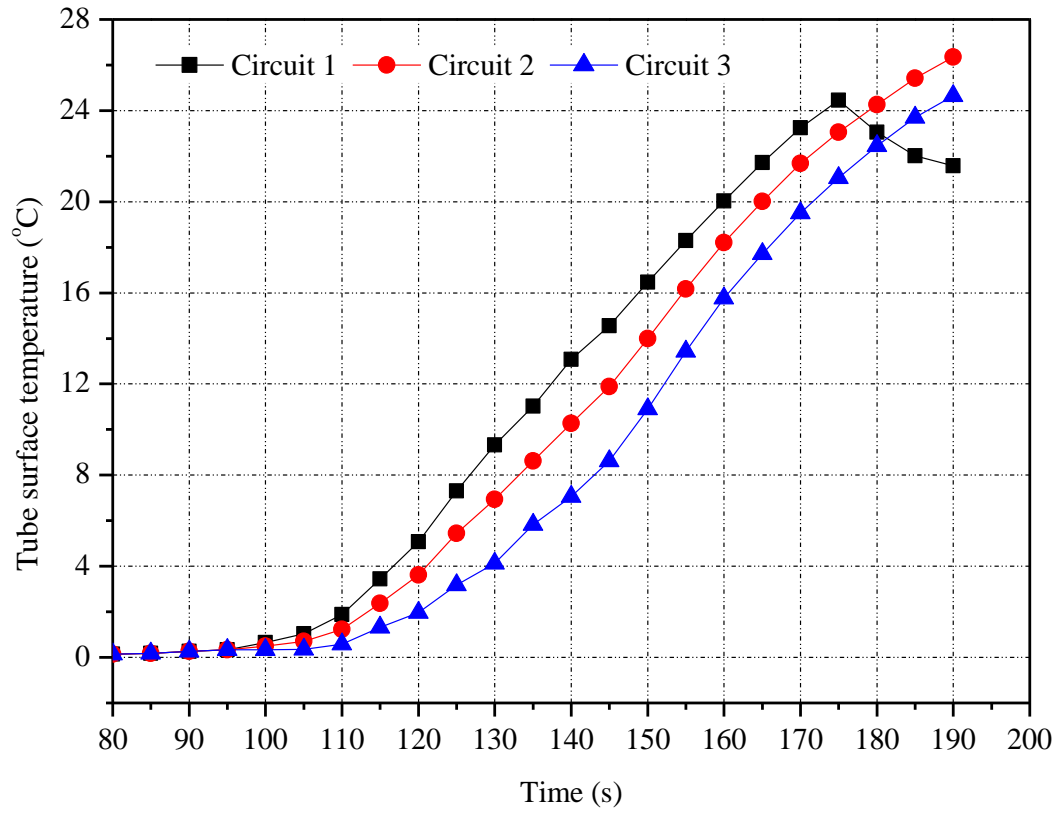


Fig. 7.7 Predicted tube surface temperatures at circuit exits (Case 3)

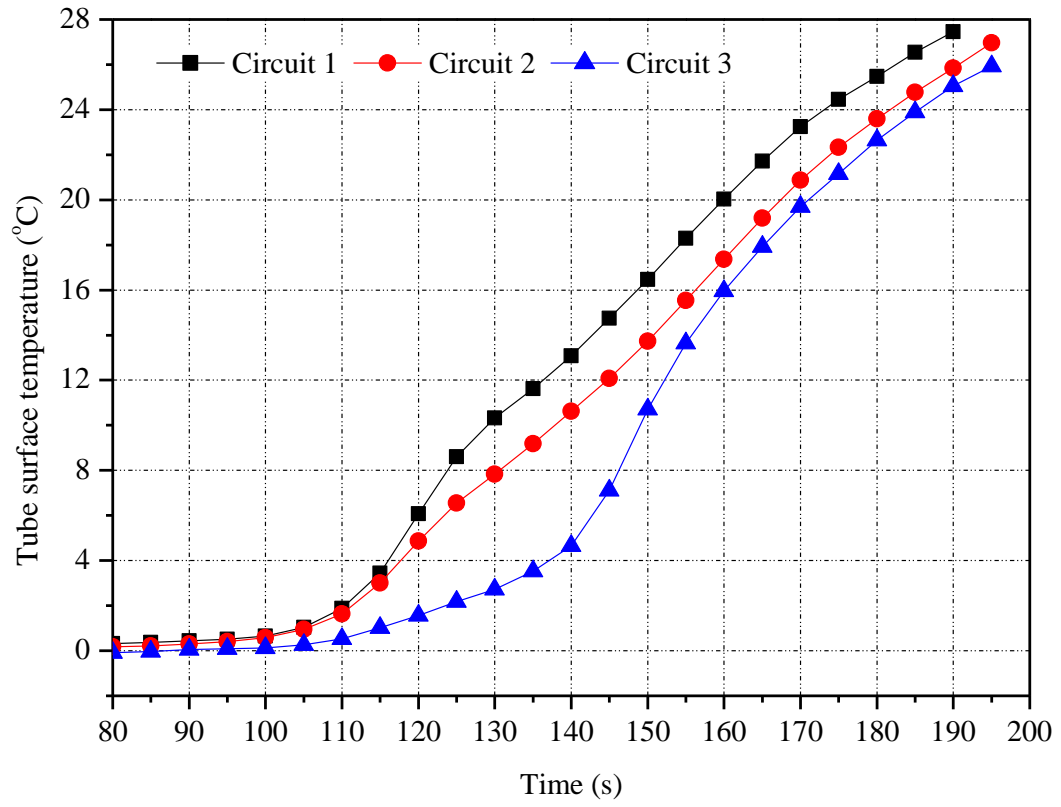


Fig. 7.8 Measured tube surface temperatures at circuit exits

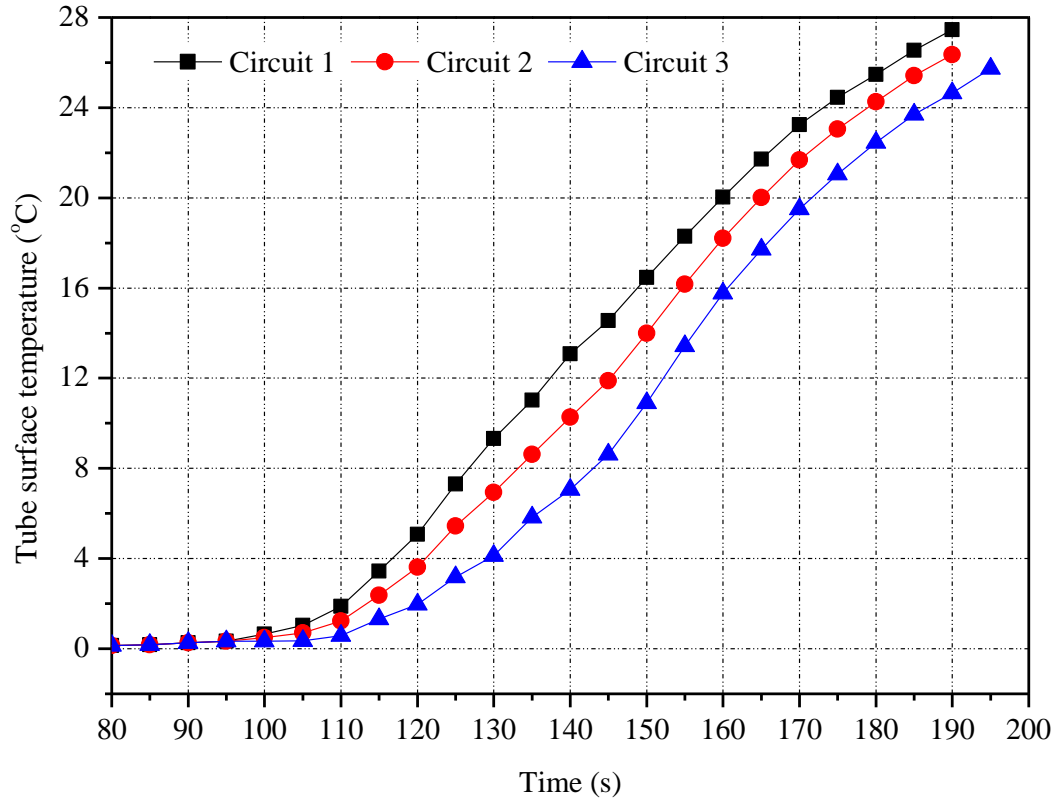


Fig. 7.9 Predicted tube surface temperatures at circuit exits

The simulation results for the three study cases are summarized in Table 7.2, where the results of the experimental and simulation studies reported in Chapters 5 and 6 are also included. It can be seen from the Table that for the three cases, Case 2 appeared to be the better one in terms of shortening the defrosting duration with the shortest duration of 179 s. Also it can be seen from the Table 7.2, the values of  $\Delta t$  for Case 1 and Case 2 were significant smaller than the experimental value and that for Case 3, suggesting that using the methods in Case Studies 1 and 2 can help alleviate uneven defrosting for a better defrosting performance. However, since different defrosting durations for the three study cases were resulted in, the energy use for defrosting was therefore different. This is further discussed in Section 7.4.

Table 7.2 Defrosting durations in the three study cases and in the previous experimental and modeling studies

Case No.	Defrosting durations for each circuit			$\Delta t$ (s)	Results shown in
	Circuit 1	Circuit 2	Circuit 3		
Case 1	178	178	183	5	Fig. 7.5
Case 2	173	176	179	6	Fig. 7.6
Case 3	172	182	186	14	Fig. 7.7
Experimental	173	181	186	13	Fig. 7.8
Simulation	172	180	186	14	Fig. 7.9

$\Delta t$  : time difference in defrosting durations between Circuit 1 and Circuit 3.

#### 7.4 Energy use for defrosting in the three study cases

For an ASHP unit, during reverse cycle defrosting, the energy is used to heat the outdoor coil metal, melt frost, heat the melted frost, heat the cold ambient air, and evaporate the retained water on the surface of outdoor coil. In this study, the total energy use for defrosting was also evaluated for the three study cases, 715.9 kJ for Case 1, 693.4 kJ for Case 2, and 727.4 kJ for Case 3, respectively. Compared with the experimental of 732.7 kJ, the defrosting energy uses in the three study cases were all less, with that defrosting energy use in Study Case 2 being the lowest at about 94.6% of the experimental value.

It is noted that in Study Case 3, compressor speed was reduced by 1/3 for possible energy saving after the tube surface temperature at the exit on Circuit 1 reached 24 °C. However,

since the total durations of defrosting operation was longer than that in Study Case 2, the total energy use in Study Case 3 was more than that in Study Case 2, and slightly lower than the experimental value.

## **7.5 Conclusions**

A modeling study on alleviating uneven defrosting for a vertical three-circuit outdoor coil in an ASHP unit during reverse cycle defrosting was undertaken and the study results are reported in this Chapter. Three study cases were included and study results suggested that the best operating defrosting performances in terms of defrosting durations and energy use were achieved in Study Case 2. Further experimental studies to validate the modeling results presented in this Chapter can be carried out. However, it is expected that with more refrigerant circuits in an outdoor coil in an ASHP unit, the method of fully closing the modulating valves on top circuits will yield better defrosting performance for the ASHP unit, as predicted by the modeling study reported in this Chapter.

## **Chapter 8**

### **Conclusions and Future Work**

#### **8.1 Conclusions**

A research project on improving defrosting performances of an ASHP unit having a multi-circuit outdoor coil has been successfully carried out and is reported in this thesis.

The conclusions of the thesis are:

- 1) An experimental study on the negative effects of allowing downwards flowing of melted frost over a vertically installed experimental three-circuit outdoor coil in an experimental ASHP unit on defrosting performance during reverse cycle defrosting has been undertaken and reported. Three experimental study cases, with different arrangements of water collecting trays placed between or under circuit(s), were designed. The temperatures of tube surface at the exits of each refrigerant circuit, coil fin surface at the center of each circuit, and the melted frost collected were measured. The experimental results and corresponding quantitative analysis, as reported in Chapter 5, revealed the negative effects of allowing melted frost to freely flow downwards due to gravity over the airside surface of the vertically installed experimental three-circuit outdoor coil in the experimental ASHP unit on defrosting performances during reverse cycle defrosting: a longer defrosting duration and more energy consumption. In addition,

the experimental study results also suggested that the use of water collecting trays between circuits for locally draining away the melted frost before flowing into down circuit(s) was effective in mitigating these negative effects.

- 2) In Chapter 6, a mathematical modeling study on the defrosting performance for the experimental ASHP unit with local drainage of the melted frost from its vertically installed three-circuit outdoor coil. Two semi-empirical mathematical models, corresponding to two settings of with and without the use of water collecting trays between circuits, were developed. In this modeling study, a defrosting process on the airside of an outdoor coil was divided into four stages: (1) preheating, (2) frost melting without water flowing away from a circuit, (3) frost melting with water flowing away from a circuit, and (4) water layer vaporizing. The two semi-empirical models were validated by comparing the experimental data obtained in the experimental study reported in Chapter 5, and the predicted data using the models for the key operating parameters of the experimental ASHP unit, with good agreements. The validated models in this chapter could adequately describe the defrosting operation for the experimental ASHP unit with local drainage of the melted frost from its vertically installed three-circuit outdoor coil.
- 3) To explore the potential methods of alleviating the negative effects of downwards flowing of melted frost and thus improving the defrosting performances of an existing ASHP unit, a modeling study on alleviating uneven defrosting for the

vertically installed three-circuit outdoor coil in the experimental ASHP unit during reverse cycle defrosting was carried out using the empirical models reported in Chapter 6 and the study results are reported in Chapter 7. To alleviate uneven defrosting for an existing ASHP unit having a multi-circuit outdoor coil, it can be effective to vary the heat supply (via refrigerant flow) to each refrigerant circuit by varying the openings of modulating valves installed at an inlet pipe to each circuit. Three study cases, with different mechanisms of both varying the openings of modulating valves and introducing other operational changes, were designed and corresponding modeling studies carried out using the validated semi-empirical model developed at the setting of without the use of water collecting trays between circuits reported in Chapter 6. Modeling results suggested that the best defrosting performances in terms of shortening defrosting durations and reducing defrosting energy use were achieved in the study case of fully closing the modulating valve on the top circuit when its tube surface temperature at the exit of the circuit reached defrosting termination point.

The project reported in this thesis has made important contributions to the advancement of heat pump technology through improving the defrosting performances of an ASHP unit having a multi-circuit outdoor coil. The use of water collecting trays between circuits could help minimize the negative effects of downwards flowing of the melted frost during reverse cycle defrosting. In addition, two semi-empirical models developed could be used to adequately describe the defrosting operation for the experimental ASHP unit with local drainage of the melted frost from its vertically installed three-circuit outdoor coil, and

therefore, may be used in further follow-up studies for improving the operating performance of ASHP units during reverse cycle defrosting, including the modeling study reported in Chapter 7. Finally, the proposed control method of fully closing the modulating valve on the top circuit when its tube surface temperature at the exit of the circuit reached defrosting termination point could be used to improve the defrosting performances for an existing ASHP unit having a multi-circuit outdoor coil. The long-term significance of the project reported in this thesis is that the outcomes helped increase operating energy efficiency of, and enhance the reliability of ASHP units. This would in turn encourage a wider use of ASHP units, contributing to energy conservation and sustainable development worldwide.

## 8.2 Proposed future work

A number of future studies following on the successful completion of the project reported in this thesis are proposed:

- 1) To ensure that frost accumulated on the surface of the three circuits of the experimental outdoor coil was even for the experimental study reported, in Chapter 5, a series of manually adjusting the degree of opening of stop valves, through trial-and-error approach to adjust the refrigerant flow into each circuit, such that the amount of frost accumulation on each of the three circuits was close to each other (difference  $< 10\%$ ). Therefore, a better control method to ensure the frost evenly accumulated on the surface of a multi-circuit outdoor coil should be explored.
- 2) As reported in Chapter 6, in developing the two semi-empirical models, there existed a number of limitations, including assumptions and empirical formulas, and using experimental data, etc. Therefore, appropriate modifications to the models reported in Chapter 6 might have to be further introduced when the models are to be used for studying ASHP units with different configurations or operating conditions.
- 3) The project reported in this thesis was based on a three-circuit outdoor coil. For ASHP units with larger capacity, more circuits will be used in their outdoor coils.

However, their operating performance during reverse cycle defrosting may be more complex, deserving further detailed studies experimentally and mathematically.

- 4) As reported in Chapter 7, the best defrosting performances in terms of shortening defrosting durations and reducing defrosting energy use were achieved in the study case of fully closing the modulating valve on the top circuit when its tube surface temperature at the exit of the circuit reached defrosting termination point. It is expected that with more refrigerant circuits in an outdoor coil in an ASHP unit, the method of fully closing the modulating valves on top circuit(s) would yield better defrosting performance for the ASHP unit. However, further experimental studies to validate the modeling results are to be carried out.

## References

- [1] Abdel-Wahed et al. 1983  
Abdel-Wahed, R.M., Hifni, M.A. and Sherif, S.A.  
Hot water defrosting of a horizontal flat plate cooling surface. *International Journal of Refrigeration*, Vol. 6, No. 3, pp. 152-154 (1983)
- [2] Aihara et al. 1997  
Aihara, T., Taku, O., Toshiyuki, S. and Hitoshi, K.  
Heat-transfer and defrosting characteristics of a horizontal array of cooled tubes immersed in a very shallow fluidized bed. *International Journal of Heat and Mass Transfer*, Vol. 40, No. 8, pp. 1807-1815 (1997)
- [3] Aganda et al. 2000a  
Aganda, A. A., Coney, J.E.R., Farrant, P.E., Sheppard, C.G.W. and Wongwuttanasatian, T.  
A comparison of the predicted and experimental heat transfer performance of a finned tube evaporator. *Applied Thermal Engineering*, Vol. 20, No. 6, pp. 499-513 (2000)
- [4] Aganda et al. 2000b  
Aganda, A. A., Coney, J.E.R. and Sheppard, C.G.W.  
Airflow maldistribution and the performance of a packaged air conditioning unit evaporator. *Applied Thermal Engineering*, Vol. 20, No. 6, pp. 515-528 (2000)
- [5] Alebrahim and Sherif 2002  
Alebrahim, Al.M. and Sherif, S.A.  
Electrical defrosting analysis of a finned tube evaporator coil using the enthalpy method. *Proceedings of the Institution of Mechanical Engineers, Part C: Journal of Mechanical Engineering Science*, Vol. 216, No. 6, pp. 655-673 (2002)
- [6] Allard and Heinzen 1988  
Allard, J. and Heinzen, R.  
Adaptive defrost. *Industry Applications, IEEE Transactions on* Vol. 24, pp. 39-42 (1988)
- [7] Al-Mutawa and Sherif 1998a  
Al-Mutawa, N.K. and Sherif, S.A.

- An analytical model for hot-gas defrosting of a cylindrical coil cooler, Part I: Model development. *ASHRAE Transactions*, Vol. 104, Part 1, pp. 1722-1730 (1998)
- [8] Al-Mutawa and Sherif 1998b  
Al-Mutawa, N.K. and Sherif, S.A.  
An analytical model for hot-gas defrosting of a cylindrical coil cooler, Part II: Model results and conclusions. *ASHRAE Transactions*, Vol. 104, Part 1, pp. 1731-1737 (1998)
- [9] Ameen et al. 1993  
Ameen, F.R., Coney, J.E.R. and Sheppard, C.G.W.  
Experimental study of warm-air defrosting of heat-pump evaporators. *International Journal of Refrigeration*, Vol. 16, No. 1, pp. 13-18 (1993)
- [10] Anand et al. 1989  
Anand, N.K., Schiesing J.S., O'Neal, D.L. and Peterson, K.T.  
Effects of outdoor coil fan pre-start on pressure transients during the reverse cycle defrost of heat pump. *ASHRAE Transactions*, Vol. 95, Part 2, pp. 699-704 (1989)
- [11] Arkar et al. 2007  
Arkar, C., Vidrih, B. and Medved, S.  
Efficiency of free cooling using latent heat storage integrated into the ventilation system of a low energy building. *International Journal of Refrigeration*, Vol. 30, No. 1, pp. 134-143 (2007)
- [12] Rahman and Jacobi 2012  
Ashiqur Rahman M and Jacobi, A.M.  
Drainage of frost melt water from vertical brass surfaces with parallel microgrooves. *International Journal of Refrigeration*, Vol. 55, pp. 1596-1605 (2012)
- [13] ASHRAE 2007  
ASHRAE  
*Handbook of HVAC Applications* (2007)
- [14] Bajnoczy et al. 1999  
Bajnoczy, G., Pálffy, E.G., Prépostffy, E. and Zöld, A.  
Heat storage by two grade phase change material. *Periodica Polytechnica-Chemical Engineering*, Vol. 43, No. 2 , pp. 137-147 (1999)
- [15] Bansal et al. 2010

- Bansal, P., Fothergill, D. and Fernandes, R.  
Thermal analysis of the defrost cycle in a domestic freezer. *International Journal of Refrigeration*, Vol. 33, No. 3, pp. 589-599 (2010)
- [16] Barrow 1985  
Barrow, H.  
A note on frosting of heat pump evaporator surfaces. *Heat Recovery System*, Vol. 5, No. 3, pp. 195-201 (1985)
- [17] Bertsch and Groll 2008  
Bertsch, S.S. and Groll, E.A.  
Two-stage air-source heat pump for residential heating and cooling applications in northern U.S. climates. *International Journal of Refrigeration*, Vol. 31, No. 7, pp. 1282-1292 (2008)
- [18] Byun et al. 2006  
Byun, J.S., Jeon, C.D., Jung, J.H. and Lee, J.  
The application of photo-coupler for frost detecting in an air-source heat pump. *International Journal of Refrigeration*, Vol. 29, No. 2, pp. 191-198 (2006)
- [19] Byun et al. 2008  
Byun, J.S., Lee, J. and Jeon, C.D.  
Frost retardation of an air-source heat pump by the hot gas bypass method. *International Journal of Refrigeration*, Vol. 31, No. 2, pp. 328-334 (2008)
- [20] Cai et al. 2011  
Cai, L., Wang, R.H., Hou, P.X. and Zhang, X.S.  
Study on restraining frost growth at initial stage by hydrophobic coating and hygroscopic coating. *Energy Buildings*, Vol. 43, pp. 1159-1163 (2011)
- [21] Chen et al. 2006  
Chen, C., Ouyang, J., Wang, X.L. and Liu, M.  
New method of heat compensation for defrosting of air source heat pump system in winter. *Journal of Refrigeration (in Chinese)*, Vol. 27, No. 4, pp. 37-40 (2006)
- [22] Chen et al. 2009  
Chen, Y.G., Guo, X.M. and Yang, Z.  
Dynamic defrosting characteristics of air source heat pump and effects of outdoor air parameters on defrost cycle performance. *Applied Thermal Engineering*, Vol. 29, No. 13, pp. 2701-2707 (2009)
- [23] Chen et al. 2012

- Chen, W., Qu, L.J., Wang, C., Yu, Z.T. and Wang J.H.  
An experimental investigation of the performance of an air-source heat pump hot-water system based on saltwater energy towers. *Journal of Zhejiang University (Engineering Science)*, Vol. 46, No. 8, pp. 1485-1489 (2012)
- [24] Cheng and Seki 1991  
Cheng, K.C. and Seki, N.  
Freezing and melting heat transfer in engineering: selected topics on ice-water systems and welding and casting processes. *Taylor & Francis*. 1991
- [25] Cheng and Shiu 2002  
Cheng, C.H. and Shiu, C.C.  
Frost formation and frost crystal growth on a cold plate. *International Journal of Heat and Mass Transfer*, Vol. 45, No. 21, pp. 4289-4303 (2002)
- [26] Cho et al. 2005  
Cho, H., Kim, Y. and Jang, I.  
Performance of a showcase refrigeration system with multi-evaporator during on-off cycling and hot-gas bypass defrost. *Energy*, Vol. 30, No. 10, pp. 1915-1930 (2005)
- [27] Choi et al. 2011  
Choi, H.J., Kim, B.S., Kang, D. and Kim, K.C.  
Defrosting method adopting dual hot gas bypass for an air-to-air heat pump. *Applied Energy*, Vol. 88, No. 12, pp. 4544-4555 (2011)
- [28] Da Silva et al. 2011  
Da Silva, D. L., Hermes, C. J. and Melo, C.  
Experimental study of frost accumulation on fan-supplied tube-fin evaporators. *Applied Thermal Engineering*, Vol. 31, pp. 1013-1020 (2011)
- [29] Datta and Tassou 1997  
Datta, D. and Tassou, S.  
Frost prediction on evaporator coils of supermarket display cabinets using artificial neural networks. *Proceedings of CLIMA 2000 Conference*, Brussels, Belgium, pp. 98 (1997)
- [30] Ciricillo 1995  
Ciricillo, S. F.  
Heat pump de-icing/controlling for energy conservation and costs. *In Proceedings of the Clima 2000 Congress on Heating, Ventilation and Air Conditioning*, Copenhagen, pp. 87-92 (1985)

- [31] Datta and Tassou 2002  
Datta, D. and Tassou, S.  
Implementation of a defrost on demand control strategy on a retail display cabinet. *Proceedings of IIF-IIR=COMMISSION D1/B1*, Urbana, IL, USA (2002)
- [32] Ding et al. 2004a  
Ding, Y.J. Ma, G.Y. and Chai, Q.H.  
Experiment investigation of reverse cycle defrosting methods on air source heat pump with TXV as the throttle regulator. *International Journal of Refrigeration*, Vol. 27, pp. 617-678 (2004)
- [33] Ding et al. 2004b  
Ding, Y.J., Chai, Q.H., Ma, G.Y. and Jiang Y.  
Experimental study of an improved air source heat pump. *Energy Conversion and Management*, Vol. 45, pp. 2393-2403 (2004)
- [34] Dittus and Boelter 1985  
Dittus, F.W. and Boelter, L.M.K.  
Heat transfer in automobile radiators of the tubular type. *International Communications in Heat and Mass Transfer*, Vol.12, No.1, pp. 3-22 (1985)
- [35] Domingorena and Ball 1980  
Domingorena, A.A. and Ball, S.J.  
Performance evaluation of a selected three-ton air-to-air heat pump in the heating mode. *ORNT/CON-34. Oak Ridge National Laboratory* (1980)
- [36] Dong et al. 2012  
Dong, J.K., Deng, S.M., Jiang Y.Q., Xia, L. and Yao, Y.  
An experimental study on defrosting heat supplies and energy consumptions during a reverse cycle defrost operation for an air source heat pump. *Applied Thermal Engineering*, Vol. 37, pp. 380-387 (2012)
- [37] Dopazo et al. 2010  
Dopazo, A.J., Fernandez-Seara, J., Uhía, F. J. and Diz, R.  
Modeling and experimental validation of the hot-gas defrost process of an air-cooled evaporator. *International Journal of Refrigeration*, Vol. 33, No. 4, pp. 829-839 (2010)
- [38] Eckman 1987  
Eckman, R.L.  
Heat pump defrost controls: a review of past, present, and future technology. *ASHRAE Transactions*, Vol. 93, Part 1 , pp. 1152-1156 (1987)

- [39] Emery and Siegel 1990  
Emery, A.F. and Siegel, B.L.  
Experimental measurements of the effects of frost formation on heat exchanger performance. *Proceedings of AIAA/ASME Thermo Physics and Heat Transfer Conference*, ASME HTD 139, pp. 1-7 (1990)
- [40] Esen and Ayhan 1996  
Esen, M. and Ayhan, T.  
Development of a model compatible with solar assisted cylindrical energy storage tank and variation of stored energy with time for different phase change materials. *Energy Conversion Management*, Vol. 37, No. 12, pp. 1775-1785 (1996)
- [41] Factor and Grossman 1980  
Factor, H. and Grossman, G.A.  
A packed bed dehumidifier/regenerator for solar air-conditioning with liquid desiccants. *Journal of Solar Energy Engineering*, Vol. 24, pp. 541-550 (1980)
- [42] Fei and Mao 2000  
Fei, Q. and Mao, Y.B.  
Research on defrost of air cooler by use of compressed air jet sweeping. *Mechanical and Electrical Equipment*, Vol. 5, pp. 8-12 (2000)
- [43] Fossa and Tanda 2002  
Fossa, M. and Tanda, G.  
Study of free convection frost formation on a vertical plate. *Experimental Thermal and Fluid Science*, Vol. 26, No. 6-7, pp. 661-668 (2002)
- [44] Fu et al. 2009  
Fu, W.C., Guo, X.M. and Tao, X.C.  
Experiment on a novel defrost cycle for air source heat pump. *Journal of Refrigeration (in Chinese)*, Vol. 30, No. 3, pp. 16-24(2009)
- [45] Gerald and Wheatley 2003  
Gerald, C.F. and Wheatley, P.O.  
Applied numerical analysis, 7th ed. *Addison-Wesley Publishing Co.* 2003
- [46] Gong et al. 2007  
Gong, J.Y., Yuan, X.L., Huang, D. and Zhang, X.Q.

- Influence of airflow maldistribution on performance of air-to-water heat pump system under frosting conditions. *Journal of Xi'an Jiaotong University (in Chinese)*, Vol. 41, No. 9, pp. 1058-1061 (2007)
- [47] Goodman and Shea 1960  
Goodman, T.R. and Shea, J.J.  
The melting of finite slabs. *Journal of Applied Mechanics*, Vol. 27, pp. 16-24 (1960)
- [48] Gu et al. 2004  
Gu, Z., Liu, H. and Li, Y.  
Thermal energy recovery of air conditioning system-heat recovery system calculation and phase change materials development. *Applied Thermal Engineering*, Vol. 24, No. 17-18, pp. 2511-2526 (2004)
- [49] Guo et al. 2006  
Guo, X.M., Chen, Y.G., Wang, W.H. and Chen, C.Z.  
Effects of outdoor air parameters on frosting characteristics of fin-tube evaporator for air source heat pump unit. *Journal of Refrigeration(in Chinese)*, Vol. 27, No. 6, pp. 29-33 (2006)
- [50] Guo et al. 2008  
Guo, X.M., Chen, Y.G., Wang, W.H. and Chen, C.Z.  
Experimental study on frost growth and dynamic performance of air source heat pump system. *Applied Thermal Engineering*, Vol. 28, No. 17-18, pp. 2267-2278 (2008)
- [51] Hambraeus 1995  
Hambraeus, K.  
Heat transfer of oil-contaminated HFC134a in a horizontal evaporator. *International Journal of Refrigeration*, Vol. 18, No. 2, pp. 87-99 (1995)
- [52] Hao et al. 2002  
Hao, Y. L., Iragorry, J., Castro, D., Tao, Y. X. and Jia, S.  
Microscopic characterization of frost surface during liquid-ice phase change period. *Proceedings of the 2002 ASME International Mechanical Engineering Congress & Exposition*, New Orleans, LA, No. IMECE2002-32797 (2002)
- [53] Hayashi et al. 1977  
Hayashi, Y., Aoki, A., Adachi, S. and Hori, K.  
Study of frost properties correlating with frost formation types. *Journal of Heat Transfer*, Vol. 99, No. 2, pp. 239-244 (1977)

- [54] He et al. 2003  
He, Z., Peng, X., Xing, Z. and Shu, P.  
Operating characteristics of an air-source heat pump under frosting defrosting conditions. *Proceedings of the Institution of Mechanical Engineers, Part A: Journal of Power and Energy*, Vol. 217, No. 6, pp. 623-629 (2003)
- [55] Heinzen 1988  
Heinzen, R. A.  
How adaptive defrost maintains refrigeration system efficiency. *Australian Refrigeration, Air Conditioning and Heating*, Vol. 42, No. 4, pp.16-16 (1988)
- [56] Heo et al. 2010  
Heo, J., Jeong, M.W. and Kim, Y.  
Effects of flash tank vapor injection on the heating performance of an inverter-driven heat pump for cold regions. *International Journal of Refrigeration*, Vol. 33, No. 6, pp. 848-855 (2010)
- [57] Hewitt and Huang 2008  
Hewitt, N. and Huang, M.J.  
Defrost cycle performance for a circular shape evaporator air source heat pump. *International Journal of Refrigeration*, Vol. 31, No. 3, pp. 444-452 (2008)
- [58] Hoffenbecker et al. 2005  
Hoffenbecker, N., Klein, S.A. and Reindl, D.T.  
Hot gas defrost model development and validation. *International Journal of Refrigeration*, Vol. 28, No. 4, pp. 605-615 (2005)
- [59] Hosoda and Uzuhashi 1967  
Hosoda, T. and Uzuhashi, H.  
Effects of frost on the heat transfer coefficient. *Hitachi Review*, Vol. 16, No. 6, pp. 254-259 (1967)
- [60] Hu 2010  
Hu, W.J.  
Study on the dynamic characteristic of a novel PCM based defrosting for air source heat pump. PhD Thesis (in Chinese), Harbin Institute of Technology, (2010)
- [61] Hu et al. 2011  
Hu, W.J., Jiang, Y.Q., Qu, M.L., Yao, Y. and Deng, S.M.  
An experimental study on the operating performance of a novel reverse-cycle hot gas defrosting method for air source heat pumps. *Applied Thermal Engineering*, Vol. 31, No. 2, pp. 363-369 (2011)

- [62] Huang et al. 1998  
Huang, H., Shu, P.C. and Li, Z.H.  
Experimental study of operating characteristics under frosting in air source heat pump water chiller/heater. *Fluid Machinery*, Vol. 12, pp. 43-47 (1998)
- [63] Huang et al. 2004  
Huang, D., Yuan, X.L. and Zhang, X.Q.  
Effects of fan-starting methods on the reverse-cycle defrost performance of an air-to-water heat pump. *International Journal of Refrigeration*, Vol. 27, No. 8, pp. 869-875 (2004)
- [64] Huang et al. 2007  
Huang, D., He, Z.L. and Yuan, X.L.  
Dynamic characteristics of an air-to-water heat pump under frosting/defrosting conditions. *Applied Thermal Engineering*, Vol. 27, No. 11-12, pp. 1996-2002 (2007)
- [65] Huang et al. 2008  
Huang, J.M., Hsieh, W.C., Kea, X.J. and Wang, C.C.  
The effects of frost thickness on the heat transfer of finned tube heat exchanger subject to the combined influence of fan types. *Applied Thermal Engineering*, Vol. 28, No. 7, pp. 728-737 (2008)
- [66] Huang et al. 2009  
Huang, D., Li, Q. and Yuan, X.  
Comparison between hot-gas bypass defrosting and reverse-cycle defrosting methods on an air-to-water heat pump. *Applied Energy*, Vol. 86, No. 9, pp. 1697-1703 (2009)
- [67] Huang et al. 2013  
Huang, D., Ri-Jing, Z., Liu, Y. and Yi, D.B.  
Effect of fin types of outdoor fan-supplied finned-tube heat exchanger on periodic frosting and defrosting performance of a residential air-source heat pump. *Applied Thermal Engineering*, Vol.69, pp. 251-260 (2014)
- [68] Irarorri and Tao 2005  
Irarorri, J. and Tao, Y.X.  
Frost temperature relations for defrosting sensing system. *Journal of Heat Transfer*, Vol. 127, No. 3, pp. 344-349 (2005)
- [69] Ismail and Jesus 2001  
Ismail, K.A.R. and Jesus, A.B.

Parametric study of solidification of PCM around a cylinder for ice-bank applications. *International Journal of Refrigeration*, Vol. 24, No. 8, pp. 809-822 (2001)

- [70] Ismail et al. 2001  
Ismail, K.A.R., Alves, C.L.F. and Modesto, M.S.  
Numerical and experimental study on the solidification of PCM around a vertical axially finned isothermal cylinder. *Applied Thermal Engineering*, Vol. 21, No. 1, pp. 53-77 (2001)
- [71] Jhee et al. 2002  
Jhee, S., Lee, K.S. and Kim, W.S.  
Effect of surface treatments on the frosting/defrosting behavior of a fin-tube heat exchanger. *International Journal of Refrigeration*, Vol. 25, No. 8, pp. 1047-1053 (2002)
- [72] Jain and Bansal 2007  
Jain, S. and Bansal, P.K.  
Performance analysis of liquid desiccant dehumidification systems. *International Journal of Refrigeration*, Vol. 30, pp. 861-872 (2007)
- [73] Jaluria 1980  
Jaluria, Y.  
Natural convection, HMT, the science and applications of heat and mass transfer. Vol. 5. *Pergamon Press*, New York (1980)
- [74] Jones and Parker 1975  
Jones, B.W. and Parker, J.D.  
Frost formation with varying environmental parameters. *Journal of Heat Transfer*, Vol. 97, No. 2, pp. 255-259 (1975)
- [75] Kelly and Bean 1977  
Kelly, G. and Bean, J.  
Dynamic performance of a residential air-to-air heat pump. *National Bureau of Standards Building Science Series*, BSS 93, Washington, D.C., March (1977)
- [76] Kim et al. 2006  
Kim, Y., Tikhonov, A., Shin, Y. and Lee, J.  
Experimental study on high performance defrosting heater for household refrigerator. *13th International Heat Conference*, Sydney, Australia (2006)
- [77] Kim et al. 2009a  
Kim, J.H., Braun, J.E. and Groll, E.A.

A hybrid method for refrigerant flow balancing in multi-circuit evaporators: Upstream versus downstream flow control. *International Journal of Refrigeration*, Vol. 32, No. 6, pp. 1271-1282 (2009)

- [78] Kim et al. 2009b  
Kim, J. H., Braun, J. E. and Groll, E. A.  
Evaluation of a hybrid method for refrigerant flow balancing in multi-circuit evaporators. *International Journal of Refrigeration*, Vol. 32, No. 6, pp. 1283-1292 (2009)
- [79] Kim et al. 2013  
Kim, K., Kim, D.R. and Lee, K.S.  
Local frosting behavior of a plated-fin and tube heat exchanger according to the refrigerant flow direction and surface treatment. *International Journal of Heat and Mass Transfer*, Vol. 64, pp. 751-758 (2013)
- [80] Kinsara et al. 1996  
Kinsara, A.A., Elsayed, M.M. and Al-Rabghi, O.M.  
Proposed energy-efficient air-conditioning system using liquid desiccant. *Applied Thermal Energy*, Vol. 16, No. 10, pp. 791-806 (1996)
- [81] Kondepudi et al. 1995  
Kondepudi, S., Murali, K., Lorsch, H. and Bhalerao, A.  
Voiding heat pump evaporator frost through the use of desiccants. *ASME-JSES-JSME International Solar Energy Conference*, New York, Part 1, pp. 25-29 (1995)
- [82] Kondepudi and O'Neal 1989  
Kondepudi, S.N. and O'Neal, D.L.  
Effect of frost growth on the performance of louvered finned tube heat exchangers. *International Journal of Refrigeration*, Vol.12, No. 3, pp. 151-158 (1989)
- [83] Kondepudi and O'Neal 1990  
Kondepudi, S.N. and O'Neal, D.L.  
The effects of different fin configuration on the performance of finned-tube heat exchanger under frosting conditions. *ASHRAE Transactions*, Vol. 96, Part 2, pp. 439-444 (1990)
- [84] Kondepudi and O'Neal 1991  
Kondepudi, S.N. and O'Neal, D.L.

Frosting performance of finned-tube heat exchanger with wavy and corrugated fins. *Experimental Thermal and Fluid Science*, Vol. 4, No. 5, pp. 613-618 (1991)

- [85] Krakow et al. 1992a  
Krakow, K.I., Yan, L. and Lin, S.  
A model of hot gas defrosting of evaporators, Part 1: Heat and mass transfer theory. *ASHRAE Transactions*, Vo. 198, Part 1, pp. 451-461 (1992)
- [86] Krakow et al. 1992b  
Krakow, K.I., Yan, L. and Lin, S.  
A model of hot gas defrosting of evaporators, Part 2: Experimental analysis. *ASHRAE Transactions*, Vo. 198, Part 1, pp. 462-474 (1992)
- [87] Krakow et al. 1993a  
Krakow, K.I., Yan, L. and Lin, S.  
An idealized model of reversed-cycle hot gas defrosting of evaporators, Part 1: Theory. *ASHRAE Transactions*, Vol. 99, Part 2, pp. 317-328 (1993)
- [88] Krakow et al. 1993b  
Krakow, K.I., Lin, S. and Yan, L.  
An idealized model of reversed-cycle hot gas defrosting of evaporators, Part 2: Experimental analysis and validation. *ASHRAE Transactions*, Vol. 99, Part 2, pp. 329-338 (1993)
- [89] Krakow and Lin 1996  
Krakow, K.I. and Lin, S.  
Hot gas defrosting of evaporators utilizing a vaporizer. *ASHRAE Transactions*, Vol. 102, Part 1, pp. 385-394 (1996)
- [90] Kuwahara et al. 1986  
Kuwahara, E., Kuwahara, T. and Yamazaki, M.  
Shortening the defrost time on a heat-pump air conditioner. *ASHRAE Transactions*, Vol. 92, Part 1, pp. 20-29 (1986)
- [91] Kwak and Bai 2010  
Kwak, K. and Bai, C.  
A study on the performance enhancement of heat pump using electric heater under the frosting condition Heat pump under frosting condition. *Applied Thermal Engineering*, Vol. 30, No. 6-7, pp. 539-543 (2010)
- [92] Kragh et al. 2005  
Kragh, J., Jørgen, R. and Svend, S.

Mechanical ventilation with heat recovery in cold climates. *In: Proceedings of the seventh Nordic symposium on building physics in Nordic countries.* Technical University of Denmark, pp.1-8 (2005)

- [93] Kwon et al. 2006  
Kwon, J.T., Lim, H.J., Kwon, Y.C., Koyama, S., Kim, D.H. and Kondou, C.  
An experimental study on frosting of laminar air flow on a cold surface with local cooling. *International Journal of Refrigeration*, Vol. 29, No. 5, pp. 754-760 (2006)
- [94] Lawrence and Evans 2008  
Lawrence, J.M.W. and Evans, J.A.  
Refrigerant flow instability as a means to predict the need for defrosting the evaporator in a retail display freezer cabinet. *International Journal of Refrigeration*, Vol. 31, No. 1, pp. 107-112 (2008)
- [95] Lee and Ro 2001  
Lee, Y.B. and Ro, S.T.  
An experimental study of frost formation on a horizontal cylinder under cross flow. *International Journal of Refrigeration*, Vol. 24, No. 6, pp. 468-474 (2001)
- [96] Lee and Ro 2002  
Lee, Y.B. and Ro, S.T.  
Frost formation on a vertical plate in simultaneously developing flow. *Experimental Thermal and Fluid Science*, Vol. 26, No. 8, pp. 939-945 (2002)
- [97] Li et al. 2010  
Li, D., Chen, Z. and Shi, M.  
Effect of ultrasound on frost formation on a cold flat surface in atmospheric air flow. *Experimental Thermal and Fluid Science*, Vol. 34, No. 8, pp. 1247-1252 (2010)
- [98] Li et al. 2011  
Li, Y., Chen, G., Tang, L. and Liu, L.  
Analysis on performance of a novel frost-free air-source heat pump system. *Building and Environment*, Vol. 46, No. 10, pp. 2051-2059 (2011)
- [99] Lee et al. 2010  
Lee, M., Kim, Y., Lee, H. and Kim, Y.  
Air-side heat transfer characteristics of flat plate finned-tube heat exchangers with large fin pitches under frosting conditions. *International Journal of Heat and Mass Transfer*, Vol.53 , pp. 2655-2661 (2010)

- [100] Liang et al. 2005  
Liang, C.H., Zhang, X.S., Chao, L.Z. and Liu, Y.M.  
Experimental comparison of sensible heat defrost and the conventional reverse cycle defrost. *Journal of Refrigeration (in Chinese)*, Vol. 26, No.4, pp. 20-24 (2005)
- [101] Liang et al. 2010  
Liang, C.H., Zhang, X.S., Li, X.W. and Chen, Z.Q.  
Control strategy and experimental study on a novel defrosting method for air-source heat pump. *Applied Thermal Engineering*, Vol. 30, No. 8-9, pp. 892-899 (2010)
- [102] Lin et al. 2013  
Lin, C., Li, Y.Z., Cai, W.J., Yan, J. and Hu, Y.  
Experimental investigation of the adjustable ejector in a multi-evaporator refrigeration system. *Applied Thermal Engineering*, Vol. 61, No.2, pp. 2-10 (2013)
- [103] Liu et al. 2003  
Liu, Z.Q., Tang, G.F. and Zhao, F.Y.  
Dynamic simulation of air-source heat pump during hot-gas defrost. *Applied Thermal Engineering*, Vol. 23, No. 6, pp. 675-685 (2003)
- [104] Liu 2004  
Liu, B.  
Analysis of frosting model and its affecting factors. *Journal of Refrigeration (in Chinese)*, Vol. 4, pp. 40-42 (2004)
- [105] Liu et al. 2006  
Liu, L., Wang, H.Y., Zhang, X.H., Meng, S. and Ma, C.F.  
An experimental study on minimizing frost deposition on a cold surface under natural convection conditions by use of a novel anti-frosting paint, Part I: Anti-frosting performance and comparison with the uncoated metallic surface. *International Journal of Refrigeration*, Vol. 29, No. 2, pp. 229-236 (2006)
- [106] Liu et al. 2007  
Liu, D., Zhao, F.Y. and Tang, G.F.  
Frosting of heat pump with heat recovery facility. *Renewable Energy (in Chinese)*, Vol. 32, No. 6, pp.1228-1242 (2007)
- [107] Llewelyn 1984

- Llewelyn, D. S.  
A significant advance in defrost control. *International Journal of Refrigeration*, Vol. 7, No. 5, pp. 334-335 (1984)
- [108] Lüer and Beer 2000  
Lüer, A. and Beer, H.  
Frost deposition in a parallel plate channel under laminar flow conditions. *International Journal of Thermal Science*, Vol. 39, No. 1, pp. 85-95 (2000)
- [109] Ma and Zhao 2008  
Ma, G. and Zhao, H.  
Experimental study of a heat pump system with flash-tank coupled with scroll compressor. *Energy and Buildings*, Vol. 40, pp. 697-701 (2008)
- [110] Machielsen and Kerschbaumer 1989  
Machielsen, C.H.M. and Kerschbaumer, H.G.  
Influence of frost formation and defrosting on the performance of air coolers: standards and dimensionless coefficients for the system designer. *International Journal of Refrigeration*, Vol. 12, No. 5, pp. 283-290 (1989)
- [111] Mader and Thybo 2012  
Mader, G. and Thybo, C.  
A new method of defrosting evaporator coils. *Applied Thermal Engineering*, Vol. 39, pp. 78-85 (1989)
- [112] Mago and Sherif 2003  
Mago, P.J. and Sherif, S.A.  
Heat and mass transfer on a cylinder surface in cross flow under supersaturated frosting conditions. *International Journal of Refrigeration*, Vol. 26, No. 8, pp. 889-899 (2003)
- [113] Mao et al. 1999  
Mao, Y., Besant, R.W. and Chen, H.  
Frost characteristics and heat transfer on a flat plate under freezer operating conditions, Part I: Experimentation and correlations. *ASHRAE Transactions*, Vol. 105, Part 2, pp. 231-251 (1999)
- [114] Martinez-Frias and Aceves 1999  
Martinez-Frias, J. and Aceves, S.M.  
Effects of evaporator frosting on the performance of an air to air heat pump. *Journal of Energy Resources Technology, Transactions of the ASME*, Vol. 121, No. 1, pp. 60-65 (1999)

- [115] Masaji 1998  
Masaji, Y.  
Development of burners for room air conditioners. *Technical Review-Mitsubishi Heavy Industries (in Japanese)*, Vol. 35, No. 2 (1998)
- [116] Masoero 1984  
Masoero, M.  
Refrigeration systems based on long-term storage of ice. *International Journal of Refrigeration*, Vol. 7, No. 2, pp. 93-100 (1984)
- [117] Matsuki et al. 1999  
Matsuki, N., Nakano, Y., Miyanaga, T., Yokoo, N. and Oka, T.  
Performance of radiant cooling system integrated with ice storage. *Energy and Buildings*, Vol. 30, No. 2, pp. 177-183 (1999)
- [118] Mei et al. 2002  
Mei, V.C., Gao, Z. and Tomlinson, J.J.  
Frost-less heat pump. *ASHRAE Transactions*, Vol. 108, Part 1, pp. 452-459 (2002)
- [119] Melo et al. 2013  
Melo, C., Knabben, F. T. and Pereira, P. V.  
An experimental study on defrost heaters applied to frost-free household refrigerators. *Applied Thermal Engineering*, Vol. 51, pp. 239-245 (2013)
- [120] Miller 1984  
Miller, W.A.  
Frosting experiments for a heat pump having a one-row spine-fin outdoor coil. *ASHRAE Transactions*, Vol. 90, Part 1, pp. 1009-1025 (1984)
- [121] Miller 1987  
Miller, W.A.  
Laboratory examination and seasonal analysis of frosting and defrosting for an air-to-air heat pump. *ASHRAE Transactions*, Vol. 93, Part 1, pp. 1447-1489 (1987)
- [122] Mills 1999  
Mills, A.F.  
Basic heat and mass transfer. *Upper Saddle River, NJ: Prentice hall*, 1999
- [123] Moallem et al. 2013  
Moallem, E., Hong, T., Cremaschi, L. and Fisher, D.E.

Experimental investigation of adverse effect of frost formation on microchannel evaporators, Part 1: Effect of fin geometry and environmental effects. *International Journal of Refrigeration*, Vol. 36, pp. 1762-1775 (2013)

- [124] Mohanraj et al. 2012  
Mohanraj, M., Jayaraj, S. and Muraleedharan C.  
Applications of artificial neural networks for refrigeration, air-conditioning and heat pump systems-A review. *Renewable and Sustainable Energy Reviews*, Vol. 16, Part 2, pp. 1340-1358 (2012)
- [125] Muller 1975  
Muller, E. D.  
A new concept for defrosting refrigeration plants. *Kalte*, Vol. 28, Part 2, pp. 52-54 (1975)
- [126] Niederer 1976  
Niederer, D.H.  
Frost and defrosting effects on coil heat transfer. *ASHRAE Transactions*, Vol. 82, Part 1, pp. 467-473 (1976)
- [127] Nishimura 2002  
Nishimura, T.  
“Heat pumps-status and trends” in Asia and the Pacific. *International Journal of Refrigeration*, Vol. 25, No. 4, pp. 405-413 (2002)
- [128] Nguyen et al. 2007  
Nguyen, M., Hewitt, N. and Huang, M.  
Performance evaluation of an air source heat pump using economized vapor injection compressor and flash tank coupled with capillary tubes. *In: Proceedings of International Congress of Refrigeration*, Beijing, China, ICR07-E2-1110 (2007)
- [129] Nutter et al. 1996  
Nutter, D.W., O’Neal, D.L. and Payne, W.V.  
Impact of the suction line accumulator on the frost/defrost performance air-source heat pump with a scroll compressor. *ASHRAE Transactions*, Vol. 102, Part 2, pp. 689-698 (1996)
- [130] O’Neal et al. 1989  
O’Neal, D.L., Peterson, K.T., Anand, N.K. and Schliesing, J.S.  
Refrigeration system dynamics during the reverse cycle defrost. *ASHRAE Transactions*, Vol. 95, Part 2, pp. 689-698 (1989)

- [131] Okoroafor and Newborough 2000  
Okoroafor, E.U. and Newborough, M.  
Minimizing frost growth on cold surfaces exposed to humid air by means of crosslinked hydrophilic polymeric coatings. *Applied Thermal Engineering*, Vol. 20, pp. 737-758 (2000)
- [132] Ozkan et al. 2012  
Ozkan, D.B., Ozil, P. and Inan, C.  
Experimental investigation of the defrosting process on domestic refrigerator finned tube evaporators. *Heat Transfer Engineering*, Vol. 33, No. 6, pp. 548-557 (2012)
- [133] Padki et al. 1989  
Padki, M.M., Sherif, S.A. and Nelson, R.M.  
A simple method for modeling the frost formation phenomenon in different geometries. *ASHRAE Transactions*, Vol.95, pp. 1127-1137 (1989)
- [134] Paone and Rossi 1991  
Paone, N. and Rossi, G.  
Fiber-optic ice sensors for refrigerators. *Proceedings of SPIE*, Vol. 1511, pp. 129-139 (1991)
- [135] Paris et al. 1993  
Paris, J., Falardeau, M. and Villeneuve, C.  
Thermal storage by latent heat: a viable option for energy conservation in buildings. *Energy Sources*, Vol. 15, No. 1, pp. 85-93 (1993)
- [136] Pasupathy et al. 2008  
Pasupathy, A., Velraja, R. and Seeniraj, R.V.  
Phase change material-based building architecture for thermal management in residential and commercial establishments. *Renewable and Sustainable Energy Reviews*, Vol. 12, No. 1, pp. 39-64 (2008)
- [137] Payne and O'Neal 1995  
Payne, V. and O'Neal, D.L.  
Defrost cycle performance for an air-source heat pump with a scroll and a reciprocating compressor. *International Journal of Refrigeration*, Vol. 18, No. 2, pp. 107-112 (1995)
- [138] Phillips et al. 1989  
Phillips, E.G., Bradley, B.C., Chant, R.E. and Fisher, D.R.

Comparison of freezing control strategies for residential air-to-air heat recovery ventilators. *ASHRAE Transactions*, Vol. 95, Part 2, (CONF-890609-) (1989)

- [139] Phillips et al. 1992  
Phillips, E.G., Fisher, D.R. and Chant, R.E.  
Freeze-control strategy and air-to-air energy recovery performance. *ASHRAE Journal*, pp. 44-9 (1992)
- [140] Qu et al. 2010  
Qu, M.L., Xia, L., Deng, S.M. and Jiang, Y.Q.  
Improved indoor thermal comfort during defrost with a novel reverse-cycle defrosting method for air source heat pumps. *Building and Environment*, Vol. 45, No. 11, pp. 2354-2361 (2010)
- [141] Qu et al. 2012a  
Qu, M.L., Xia, L., Deng, S.M. and Jiang, Y.Q.  
A study of the reverse cycle defrosting performance on a multi-circuit outdoor coil unit in an air source heat pump-Part I: Experiments. *Applied Energy*, Vol. 91, No. 1, pp. 122-129 (2012)
- [142] Qu et al. 2012b  
Qu, M.L., Pan, D.M., Xia, L., Deng, S.M. and Jiang, Y.Q.  
A study of the reverse cycle defrosting performance on a multi-circuit outdoor coil unit in an air source heat pump-Part II: Modeling analysis. *Applied Energy*, Vol. 91, No. 1, pp. 274-280 (2012)
- [143] Rabin et al. 1995  
Rabin, Y., Bar-Niv, I., Korin, E. and Mikic, B.  
Integrated solar collector storage system based on a salt hydrate phase change material. *Solar Energy*, Vol. 55, No. 6, pp. 435-444 (1995)
- [144] Rafati Nasr et al. 2014  
Rafati Nasr, M., Fauchoux, M., Besant, R.W. and Simonson, C. J.  
A review of frosting in air-to-air energy exchangers. *Renewable and Sustainable Energy Reviews*, Vol. 30, pp. 538-554 (2014)
- [145] Rite and Crawford 1991a  
Rite, R.W. and Crawford, R.R.  
The effect of frost accumulation on the performance of domestic refrigerator-freezer finned-tube evaporator coils. *ASHRAE Transactions*, Vol. 97, Part 2, pp. 428-437 (1991)

- [146] Rite and Crawford 1991b  
Rite, R.W. and Crawford, R.R.  
A parametric study of the factors governing the rate of frost accumulation on domestic refrigerator-freezer finned-tube evaporator coils. *ASHRAE Transactions*, Vol. 97, Part 2, pp. 438-446 (1991)
- [147] Sanders 1974  
Sanders, C.T.  
Frost formation: the influence of frost formation and defrosting on the performance of air coolers. PhD. Thesis, Technische Hogeschool, Delft, The Netherlands (1974)
- [148] Seker et al. 2004a  
Seker, D., Kartas, H. and Egrican, N.  
Frost formation on fin-and-tube heat exchangers, Part I: Modeling of frost formation on fin-and-tube heat exchangers. *International Journal of Refrigeration*, Vol. 27, No. 4, pp. 367-374 (2004)
- [149] Seker et al. 2004b  
Seker, D., Kartas, H. and Egrican, N.  
Frost formation on fin-and-tube heat exchangers, Part II: Experimental investigation of frost formation on fin-tube heat exchangers. *International Journal of Refrigeration*, Vol. 27, No. 4, pp. 375-377 (2004)
- [150] Shah 1979  
Shah, M.M.  
A general correlation for heat transfer during film condensation inside pipes. *International Journal of Heat and Mass Transfer*, Vol. 22, No.4, pp. 547-556 (1979)
- [151] Sharma and Sagara 2005  
Sharma, S.D. and Sagara, K.  
Latent heat storage materials and systems: a review. *International Journal of Green Energy*, Vol. 2, No. 1, pp. 1-56 (2005)
- [152] Shao et al. 2002  
Shao, S., Wang, B., Xia, J., Ma, G. and Yan, Q.  
Study on heat pump cycle for cold regions with two-stage compression in one scroll compressor. *In: 7th IEA Heat Pump Conference*, Beijing, China (2002)
- [153] Sherif and Hertz 1998  
Sherif, S.A. and Hertz, M.G.

A semi-empirical model for electric defrosting of a cylindrical coil cooler. *International Journal of Energy Research*, Vol. 22, No. 1, pp. 85-92 (1998)

- [154] Sherif and Sherif 1992  
Sherif, S.A. and Sherif, R.A.  
Hot gas defrosting analysis of a flat plate cooler. *Proceedings of the 15th World Energy Engineering Congress and the 1992 World Environmental Engineering Congress*, Atlanta, Georgia, pp. 583-586 (1992)
- [155] Siegel 1977  
Siegel, R.  
Solidification of low conductivity material containing dispersed high conductivity particles. *International Journal of Heat and Mass Transfer*, Vol. 20, No. 10, pp. 1087-1089 (1977)
- [156] Sommers and Jacobi 2005  
Sommers, A.D. and Jacobi, A.M.  
Air-side heat transfer enhancement of a refrigerator evaporator using vortex generation. *International Journal of Refrigeration*, Vol. 28, No. 7, pp. 1006-1017 (2005)
- [157] Stoecker 1957  
Stoecker, W.F.  
How frost formation on coils affects refrigeration systems. *Refrigeration Engineering*, Vol. 65, Part 2, pp. 42-46 (1957)
- [158] Stoecker et al. 1983  
Stoecker, W. F., Jr Lux, J. J. and Kooy, R.J.  
Energy consideration in hot-gas defrosting of industrial refrigeration coils. *ASHRAE Transactions*, Vol. 89, Part 2, pp. 549-573 (1983)
- [159] Tanda and Fossa 2006  
Tanda, G. and Fossa, M.  
Free convection frost growth in a narrow vertical channel. *International Journal of Heat and Mass Transfer*, Vol. 49, No. 11-12, pp. 1946-1957 (2006)
- [160] Tanker 1941  
Tanker, C. R.  
U.S. Patent No. 2,300,085. *Washington, DC: U.S. Patent and Trademark Office*. (1941)
- [161] Threlkeld 1970

- Threlkeld, J.L.  
Thermal environmental engineering. *Englewood Cliffs, NJ: Prentice-Hall, 1970.*
- [162] Tso et al. 2006a  
Tso, C.P., Cheng, Y.C. and Lai, A.C.K.  
Dynamic behavior of a direct expansion evaporator under frosting condition. Part I: Distributed model. *International Journal of Refrigeration*, Vol. 29, No. 4, pp. 611-623 (2006)
- [163] Tso et al. 2006b  
Tso, C.P., Cheng, Y.C. and Lai, A.C.K.  
Dynamic behavior of a direct expansion evaporator under frosting condition, Part II: Field investigation on a shipping container. *International Journal of Refrigeration*, Vol. 29, No. 4, pp. 624-631 (2006)
- [164] Umezu and Suma 1984  
Umezu, K. and Suma, S.  
Heat pump room air-conditioner using variable capacity compressor. *ASHRAE Transactions*, Vol. 90, No. 1a, pp. 335-349 (1984)
- [165] Vakialtojjar and Saman 2001  
Vakialtojjar, S.M. and Saman, W.  
Analysis and modeling of a phase change storage system for air conditioning applications. *Applied Thermal Engineering*, Vol. 21, No. 3, pp. 249-263 (2001)
- [166] Verma et al. 2002  
Verma, P., Carlson, D.M., Wu, Y., Hrnjak, P.S. and Bullard, C.W.  
Experimentally validated model for frosting of plain-fin-round-tube heat exchangers. *Proceedings of the 2002 International Conference of New Technologies in Commercial Refrigeration at University of Illinois at Urbana-Champaign*, pp. 152-162 (2002)
- [167] Votsis et al. 1989  
Votsis, P.P., Tassou, S.A., Wilson, D.R. and Marquand, C.J.  
Investigation of the performance of a heat pump under frosting and defrosting conditions. *Heat Recovery System & CHP*, Vol. 9, No. 5, pp. 399-406 (1989)
- [168] Wang and Liu 2005  
Wang, S.W. and Liu, Z.Y.  
A new method for preventing heat pump from frosting. *Renewable Energy*, Vol. 30, No. 5, pp. 753-761 (2005)

- [169] Wang et al. 2008  
Wang, Z.Y., Wang, X.X. and Dong, Z.M.  
Defrost improvement by heat pump refrigerant charge compensating. *Applied Energy*, Vol. 85, No. 11, pp. 1050-1059 (2008)
- [170] Wang et al. 2009  
Wang, X., Hwang, Y. and Radermacher, R.  
Two-stage heat pump with vapor-injected scroll compressor using R410A as a refrigerant. *International Journal of Refrigeration*, Vol. 32, No. 2, pp. 1442-1451 (2009)
- [171] Wang et al. 2011a  
Wang, R.X., Xie, G.Z., Wu, Q.P., Wu, Y.Z. and Yuan, J.W.  
An air source heat pump with an advanced cycle for heating buildings in Beijing. *Energy Conversion and Management*, Vol. 52, No. 2, pp. 1493-1500 (2011)
- [172] Wang et al. 2011b  
Wang, W., Xiao, J., Guo, Q.C., Lu, W.P. and Feng, Y.C.  
Field test investigation of the characteristics for the air source heat pump under two typical mal-defrost phenomena. *Applied Energy*, Vol. 88, pp. 4470-4480 (2011)
- [173] Wang et al. 2012a  
Wang, Q., He, W., Liu, Y.Q., Liang, G.F., Li, J.R., Han, X.H. and Chen, G.M.  
Vapor compression multifunctional heat pumps in China: A review of configurations and operational modes. *Renewable and Sustainable Energy Reviews*, Vol. 16, No. 9, pp. 6522-6538 (2012)
- [174] Wang et al. 2012b  
Wang, W., Guo, Q.C., Lu, W.P., Feng, Y.C. and Na, W.  
A generalized simple model for predicting frost growth on cold flat plate. *International Journal of Refrigeration*, Vol. 35, pp. 475-486 (2012)
- [175] Wang et al. 2012c  
Wang, D., Tao, T., Xu, G., Luo, A. and Kang, S.  
Experimental study on frosting suppression for a finned-tube evaporator using ultrasonic vibration. *Experimental Thermal and Fluid Science*, Vol. 36, pp. 1-11 (2012)
- [176] Wang et al. 2013a  
Wang, W., Xiao, J., Feng, Y.C., Guo, Q.C. and Wang, L.C.

Characteristics of an air source heat pump with novel photoelectric sensors during periodic frostedefrost cycles. *Applied Thermal Engineering*, Vol. 50, pp. 177-186 (2013)

- [177] Wang et al. 2013b  
Wang, W., Feng, Y.C., Zhu, J.H., Li, L.T., Guo, Q.C. and Lu, W.P.  
Performances of air source heat pump system for a kind of mal-defrost phenomenon appearing in moderate climate conditions. *Applied Energy*, Vol. 112, pp. 1138-1145 (2013)
- [178] Watters et al. 2002  
Watters, R.J., O'Neal, D.L. and Yang, J.X.  
Frost/defrost performance of a three-row fin staged heat pump evaporator. *ASHRAE Transactions*, Vol. 108, Part 2, pp. 318-329 (2002)
- [179] Winandy and Lebrun 2002  
Winandy, E.L. and Lebrun, J.  
Scroll compressor using gas and liquid injection: experimental analysis and modeling. *International Journal of Refrigeration*, Vol. 25, pp. 1143-1156 (2002)
- [180] Woodley 1989  
Woodley, C. B. C.  
Saving on the defrost. *Air Conditioning Refrigeration News*, August, pp. 62 (1989)
- [181] Wu and Webb 2001  
Wu, X.M. and Webb, R. L.  
Investigation of the possibility of frost release from a cold surface. *Experimental Thermal and Fluid Science*, Vol. 24, No. 3-4, pp. 151-156 (2001)
- [182] Xia et al. 1998  
Xia, J., Zhou, X.X. and Zhou, Z.Y.  
Effect of different parameters on performance of finned-tube evaporators and optimal defrosting period of heat pump. *Journal of Shanghai Jiaotong University (in Chinese)*, Vol. 32, No. 7, pp. 114-116 (1998)
- [183] Xia et al. 2004  
Xia, Y., Hrnjak, P.S. and Jacobi, A.M.  
An empirical study about frost accumulation effects on louvered-fin micro channel heat exchangers. *Proceedings of International Refrigeration and Air Conditioning Conference*, Purdue, July 12-15 (2004)

- [184] Xia et al. 2006  
 Xia, Y., Zhong, Y., Hrnjak, P.S. and Jacobi, A.M.  
 Frost, defrost, and refrost and its impact on the air-side thermal-hydraulic performance of louvered-fin, flat-tube heat exchangers. *International Journal of Refrigeration*, Vol. 29, No. 7, pp. 1066-1079 (2006)
- [185] Xiao et al. 2009  
 Xiao, J., Wang, W., Zhao, Y.H. and Zhang, F.R.  
 An analysis of the feasibility and characteristics of photoelectric technique applied in defrost-control. *International Journal of Refrigeration*, Vol. 32, pp. 1350-1357 (2009)
- [186] Xiao et al. 2010  
 Xiao, J., Wang, W., Guo, Q.C. and Zhao, Y.H.  
 An experimental study of the correlation for predicting the frost height in applying the photoelectric technology. *International Journal of Refrigeration*, Vol. 33, No. 5, pp. 1006-1014 (2010)
- [187] Yan et al. 2003a  
 Yan, W.M., Li, H.Y., Wu, Y.J., Lin, J.Y. and Chang, W.R.  
 Performance of finned tube heat exchangers operating under frosting conditions. *International Journal of Heat and Mass Transfer*, Vol. 46, No. 5, pp. 871-877 (2003)
- [188] Yan et al. 2003b  
 Yan, Q.L., Zhu, L., Zhang, M.E., Yan, N.X. and Hui, X.Y.  
 Study on ultrasonic defrost technology of refrigeration fan. *Transactions of the Chinese Society for Agricultural Machinery*, Vol. 34, No. 4, pp. 74-85 (2003)
- [189] Yan et al. 2005  
 Yan, W.M., Li, H.Y. and Tsay, Y.L.  
 Thermofluid characteristics of frosted finned-tube heat exchangers. *International Journal of Heat and Mass Transfer*, Vol. 48, No. 15, pp. 3073-3080 (2005)
- [190] Yang et al. 2006a  
 Yang, D.K., Lee, K.S. and Song, S.  
 Fin spacing optimization of a fin-tube heat exchanger under frosting conditions. *International Journal Heat Mass Transfer*, Vol. 49, pp. 2619-2625 (2006)
- [191] Yang et al. 2006b  
 Yang, D.K., Lee, K.S. and Song, S.

- Modeling for predicting frosting behavior of a fin-tube heat exchanger. *International Journal Heat Mass Transfer*, Vol. 49, No. 7-8, pp. 1472-1479 (2006)
- [192] Yao et al. 2003  
Yao, Y. and Ma, Z.L.  
Modeling and analyzing of airside heat exchanger under frosting in air source heat pump water chiller/heater. *International Journal of Harbin Institute of Technology*, Vol. 35, No. 7, pp. 781-783 (2003)
- [193] Yao et al. 2004  
Yao, Y., Jiang, Y.Q., Deng, S.M. and Ma, Z.L.  
A study on the performance on the airside heat exchanger under frosting in air-source heat pump water heater/chiller unit. *International Journal of Heat and Mass Transfer*, Vol. 47, No. 17-18, pp. 3745-3756 (2004)
- [194] Yasuda et al. 1990  
Yasuda, Y., Senshu, T., Kuroda, S., Atsumi, T. and Oguni, K.  
Heat pump performance under frosting conditions: Part II-Simulation of heat pump cycle characteristics under frosting conditions. *ASHRAE Transactions*, Vol. 96, No.1, pp. 330-336 (1990)
- [195] Ye and Lee 2013  
Ye, H.Y. and Lee, K.S.  
Performance prediction of a fin-and-tube heat exchanger considering air-flow reduction due to the frost accumulation. *International Journal of Heat and Mass Transfer*, Vol.67, pp. 225-233 (2013)
- [196] Yin et al. 2012  
Yin, H. J., Yang, Z., Chen, A. Q. and Zhang, N.  
Experimental research on a novel cold storage defrost method based on air bypass circulation and electric heater. *Energy*, Vol. 37, Part 1, pp. 623-631 (2012)
- [197] Yonko and Sepsy 1967  
Yonko, J.D. and Sepsy, C.F.  
An investigation of the thermal conductivity of frost while forming on a flat horizontal plate. *ASHRAE Transactions*, Vol. 73, Part 2, pp. x1.1-x1.10 (1967)
- [198] Young 1980  
Young, D.J.  
Development of a northern climate residential air-source heat pump. *ASHRAE Transactions*, Vol. 86, Part 1, pp. 671-686 (1980)

- [199] Zakrzewski 1984  
Zakrzewski, B.  
Optimal defrost cycle for the air cooler. *International Journal of Refrigeration*, Vol. 7, No. 1, pp. 41-45 (1984)
- [200] Zhang and Hrnjak 2009  
Zhang, P. and Hrnjak, P.S.  
Air-side performance evaluation of three types of heat exchangers in dry, wet and periodic frosting conditions. *International Journal of Refrigeration*, Vol. 32, pp. 911-921 (2009)
- [201] Zhnder et al. 2002  
Zhnder, M., Favrat, D., Hohl, H., Olivier, C. and Perevozchikov, M.  
High performance air-water heat pump with extended application range for residential heating. *In: 7th IEA Heat Pump Conference*, Beijing, China (2002)

## Appendix A

### Photos of the Experimental Setup

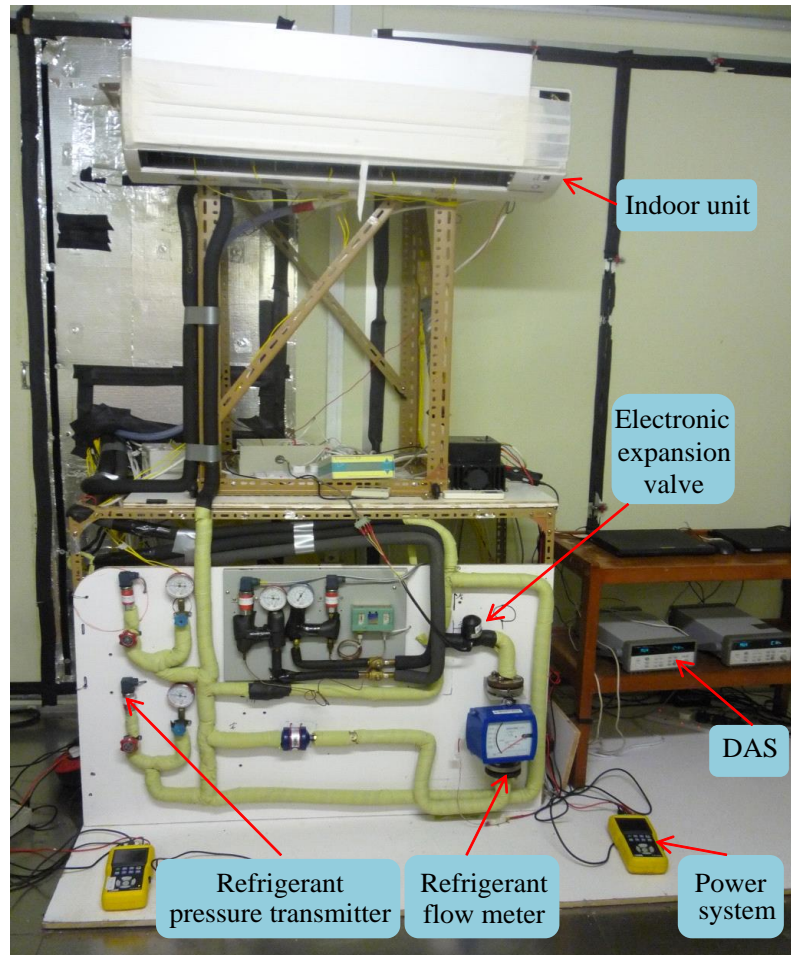


Photo 1 Overview of the indoor part of the experimental setup

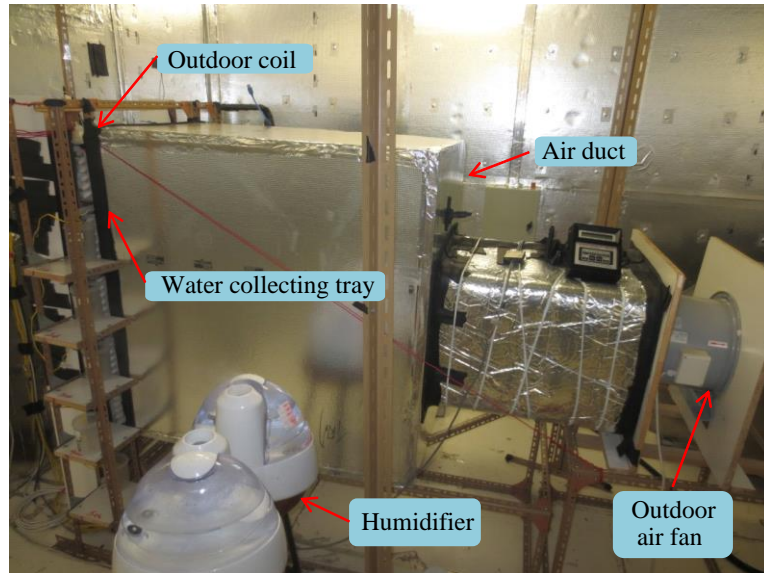


Photo 2 Overview of the outdoor part of the experimental setup

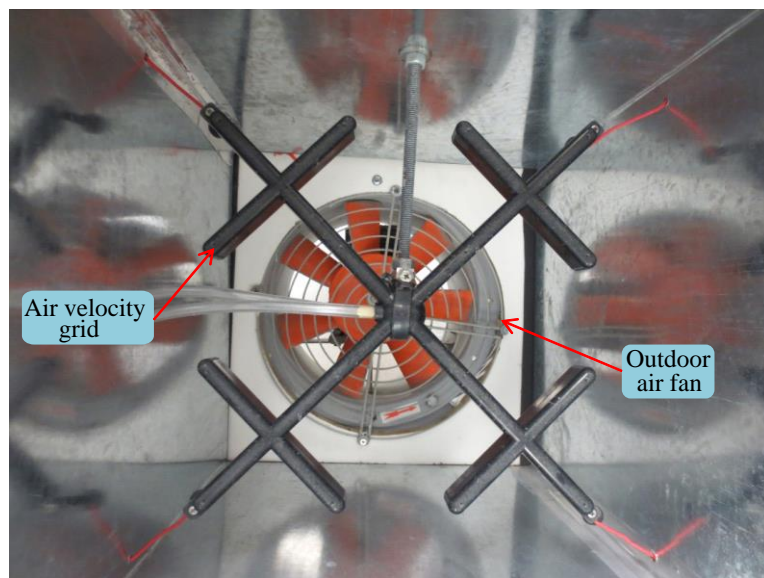


Photo 3 Air velocity grid in the outdoor part of the experimental setup

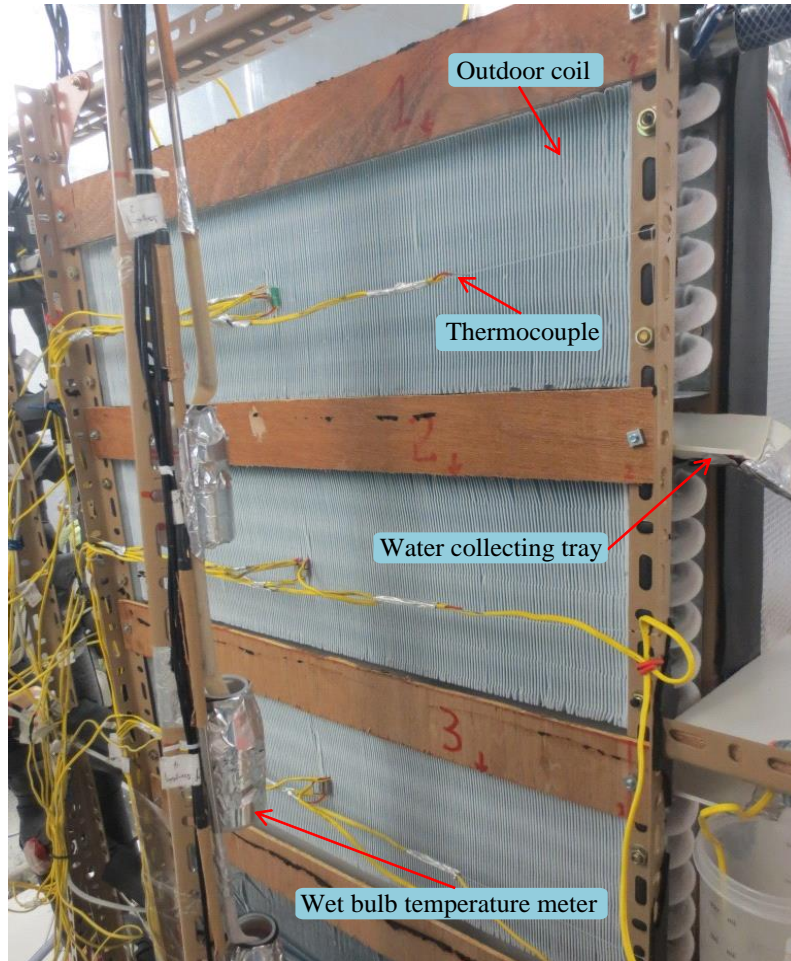


Photo 4 Outdoor coil of the experimental setup

## Appendix B

### Program Listing of Model 1

% The following program written in Matlab R2012a was used for modeling study the negative effects of downwards flowing of melted frost on defrosting performance for an ASHP unit having a vertically installed three-circuit outdoor coil during reverse cycle defrosting without using any water collecting trays between circuits, named as Model 1 in Chapter 6 in this thesis.

```
clear all;
```

```
clc;
```

```
hri=zeros(45,3); % the enthalpy value of input refrigerant, kJ/kg
```

```
Mr=zeros(45,3); % the mass flow rate of refrigerant, kg/s
```

```
Tri=zeros(45,3); % the temperature of input refrigerant, °C
```

```
Rr=zeros(45,3); % thermal resistance of refrigerant during defrosting, (K·m2)/W
```

```
% input all the known parameters
```

```
hri=xlsread('song20130828','hri');
```

```
Mr=xlsread('song20130828','Mr');
```

```
Tri=xlsread('song20130828','Tri');
```

```
Rr=xlsread('song20130828','Rr');
```

```
% input all the known parameters from the excel with the experimental results
```

```
mf=zeros(45,3); % the mass of melted frost, when it comes to 4th stage, it is 0 kg/5s
```

Tw=zeros(45,3); % the temperature of retained water on the coil, °C  
 qr=zeros(45,3); % the energy used from the refrigerant during the 5 seconds, J  
 qr2=zeros(46,3); % use refrigerant (R22) to calculate the energy used in defrosting; and  
 another way is to measure and calculated the energy used with Power system, J  
 Tro=zeros(45,3); % the temperature of exit refrigerant, °C  
 qm=zeros(45,3); % the energy used in frost melting during the 5 seconds, J; melting and  
 energy comes from the refrigerant, J  
 sfrost=zeros(45,3); % the total mass of frost melted before the moment, kg  
 qair=zeros(45,3); % the energy used in the ambient air, J  
 hair=zeros(45,3); % the coefficient of natural convective heat transfer, W/(m<sup>2</sup>°C)  
 mvaw=zeros(45,3); % the mass of vaporized water into the ambient air, kg/5s  
 smvaw=zeros(45,3); % the sum of vaporized water before this moment, kg  
 mrw=zeros(45,3); % the mass of retained water on this coil, kg/5s  
 hd=zeros(45,3); % the coefficient of convective mass transfer, W/(m<sup>2</sup>°C)  
 qvap=zeros(45,3); % the energy used in the water vaporized, J  
 s\_qvap=zeros(45,3); % total energy used in the water vaporized, J  
 watertray=zeros(45,3); % the mass of water flowing away from the water collecting tray,  
 kg/5s  
 swatertray=zeros(45,3); % the total mass of water flowing away from the water collecting  
 tray in the 5 seconds, kg  
 s\_qr2=zeros(45,3); % the energy taken in the refrigerant, J  
 hro=zeros(45,3); % the enthalpy value of output refrigerant, kJ/kg  
 % list the unknown parameters, and initialize these parameters with zeroes

for i=1:3 % three circuits in this study based on the experiment results

for j=1:18 % about 18\*5 seconds in the first two stages, obtained from the experimental results

if j==1

khri=hri(j,i); % , kJ/kg

```

kMr=Mr(j,i); % kg / s
kTri=Tri(j,1); % °C
kRr=Rr(j,i); % (K·m2)/W
ksmrw=0.0001; % the total retained water at the beginning is 0 kg, choose 0.0001
as the value for debugging, kg
kTw1=0.01; % the temperature of the melted frost at the beginning is 0 °C, choose
0 °C as the value for debugging
% all the input parameters in the function listed here

x0=[0.0001 0.0001 0.01 1200 0.001]; % mf=x(1), mrw=x(2), Tw=x(3); qr=x(4);
Tro=x(5) the values of debugging
options=optimset('display','off','MaxIter',100000,'MaxFunEvals',20000); % number
[A,fval,exit]=fsolve(@(x)
mystage1(x,ksmrw,kTw1,i,kRr,kTri,khri,kMr),x0,options); % x, ksmrw, kTw1, i, kTri,
kRr, kqr

mf(j,i)=A(1); % the mass of melted frost, kg/s
mrw(j,i)=A(2); % the mass of retained water, kg/s
Tw(j,i)=A(3); % the temperature of retained water, °C
qr(j,i)=A(4); % the energy used in defrosting from refrigerant, W
Tro(j,i)=A(5); % the temperature of tube surface at exit of each circuit, °C

A;
x00=real(A);
fval
exit
qm(j,i)=334000*mf(j,i); % W
sfrost(j,i)=5*sum(mf(:,i)); % kg
mvaw(j,i)=0; % kg/s
smvaw(j,i)=5*sum(mvaw(:,i)); % kg
qvap(j,i)=mvaw(j,i)*2443*1000; % J

```

```

s_qvap(j,i)=sum(qvap(:,i))*5; % J

watertray(j,i)=0; % kg/s
swatertray(j,i)=sum(watertray(:,i)); % kg
hro(j,i)=44518+1170.36*Tro(j,i)+1.68674*Tro(j,i)^2+5.2703/1000*Tro(j,i)^3;
qr2(j,i)=kMr*(khri-hro(j,i)); % W
s_qr2(j,i)=sum(qr2(:,i))*5; % W

%%%%%%%%%%%%%%%%%%%%%%%%%%%%%%%%%%%%%%%%%%%%%%%%%%%%%%%%%%%%%%%%%%%%%%%%

else if j<8
    khri=hri(j,i); % , kJ/kg
    kMr=Mr(j,i); % kg/s
    kTri=Tri(j,i); % , °C
    kRr=Rr(j,i); % (K·m2)/W
    ksmrw=sfrost(j-1,i); % the total retained water on 5*j seconds is the summate
value of 0-5*(j-1)seconds
    kTw1=Tw(j-1,i); % the temperature of the melted frost on 5*j seconds
    % all the input parameters in the function listed here

    x0=[0.0001 0.0001 0.01 1200 0.001]; % mf=x(1), mrw=x(2), Tw=x(3); qr=x(4);
Tro=x(5) the values for debugging

options=optimset('display','off','MaxIter',100000,'MaxFunEvals',20000); % number
[A,fval,exit]=fsolve(@x)
mystage1(x,ksmrw,kTw1,i,kRr,kTri,khri,kMr),x0,options); % x, ksmrw, kTw1, i, kTri,
kRr, kqr

mf(j,i)=A(1); % the mass of melted frost, kg/s
mrw(j,i)=A(2); % the mass of retained water, kg/s

```

```

Tw(j,i)=A(3); % the temperature of retained water, °C
qr(j,i)=A(4); % the energy used in defrosting from refrigerant, W
Tro(j,i)=A(5); % the temperature of tube surface at exit of each circuit, °C

```

```

A
x00=real(A);
fval
exit
qm(j,i)=334000.*mf(j,i); % W
sfrost(j,i)=5.*sum(mf(:,i)); % kg
mvaw(j,i)=0; % kg/s
smvaw(j,i)=5.*sum(mvaw(:,i)); % kg
hair(j,i)=0; % W/(m2°C)
qair(j,i)=0; % W
s_qair(j,i)=sum(qair(:,i))*5; % W
hd(j,i)=0; % W/(m2°C)
qvap(j,i)=mvaw(j,i)*2443*1000; % W
s_qvap(j,i)=sum(qvap(:,i))*5; % W
watertray(j,i)=0; % kg/s
swatertray(j,i)=sum(watertray(:,i)); % kg

```

```

hro(j,i)=44518+1170.36*Tro(j,i)+1.68674*Tro(j,i)^2+5.2703/1000*Tro(j,i)^3;
qr2(j,i)=kMr*(khri-hro(j,i)); % W
s_qr2(j,i)=sum(qr2(:,i))*5; % W

```

```

% here is the end of stage 1: preheating stage
%%%%%%%%%%%%%%%%%%%%%%%%%%%%%%%%%%%%%%%%%%%%%%%%%%%%%%%%%%%%%%%%%%%%%%%%

```

```

else if j>=8
    khri=hri(j,i); % kJ/kg

```

```

kMr=Mr(j,i); % kg/s
kTri=Tri(j,i); % °C
kRr=Rr(j,i); % (K·m2)/W
ksmrw=sfrost(j-1,i); % the total retained water on 5*j seconds, kg
kTw1=Tw(j-1,i); % the temperature of the melted frost on 5*j seconds, °C
% all the input parameters in the function listed here

x0=[0.0034 0.0034 0.35 1200 0.001]; % mf=x(1), mrw=x(2), Tw=x(3);
qr=x(4); Tro=x(5) the values for debugging;

options=optimset('display','off','MaxIter',100000,'MaxFunEvals',20000); % number
[A,fval,exit]=fsolve(@x)
mystage2(x,ksmrw,kTw1,i,kRr,kTri,khri,kMr),x0,options); % kRr1, kTr1 %
uw(j,i)=A(1);

mf(j,i)=A(1); % the mass of melted frost, kg/s
mrw(j,i)=A(2); % the mass of retained water, kg/s
Tw(j,i)=A(3); % the temperature of retained water, °C
qr(j,i)=A(4); % the energy used in defrosting from refrigerant, W
Tro(j,i)=A(5); % the temperature of tube surface at exit of each circuit, °C

A
x00=real(A);
fval
exit
qm(j,i)=334000.*mf(j,i); % W
effq(j,i)=qm(j,i)/qr(j,i); % 1
sfrost(j,i)=5.*sum(mf(:,i)); % kg
mvaw(j,i)=0; % kg/s
smvaw(j,i)=5.*sum(mvaw(:,i)); % kg
hair(j,i)=0; % W/(m2°C)

```

```

    qair(j,i)=0; % W
    s_qair(j,i)=sum(qair(:,i))*5; % W
    hd(j,i)=0; % W/(m2°C)
    qvap(j,i)=mvaw(j,i)*2443*1000; % W
    s_qvap(j,i)=sum(qvap(:,i))*5; % W
    watertray(j,i)=0; % kg/s
    swatertray(j,i)=sum(watertray(:,i)); % kg

hro(j,i)=44518+1170.36*Tro(j,i)+1.68674*Tro(j,i)^2+5.2703/1000*Tro(j,i)^3;
% kJ/kg
    qr2(j,i)=kMr*(khri-hro(j,i)); % W
    s_qr2(j,i)=sum(qr2(:,i))*5; % W

% here is the end of stage 2: frost melting without water flow to down circuit
%%%%%%%%%%%%%%%%%%%%%%%%%%%%%%%%%%%%%%%%%%%%%%%%%%%%%%%%%%%%%%%%%%%%%%%%

    end
    end
    end
end
end
%%%%%%%%%%%%%%%%%%%%%%%%%%%%%%%%%%%%%%%%%%%%%%%%%%%%%%%%%%%%%%%%%%%%%%%%

for i=1
    for j=18:45
        % for the 18*5 seconds for the 1st Circuit

        kmw1=mf(j-1,i)+0.0192; % 0.0192 kg stands for the mass of flowing water is
the sum of the melting and the melted on the coil, kg/s

```

```

    ksmrw=sfrost(17,i); % the total mass of water retained on the coil, the flowing
part 0.0192 kg was neglected, kg
    kTw1=Tw(j-1,i); %, °C
    kTri=Tri(j,i); %, °C
    kRr=Rr(j,i); % (K·m2)/W
    kMr=Mr(j,i); % kg/s
    khri=hri(j,i); % kJ/kg
    % all the input parameters in the function listed here

    x0=[0.0042 0.0042 0.335 1200 0.001]; % mf=x(1), mr=x(2), Tw=x(3); qr=x(4);
Tro=x(5) the values for debugging;
    options=optimset('display','off','MaxIter',100000,'MaxFunEvals',20000); %
number
    [A,fval,exit]=fsolve(@x)
mystage31(x,kmw1,ksmrw,kTw1,i,kTri,kRr,kMr,khri),x0,options);

    mf(j,i)=A(1); % melted water, kg/s; after this stage, mf is 0 kg/s
    mrw(j,i)=A(2); % retained water, kg/s
    Tw(j,i)=A(3); % retained water temperature, °C
    qr(j,i)=A(4); % energy used in defrosting from refrigerant, W
    Tro(j,i)=A(5); % the temperature of tube surface at exit of each circuit, °C

    A
    x00=real(A);
    fval
    exit
    qm(j,i)=334000.*mf(j,i); % W
    sfrost(j,i)=5.*sum(mf(:,i)); % after this stage, sfrost(j,i)=0.350 kg, obtained
from the experimental study, kg
    qair(j,i)=1.4748.*Tw(j,i).^4/3).*2.6852*2.5*0.55*((sfrost(j-
1,i))./0.323).^1.5; % W

```

```

s_qair(j,i)=sum(qair(:,i))*5; % W
hair(j,i)=1.4748.*Tw(j,i).^(1/3); % W/(m2°C)
smvaw(j,i)=5.*sum(mvaw(:,i)); % kg/s
hd(j,i)=0; % W/(m2°C)
qvap(j,i)=mvaw(j,i)*2443*1000; % W
s_qvap(j,i)=sum(qvap(:,i))*5; % W
watertray(j,i)=kmw1; % kg/s
swatertray(j,i)=sum(watertray(:,i)); % kg
hro(j,i)=44518+1170.36*Tro(j,i)+1.68674*Tro(j,i)^2+5.2703/1000*Tro(j,i)^3; %
kJ/kg
qr2(j,i)=kMr*(khri-hro(j,i)); % W
s_qr2(j,i)=sum(qr2(:,i))*5; % W

if sfrost(j,i)>=0.35;
    sfrost(j,i)=0.35; % after this stage, sfrost(j,i)=0.350 kg
    mf(j,i)=0; % at the fourth stage, the mf is always 0 kg/s
    kTw1=Tw(j-1,i); % the initial values are different for each circuit, °C
    mr0=0.008; % the water left on the first coil; kg/s
    smvaw=smvaw(j-1,i); % at the beginning of this stage, it is 0 kg

    % Coef7=-5800.2206;
    % Coef8=1.3914993;
    % Coef9=-0.04860239;
    % Coef10=0.000041764768;
    % Coef11=-0.000000014452093;
    % Coef12=6.5459673;

    T=Tri(j,i)+273.15; % K
    denspipe=exp(-5800.2206*T.^(-1)+1.3914993*T.^(0)-
0.04860239*T.^(1)+0.000041764768*T.^(2)-

```

0.000000014452093\*T.^(3)+6.5459673\*log(T))/(8314./18.\*T); % calculate the density of humidity air

Tair=0+273.15;% K; % Tair=0 % °C

PwSat\_Air=exp(-5800.2206\*Tair.^(-1)+1.3914993\*Tair.^(0)-  
0.04860239\*Tair.^(1)+0.000041764768\*Tair.^(2)-  
0.000000014452093\*Tair.^(3)+6.5459673\*log(Tair)); % Pa

dens\_air=0.80\*PwSat\_Air/(8314/18\*(273.15+0));

% relative\_Humi\_air=0.80

% 0.0039 density of component outside boundary layer, kg/m<sup>3</sup>

% PwSat\_pipeAir(1,t)=Pressure\_Air\_Water(Tr(1,t))

% dens\_pipe(c,t)=Pressure\_Air\_Water(Tw(c,t-  
1)).\*10^6./(8314./18.\*(273.15+Tw(c,t-1)));

% density of gas at interface (saturation density), kg/m<sup>3</sup>

kTri=Tri(j,i); % °C

kRr=Rr(j,i); % (K·m<sup>2</sup>)/W

kMr=Mr(j,i); % kg/s

khri=hri(j,i); % kJ/kg

% all the input parameters in the function listed here

x0=[0.0042 0.0042 0.335 1200 0.001];

options=optimset('display','off','MaxIter',10000,'MaxFunEvals',20000); %  
number

[A,fval,exit]=fsolve(@x)

mystage41(x,kTw1,mr0,smvaw,i,denspipe,dens\_air,kTri,kRr,kMr,khri),x0,options);

mrw(j,i)=A(1); % retained water, kg/s

mvaw(j,i)=A(2); % vaporized water, kg/s

Tw(j,i)=A(3); % retained water temperature, °C

qr(j,i)=A(4); % energy used in defrosting from refrigerant, W

```

Tro(j,i)=A(5); % the temperature of tube surface at exit of each circuit, °C

A
x00=real(A);
fval
exit
hair(j,i)=1.4748.*Tri(j,1).^(1/3); % W/(m2 °C)
qair(j,i)=1.4748.*Tri(j,1).^(4/3).*2.6852*2.5*2; % W
s_qair(j,i)=sum(qair(:,i))*5; % W
hd(j,i)=hair(j,i)/1005./1.258./0.845^(2/3); % W/(m2 °C)
smvaw(j,i)=5.*sum(mvaw(:,i)); % kg
qm(j,i)=334000.*mf(j,i); % W
qvap(j,i)=mvaw(j,i)*2443*1000; % W
s_qvap(j,i)=sum(qvap(:,i))*5; % W
watertray(j,i)=0; % kg/s
swatertray(j,i)=sum(watertray(:,i)); % kg

hro(j,i)=44518+1170.36*Tro(j,i)+1.68674*Tro(j,i)^2+5.2703/1000*Tro(j,i)^3;
% kJ/kg
qr2(j,i)=kMr*(khri-hro(j,i)); % W
s_qr2(j,i)=sum(qr2(:,i))*5; % W

end
end
end
% here is the end of stage 4 for Circuit 1: water layer evaporating stage
%%%%%%%%%%

for i=2
    for j=18:45

```

```

% for the 18*5 seconds for the 2nd circuit;
    kmw1=mf(j-1,i-1)+0.0192; % the water comes from 1st circuit, kg/s
    kmw2=kmw1+mf(j-1,i)+0.0192; % the water left from this 2nd circuit, kg/s
    ksmrw=sfrost(17,i); % the sum of water retained on the coil, kg

    kTw1=Tw(j-1,i); % °C
    kTri=Tri(j,i); % °C
    kRr=Rr(j,i); % (K·m2)/W
    kMr=Mr(j,i); % kg/s
    khri=hri(j,i); % kJ/kg
    % all the input parameters in the function listed here

    x0=[0.0042 0.0042 0.335 1200 0.001]; % mf=x(1), mr=x(2), Tw=x(3); qr=x(4);
Tro=x(5) the values of debugging;
    options=optimset('display','off','MaxIter',100000,'MaxFunEvals',20000);%
number
    [A,fval,exit]=fsolve(@(x)
mystage32(x,kmw1,kmw2,ksmrw,kTw1,i,kTri,kRr,kMr,khri),x0,options);

    mf(j,i)=A(1); % melted water, kg/s; after this stage, mf is 0 kg/s
    mrw(j,i)=A(2); % retained water, kg/s
    Tw(j,i)=A(3); % retained water temperature, °C
    qr(j,i)=A(4); % energy used in defrosting from refrigerant, W
    Tro(j,i)=A(5); % the temperature of tube surface at exit of each circuit, °C

    A
    x00=real(A);
    fval
    exit

    qm(j,i)=334000.*mf(j,i); % W

```

```

sfrost(j,i)=5.*sum(mf(:,i)); % after this stage, sfrost(j,i)=0.350, kg
qair(j,i)=1.4748.*Tw(j,i).^(4/3).*2.6852*2.5*0.50*((sfrost(j-1,i))./0.323).^1.5;
% W
s_qair(j,i)=sum(qair(:,i))*5; % W
hair(j,i)=1.4748.*Tw(j,i).^(1/3); % W/(K·m²)
smvaw(j,i)=5.*sum(mvaw(:,i)); % kg
hd(j,i)=0; % W/(K·m²)
qvap(j,i)=mvaw(j,i)*2443*1000; % W
s_qvap(j,i)=sum(qvap(:,i))*5; % W
watertray(j,i)=kmw2; % kg/s
swatertray(j,i)=sum(watertray(:,i)); % kg

hro(j,i)=44518+1170.36*Tro(j,i)+1.68674*Tro(j,i)^2+5.2703/1000*Tro(j,i)^3; %
W/(m² °C)
qr2(j,i)=kMr*(khri-hro(j,i)); % W
s_qr2(j,i)=sum(qr2(:,i))*5; % W

% here is the end of stage 3 for Circuit 2: frost melting with water flow to down circuit
%%%%%%%%%%%%%%%%%%%%%%%%%%%%%%%%%%%%%%%%%%%%%%%%%%%%%%%%%%%%%%%%%%%%%%%%

if sfrost(j,i)>=0.35;
    sfrost(j,i)=0.35; % kg
    mf(j,i)=0; % at fourth stage, the mf is always 0 kg/s
    kTw1=Tw(j-1,i); % the initial values are different for each circuit, °C
    mr0=0.008 ; % the water left on the first coil, kg/s
    smvaw=smvaw(j-1,i); % at the beginning of this stage, it is 0 kg

    % Coef7=-5800.2206;
    % Coef8=1.3914993;
    % Coef9=-0.04860239;

```

```

% Coef10=0.000041764768;
% Coef11=-0.000000014452093;
% Coef12=6.5459673;

T=Tri(j,i)+273.15; % K
denspipe=exp(-5800.2206*T.^(-1)+1.3914993*T.^(0)-
0.04860239*T.^(1)+0.000041764768*T.^(2)-
0.000000014452093*T.^(3)+6.5459673*log(T))/(8314./18.*T);
% calculate the density of humidity air, kg/m3

Tair=0+273.15;% K; %Tair=0; % °C;
PwSat_Air=exp(-5800.2206*Tair.^(-1)+1.3914993*Tair.^(0)-
0.04860239*Tair.^(1)+0.000041764768*Tair.^(2)-
0.000000014452093*Tair.^(3)+6.5459673*log(Tair)); % Pa;
dens_air=0.80*PwSat_Air/(8314/18*(273.15+0));
% relative_Humi_air=0.80;
% 0.0039 density of component outside boundary layer, kg/m3
% PwSat_pipeAir(1,t)=Pressure_Air_Water(Tr(1,t));
% dens_pipe(c,t)=Pressure_Air_Water(Tw(c,t-
1)).*10^6./(8314./18.*(273.15+Tw(c,t-1)));
% density of gas at interface (saturation density), kg/m3

kTri=Tri(j,i); % °C
kRr=Rr(j,i); % (K·m2)/W
kMr=Mr(j,i); % kg/s
khri=hri(j,i); % kJ/kg
% all the input parameters in the function listed here

x0=[0.0042 0.0042 0.335 1200 0.001];
options=optimset('display','off','MaxIter',10000,'MaxFunEvals',20000); %
number

```

```

[A,fval,exit]=fsolve(@(x)
mystage42(x,kTw1,mr0,smvaw,i,denspipe,dens_air,kTri,kRr,kMr,khri),x0,options);

mrw(j,i)=A(1); % retained water, kg/s;
mvaw(j,i)=A(2); % vaporized water, kg/s;
Tw(j,i)=A(3); % retained water temperature, °C;
qr(j,i)=A(4); % energy used in defrosting from refrigerant, W;
Tro(j,i)=A(5); % the temperature of tube surface at exit of each circuit, °C

A
x00=real(A);
fval
exit

hair(j,i)=1.4748.*Tri(j,1).^(1/3); % W/(K·m2)
qair(j,i)=1.4748.*Tri(j,1).^(4/3).*2.6852*2.5*2; % W
s_qair(j,i)=sum(qair(:,i))*5; % W
hd(j,i)=hair(j,i)/1005./1.258./0.845^(2/3); % W/(K·m2)
qvap(j,i)=mvaw(j,i)*2443*1000; % W
smvaw(j,i)=5.*sum(mvaw(:,i)); % kg
qm(j,i)=334000.*mf(j,i); % W
qvap(j,i)=mvaw(j,i)*2443*1000; % W
s_qvap(j,i)=sum(qvap(:,i))*5; % W
watertray(j,i)=0; % kg/s
swatertray(j,i)=sum(watertray(:,i)); % kg

hro(j,i)=44518+1170.36*Tro(j,i)+1.68674*Tro(j,i)^2+5.2703/1000*Tro(j,i)^3;
% W/(K·m2)
qr2(j,i)=kMr*(khri-hro(j,i)); % W
s_qr2(j,i)=sum(qr2(:,i))*5; % W

```

```

        end
    end
end
% here is the end of stage 4 for Circuit 2: water layer evaporating stage
%%%%%%%%%%%%%%%%%%%%%%%%%%%%%%%%%%%%%%%%%%%%%%%%%%%%%%%%%%%%%%%%%%%%%%%%

for i=3
    for j=18:45
        % for the 18*5 seconds for the 1st circuit;

        kmw2=mf(j-1,i-2)+mf(j-1,i-1)+0.0192*2.0; % kg/s
        kmw3=kmw2+mf(j-1,i)+0.0192; % kg/s
        ksmrw=sfrost(17,i); % kg
        kTw1=Tw(j-1,i); % °C
        kTri=Tri(j,i); % °C
        kRr=Rr(j,i); % (K·m²)/W
        kMr=Mr(j,i); % kg/s
        khri=hri(j,i); % kJ/kg
        % all the input parameters in the function listed here

        x0=[0.0042 0.0042 0.335 1200 0.001];%mf=x(1), mr=x(2), Tw=x(3);
qr=x(4); Tro=x(5) the values of debugging
        options=optimset('display','off','MaxIter',100000,'MaxFunEvals',20000); %
number
        [A,fval,exit]=fsolve(@(x)
mystage33(x,kmw2,kmw3,ksmrw,kTw1,i,kTri,kRr,kMr,khri),x0,options);

        mf(j,i)=A(1); % melted water, kg/s; after this stage, mf is 0 kg/s
        mrw(j,i)=A(2); % retained water, kg/s
        Tw(j,i)=A(3); % retained water temperature, °C

```

```

qr(j,i)=A(4); % energy used in defrosting from refrigerant. W
Tro(j,i)=A(5); % the temperature of tube surface at exit of each circuit, °C

A
x00=real(A);
fval
exit
qm(j,i)=334000.*mf(j,i); % W
sfrost(j,i)=5.*sum(mf(:,i)); % after this stage, sfrost(j,i)=0.350, kg
qair(j,i)=1.4748.*Tw(j,i).^(4/3).*2.6852*2.5*0.45*((sfrost(j-
1,i))./0.323).^1.5; % W
s_qair(j,i)=sum(qair(:,i))*5; % W
hair(j,i)=1.4748.*Tw(j,i).^(1/3); % W/(K m²)
smvaw(j,i)=5.*sum(mvaw(:,i)); % kg
hd(j,i)=0; % W/(K m²)
qvap(j,i)=mvaw(j,i)*2443*1000; % W
s_qvap(j,i)=sum(qvap(:,i))*5; % W
watertray(j,i)=kmw3; % kg/s
swatertray(j,i)=sum(watertray(:,i)); % kg

hro(j,i)=44518+1170.36*Tro(j,i)+1.68674*Tro(j,i)^2+5.2703/1000*Tro(j,i)^3;
% kJ/kg
qr2(j,i)=kMr*(khri-hro(j,i)); % W
s_qr2(j,i)=sum(qr2(:,i))*5; % W
% here is the end of stage 3 for Circuit 3: frost melting with water flow to down circuit
%%%%%%%%%%%%%%

if sfrost(j,i)>=0.35;
    sfrost(j,i)=0.35; % kg
    mf(j,i)=0; % 4th stage the mf is always 0, kg/s

```

```

kTw1=Tw(j-1,i); % the initial values are different for each circuit, °C
mr0=0.008 ; % the water left on the first coil, kg/s
smvaw=smvaw(j-1,i); % at the beginning of this stage, it is 0, kg

% Coef7=-5800.2206;
% Coef8=1.3914993;
% Coef9=-0.04860239;
% Coef10=0.000041764768;
% Coef11=-0.000000014452093;
% Coef12=6.5459673;

Tair=0+273.15; % K; % Tair=0; % °C
PwSat_Air=exp(-5800.2206*Tair.^(-1)+1.3914993*Tair.^(0)-
0.04860239*Tair.^(1)+0.000041764768*Tair.^(2)-
0.000000014452093*Tair.^(3)+6.5459673*log(Tair));% Pa

dens_air=0.80*PwSat_Air/(8314/18*(273.15+0)); % relative_Humi_air=0.80;
% 0.0039 density of component outside boundary layer, kg/m3
% PwSat_pipeAir(1,t)=Pressure_Air_Water(Tr(1,t))
% dens_pipe(c,t)=Pressure_Air_Water(Tw(c,t-
1)).*10^6./(8314./18.*(273.15+Tw(c,t-1)))
% density of gas at interface (saturation density), kg/m3

T=Tri(j,i)+273.15; % K
denspipe=exp(-5800.2206*T.^(-1)+1.3914993*T.^(0)-
0.04860239*T.^(1)+0.000041764768*T.^(2)-
0.000000014452093*T.^(3)+6.5459673*log(T))/(8314./18.*T); % calculate the density
of humidity air, kg/m3

kTri=Tri(j,i); % °C
kRr=Rr(j,i); (K·m2)/W

```

```

kMr=Mr(j,i); % kg/s
khri=hri(j,i); % kJ/kg
% all the input parameters in the function listed here

x0=[0.0042 0.0042 0.335 1200 0.001];
options=optimset('display','off','MaxIter',10000,'MaxFunEvals',20000); %
number
[A,fval,exit]=fsolve(@(x)
mystage43(x,kTw1,mr0,smvaw,i,denspipe,dens_air,kTri,kRr,kMr,khri),x0,options);

mrw(j,i)=A(1); % retained water, kg/s
mvaw(j,i)=A(2); % vaporized water, kg/s
Tw(j,i)=A(3); % retained water temperature, °C
qr(j,i)=A(4); % energy used in defrosting from refrigerant, W
Tro(j,i)=A(5); % the temperature of tube surface at exit of each circuit, °C

A
x00=real(A);
fval
exit

hair(j,i)=1.4748.*Tri(j,1).^(1/3); % W/(K m2)
qair(j,i)=1.4748.*Tri(j,1).^(4/3).*2.6852*2.5*2; % W
s_qair(j,i)=sum(qair(:,i))*5; % W
hd(j,i)=hair(j,i)/1005./1.258./0.845^(2/3); % W/(K m2)
smvaw(j,i)=5.*sum(mvaw(:,i)); % kg
qm(j,i)=334000.*mf(j,i); % W
qvap(j,i)=mvaw(j,i)*2443*1000; % W
s_qvap(j,i)=sum(qvap(:,i))*5; % W
watertray(j,i)=0; % kg/s
swatertray(j,i)=sum(watertray(:,i)); % kg

```

```

hro(j,i)=44518+1170.36*Tro(j,i)+1.68674*Tro(j,i)^2+5.2703/1000*Tro(j,i)^3;
% W/(K m2)
    qr2(j,i)=kMr*(khri-hro(j,i)); % W
    s_qr2(j,i)=sum(qr2(:,i))*5; % W

    end
end
end
% here is the end of stage 4 for Circuit 3: water layer evaporating stage
%%%%%%%%%%%%%%%%%%%%%%%%%%%%%%%%%%%%%%%%%%%%%%%%%%%%%%%%%%%%%%%%%%%%%%%%

for i=1:3

    s_qm=0.350*3*334000; % this is fixed value for different cases, W
    s_qvap1=sum(s_qvap(37,:)); % W
    s_qr1=sum(s_qr2(37,:))*0.65; % W
    s_qair1=sum(s_qair(37,:)); % W
    s_q_heatingmeltedfrost=sum(swatertray(45,:)*Tw(32,3)*4.2*1000); % W
    Defrostingefficiency=(s_qm+s_qvap1)/s_qr1; % 1

end
%%%%%%%%%%%%%%%%%%%%%%%%%%%%%%%%%%%%%%%%%%%%%%%%%%%%%%%%%%%%%%%%%%%%%%%%

% The following programs are function programs used in the previous main program.

function F=mystage1(x,ksmrw,kTw1,i,kRr,kTri,khri,kMr)
% solve mf=x(1), mw=x(2), Tw=x(3), qr=x(4), kRr=x(5)
F=[x(1)-x(2); % kg/s

```

```

x(4)-334000.*x(1)-4195.2.*x(2).*x(3)-4195.2.*ksmrw.*(x(3)-kTw1); % J/s
334000.*x(1)-1480.54.*((i+1)^0.5-i^0.5).*2.6852*2.5*x(3); % 0.85 stand for the
water side modification
x(4)-0.0679*(kTri-2.*x(3))./(kRr+3.6316e-06); % 0.55 is the modification value of
refrigerant side
x(4)-0.32*kMr*(khri-44518-1170.36*x(5)-1.68674*x(5)^2-
5.2703/1000*x(5)^3)] %0.40 make the s-frost suitable. % -5.2703/1000*kTro^3, W

end

```

```

function F=mystage2(x,ksmrw,kTw1,i,kRr,kTri,khri,kMr)
% solve mf=x(1), mw=x(2), Tw=x(3), qr=x(4), Rr=x(5)
F=[x(1)-x(2); % kg/s
x(4)-334000.*x(1)-4195.2.*x(3).*x(2)-4195.2.*ksmrw.*(x(3)-kTw1)-
1.4748.*x(3).^(4/3).*2.6852*2.5*0.15; % W 0.4
1.4748.*x(3).^(4/3).*2.6852*2.5*0.15+334000.*x(1)-1480.54.*((i+1)^0.5-
i^0.5).*2.6852*2.5*0.85*x(3); % 0.85 stand for the area, which is not 2.6852*2.5*2.0
x(4)-0.0679*(kTri-2.*x(3))./(kRr+3.6316e-06); % 0.755 is the modification value of
refrigerant side
x(4)-0.32*kMr*(khri-44518-1170.36*x(5)-1.68674*x(5)^2-5.2703/1000*x(5)^3)] %
0.40 is to modify the Mr. -5.2703/1000*kTro^3, W

end

```

```

function F=mystage31(x,kmw1,ksmrw,kTw1,i,kTri,kRr,kMr,khri)
% solve mf=x(1), mrw=x(2), Tw=x(3), qr=x(4), Rr=x(5)
F=[x(1)-x(2)-kmw1; % mass conservation, frost changes to water, kg/s

```

```

x(4)-334000.*x(1)-4195.2.*ksmrw*(x(3)-kTw1)-
1.4748.*x(3).^4/3).*2.6852*2.5*0.55; % the energy in refrigerant used in frost melting,
retained water temperature improve, heating the air, W
% 2.6852*2.5*4.0*0.75 is the actual area of contact fins surface and the ambient air
1.4748.*x(3).^4/3).*2.6852*2.5*0.55+334000.*x(1)-1480.54.*((i+1)^0.5-
i^0.5).*2.6852*2.5*x(3)*0.45; % the heat transfer from water layer; 0.85 stand the area
is not 2.6852*2.5*4.0;
x(4)-0.0679*1.6*(kTri-2.*x(3))./(kRr+3.6316e-06); % 0.755 is the modification value
of refrigerant side
x(4)-0.42*kMr*(khri-44518-1170.36*x(5)-1.68674*x(5)^2-5.2703/1000*x(5)^3)] %
0.40 is to modify the Mr.-5.2703/1000*kTro^3, W

end

```

```

function F=mystage32(x,kmw1,kmw2,ksmrw,kTw1,i,kTri,kRr,kMr,khri)
% solve mf=x(1), mrw=x(2), Tw=x(3), qr=x(4), Rr=x(5)
F=[x(1)+kmw1-x(2)-kmw2; % mass conservation, frost changes to water, kg/s
x(4)-334000.*x(1)-4195.2.*(ksmrw+kmw1-kmw2)*(x(3)-kTw1)-
1.4748.*x(3).^4/3).*2.6852*2.5*0.50; % the energy in refrigerant used in frost melting,
retained water temperature improve, heating the air
% 2.6852*2.5*4.0*0.75 is the actual area of contact fins surface and the ambient air
1.4748.*x(3).^4/3).*2.6852*2.5*0.50+334000.*x(1)-1480.54.*((i+1)^0.5-
i^0.5).*2.6852*2.5*x(3)*0.50; % the heat transfer from water layer; 0.85 stand for the
area, which is not 2.6852*2.5*4.0;
x(4)-0.0679*1.3*(kTri-2*x(3))./(kRr+3.6316e-06); % 0.755 is the modification value
of refrigerant side
x(4)-0.375*kMr*(khri-44518-1170.36*x(5)-1.68674*x(5)^2-5.2703/1000*x(5)^3)] %
0.30 is to modify the Mr.-5.2703/1000*kTro^3, W

end

```

```

function F=mystage33(x,kmw2,kmw3,ksmrw,kTw1,i,kTri,kRr,kMr,khri)
% solve mf=x(1), mrw=x(2), Tw=x(3), qr=x(4), Rr=x(5)
F=[x(1)+kmw2-x(2)-kmw3; % mass conservation, frost changes to water, kg/s
  x(4)-334000.*x(1)-4195.2.*(ksmrw+kmw2-kmw3).*(x(3)-kTw1)-
  1.4748.*x(3).^(4/3).*2.6852*2.5*0.45; % the energy in refrigerant used in frost melting,
  retained water temperature improve, heating the air
  1.4748.*x(3).^(4/3).*2.6852*2.5*0.45+334000.*x(1)-1480.54.*((i+1)^0.5-
  i^0.5).*2.6852*2.5*0.55*x(3); % the heat transfer from water layer
  % 2.6852*2.5*4.0*0.75 is the actual area of contact fins surface and the ambient air;
  x(4)-0.0679*1.0*(kTri-2*x(3))./(kRr+3.6316e-06); % 0.755 is the modification value
  of refrigerant side
  x(4)-0.33*kMr*(khri-44518-1170.36*x(5)-1.68674*x(5)^2-5.2703/1000*x(5)^3)] %
  0.40 is to modify the Mr. -5.2703/1000*kTro^3, W

end

```

```

function F=mystage41(x,kTw1,mr0,smvaw,i,denspipe,dens_air,kTri,kRr,kMr,khri)
% solve mrw=x(1), mvaw=x(2), Tw=x(3), qr=x(4), Rr=x(5)
F=[x(1)-x(2); % the water left on the coil is the water vaporized from this coil; mass
  conservation law
  x(4)-4195.2*((mr0-smvaw-x(2))*x(3)-(mr0-smvaw)*kTw1)-1480.54.*((i+1)^0.5-
  i^0.5).*2.6852*2.5*0.1*x(3)-1.4748*x(3)^(4/3).*2.6852*2.5*0.9-2443*1000*x(2);
  % the energy comes from refrigerant was used in improve the temperature
  % of retained water, and heat the ambient air, and retained water
  % vaporized; energy conservation, 2.0

```

```

x(2)-1.4748.*x(3).^(1/3)./1005./1.258./0.845^(2/3).*(denspipe-
dens_air)*2.6852*2.5*0.9*((mr0-smvaw)./mr0).^1.5*7.8;
% the mass of water vaporized into the ambient air is equal with the
x(4)-0.0679*7.0*(kTri-2.0*x(3))./(kRr+3.6316e-06); % 0.755 is the modification
value of refrigerant side
x(4)-1.35*kMr*(khri-44518-1170.36*x(5)-1.68674*x(5)^2-5.2703/1000*x(5)^3)] %
0.30 is to modify the Mr. -5.2703/1000*kTro^3, W

end

```

```

function F=mystage42(x,kTw1,mr0,smvaw,i,denspipe,dens_air,kTri,kRr,kMr,khri)
% solve mrw=x(1), mvaw=x(2), Tw=x(3), qr=x(4), Rr=x(5)
F=[x(1)-x(2); % the water left on the coil is the water vaporized from this coil; mass
conservation law

```

```

x(4)-4195.2*((mr0-smvaw-x(2))*x(3)-(mr0-smvaw)*kTw1)-1480.54.*((i+1)^0.5-
i^0.5).*2.6852*2.5*0.2*x(3)-1.4748*x(3)^(4/3)*2.6852*2.5*0.8-2443*1000*x(2);
% the energy comes from refrigerant was used in improve the temperature
% of retained water, and heat the ambient air, and retained water
% vaporized; energy conservation, 2.0

```

```

x(2)-1.4748.*x(3).^(1/3)./1005./1.258./0.845^(2/3).*(denspipe-
dens_air)*2.6852*0.8*2.5*((mr0-smvaw)./mr0).^1.5*7.8;
% the mass of water vaporized into the ambient air is equal with the
x(4)-0.0679*5.5*(kTri-2.0*x(3))./(kRr+3.6316e-06); % 0.755 is the modification
value of refrigerant side
x(4)-1.25*kMr*(khri-44518-1170.36*x(5)-1.68674*x(5)^2-5.2703/1000*x(5)^3)] %
0.30 is to modify the Mr. -5.2703/1000*kTro^3, W

end

```

```

function F=mystage43(x,kTw1,mr0,smvaw,i,denspipe,dens_air,kTri,kRr,kMr,khri)
% solve mrw=x(1), mvaw=x(2), Tw=x(3), qr=x(4), Rr=x(5)
F=[x(1)-x(2); % the water left on the coil is the water vaporized from this coil; mass
conservation law

x(4)-4195.2*((mr0-smvaw-x(2))*x(3)-(mr0-smvaw)*kTw1)-1480.54.*((i+1)^0.5-
i^0.5).*2.6852*2.5*0.3*x(3)-1.4748*x(3)^(4/3)*2.6852*2.5*0.7-2443*1000*x(2);
% the energy comes from refrigerant was used in improve the temperature
% of retained water, and heat the ambient air, and retained water
% vaporized; energy conservation, 2.0

x(2)-1.4748.*x(3).^(1/3)./1005./1.258./0.845^(2/3).*(denspipe-
dens_air)*2.6852*0.7*2.5*((mr0-smvaw)./mr0).^1.5*7.8;
% the mass of water vaporized into the ambient air is equal with the

x(4)-0.0679*4.0*(kTri-2.0*x(3))./(kRr+3.6316e-06); % 0.755 is the modification
value of refrigerant side

x(4)-1.15*kMr*(khri-44518-1170.36*x(5)-1.68674*x(5)^2-5.2703/1000*x(5)^3)] %
0.30 is to modify the Mr. -5.2703/1000*kTro^3, W

end

```